
SUBSURFACE IMAGING OF LAVA TUBES

Roadway Applications

Publication No. FHWA-CFL/TD-05-005

September 2005



U.S. Department
of Transportation
**Federal Highway
Administration**



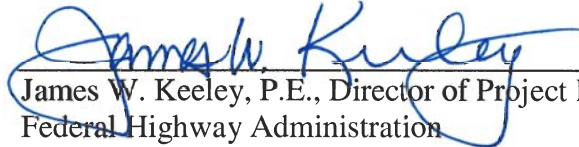
**Central Federal Lands Highway Division
12300 West Dakota Avenue
Lakewood, CO 80228**

FOREWORD

The Federal Lands Highway (FLH) promotes development and deployment of applied research and technology applicable to solving transportation related issues on Federal Lands. The FLH provides technology delivery, innovative solutions, recommended best practices, and related information and knowledge sharing to Federal agencies, Tribal governments, and other offices within the FHWA.

At many sites where road projects are planned by the FLH, unknown or undetected lava tubes (subsurface voids) may be present. To help quantify issues related to unknown voids, CFLHD undertook a preliminary investigation into non-invasive geophysical methods aimed at (1) characterizing the presence and vertical/horizontal extent of voids, (2) determining the most suitable geophysical methods for specifically conducting roadway surveys in terms of detection capabilities vs. feasibility (cost) vs. time constraints, and (3) identifying the range of applications nationwide.

This study includes background information of multiple geophysical methods and their ability to detect voids, a review of geophysical data collected over lava tubes at Lava Beds National Monument, and the results from the data. Conclusions and recommendations for economically and accurately locating lava tubes were made.



James W. Keeley, P.E., Director of Project Delivery
Federal Highway Administration
Central Federal Lands Highway Division

Notice

This document is disseminated under the sponsorship of the U.S. Department of Transportation in the interest of information exchange. The U.S. Government assumes no liability for the use of the information contained in this document. This report does not constitute a standard, specification, or regulation.

The U.S. Government does not endorse products or manufacturers. Trademarks or manufacturers' names appear in this report only because they are considered essential to the objective of the document.

Quality Assurance Statement

The Federal Highway Administration (FHWA) provides high-quality information to serve Government, industry, and the public in a manner that promotes public understanding. Standards and policies are used to ensure and maximize the quality, objectivity, utility, and integrity of its information. FHWA periodically reviews quality issues and adjusts its programs and processes to ensure continuous quality improvement.

Technical Report Documentation Page

1. Report No. FHWA-CFL/TD-05-005	2. Government Accession No.	3. Recipient's Catalog No.	
4. Title and Subtitle <i>Subsurface Imaging of Lava Tubes Roadway Applications</i>		5. Report Date September 2005	
		6. Performing Organization Code	
7. Author(s) Todd M. Meglich, Misti C. Williams, and Kanaan Hanna		8. Performing Organization Report No. 5007	
9. Performing Organization Name and Address Blackhawk, a division of ZAPATA ENGINEERING 301 Commercial Road, Suite B Golden, CO 80401		10. Work Unit No. (TRAIS)	
		11. Contract or Grant No. DTFH68-03-P-00179	
12. Sponsoring Agency Name and Address Federal Highway Administration Central Federal Lands Highway Division 12300 W. Dakota Avenue, Suite 210 Lakewood, CO 80228		13. Type of Report and Period Covered Technical Report, 2005	
		14. Sponsoring Agency Code HFTS-16.4	
15. Supplementary Notes COTR: Khamis Haramy, FHWA CFLHD; Advisory Panel Members: Roger Surdahl, Matt Demarco, and Linden Snyder, FHWA CFLHD. This project was funded under the FHWA Federal Lands Highway Technology Deployment Initiatives and Partnership Program (TDIPP).			
16. Abstract The Central Federal Lands Highway Division (CFLHD), FHWA, located in Denver, CO, is primarily responsible for the rehabilitation, reconstruction, and repaving of National Forest and Park roads in the western states region. At many sites, such as the Lava Beds National Monument (LBNM) in northern California, there are concerns that unknown near-surface voids pose possible risks to roadway construction activities, the long-term stability and maintenance of the roadway, and to public safety. To help quantify issues related to unknown voids, CFLHD undertook a preliminary investigation into non-invasive geophysical methods aimed at (1) characterizing the presence and vertical/horizontal extent of voids, (2) determining the most suitable geophysical methods for specifically conducting roadway surveys in terms of detection capabilities vs. feasibility (cost) vs. time constraints, and (3) identifying the range of applications nationwide. This report contains the details of geophysical surveys performed at the LBNM. The geophysical surveys were performed over several areas with known lava tubes. This report provides the geological site conditions, overviews of the geophysical methods, summary of the results, and overall recommendations that should be considered for future void detection.			
17. Key Words GEOPHYSICAL SURVEYS, MAGNETIC, ELECTRICAL RESISTIVITY, ELECTRICAL CONDUCTIVITY, HIGH RESOLUTION SHEAR WAVE REFLECTION, GROUND PENETRATING RADAR, VOIDS, LAVA TUBES		18. Distribution Statement No restriction. This document is available to the public from the sponsoring agency at the website http://www.cflhd.gov .	
19. Security Classif. (of this report) Unclassified	20. Security Classif. (of this page) Unclassified	21. No. of Pages 149	22. Price

SI* (MODERN METRIC) CONVERSION FACTORS

APPROXIMATE CONVERSIONS TO SI UNITS

Symbol	When You Know	Multiply By	To Find	Symbol
LENGTH				
in	inches	25.4	millimeters	mm
ft	feet	0.305	meters	m
yd	yards	0.914	meters	m
mi	miles	1.61	kilometers	km
AREA				
in ²	square inches	645.2	square millimeters	mm ²
ft ²	square feet	0.093	square meters	m ²
yd ²	square yard	0.836	square meters	m ²
ac	acres	0.405	hectares	ha
mi ²	square miles	2.59	square kilometers	km ²
VOLUME				
fl oz	fluid ounces	29.57	milliliters	mL
gal	gallons	3.785	liters	L
ft ³	cubic feet	0.028	cubic meters	m ³
yd ³	cubic yards	0.765	cubic meters	m ³
NOTE: volumes greater than 1000 L shall be shown in m ³				
MASS				
oz	ounces	28.35	grams	g
lb	pounds	0.454	kilograms	kg
T	short tons (2000 lb)	0.907	megagrams (or "metric ton")	Mg (or "t")
TEMPERATURE (exact degrees)				
°F	Fahrenheit	5 (F-32)/9 or (F-32)/1.8	Celsius	°C
ILLUMINATION				
fc	foot-candles	10.76	lux	lx
fl	foot-Lamberts	3.426	candela/m ²	cd/m ²
FORCE and PRESSURE or STRESS				
lbf	poundforce	4.45	newtons	N
lbf/in ²	poundforce per square inch	6.89	kilopascals	kPa

APPROXIMATE CONVERSIONS FROM SI UNITS

Symbol	When You Know	Multiply By	To Find	Symbol
LENGTH				
mm	millimeters	0.039	inches	in
m	meters	3.28	feet	ft
m	meters	1.09	yards	yd
km	kilometers	0.621	miles	mi
AREA				
mm ²	square millimeters	0.0016	square inches	in ²
m ²	square meters	10.764	square feet	ft ²
m ²	square meters	1.195	square yards	yd ²
ha	hectares	2.47	acres	ac
km ²	square kilometers	0.386	square miles	mi ²
VOLUME				
mL	milliliters	0.034	fluid ounces	fl oz
L	liters	0.264	gallons	gal
m ³	cubic meters	35.314	cubic feet	ft ³
m ³	cubic meters	1.307	cubic yards	yd ³
MASS				
g	grams	0.035	ounces	oz
kg	kilograms	2.202	pounds	lb
Mg (or "t")	megagrams (or "metric ton")	1.103	short tons (2000 lb)	T
TEMPERATURE (exact degrees)				
°C	Celsius	1.8C+32	Fahrenheit	°F
ILLUMINATION				
lx	lux	0.0929	foot-candles	fc
cd/m ²	candela/m ²	0.2919	foot-Lamberts	fl
FORCE and PRESSURE or STRESS				
N	newtons	0.225	poundforce	lbf
kPa	kilopascals	0.145	poundforce per square inch	lbf/in ²

TABLE OF CONTENTS

	Page
EXECUTIVE SUMMARY	1
REPORT ORGANIZATION.....	3
CHAPTER 1.0. INTRODUCTION.....	5
CHAPTER 2.0. LOCATION AND GEOLOGICAL BACKGROUND	7
CHAPTER 3.0. GEOPHYSICAL METHODS FOR MAPPING VOIDS.....	9
3.1 Electrical Resistivity.....	9
3.1.1 General Background and Data Acquisition	9
3.1.2 Advantages for Mapping Subsurface Voids	11
3.1.3 Limitations for Mapping Subsurface Voids.....	11
3.1.4 Case Studies for Mapping Subsurface Voids.....	12
3.1.5 Application of the Electrical Resistivity at LBNM.....	12
3.2 Ground Penetrating Radar	13
3.2.1 General Background and Data Acquisition	13
3.2.2 Advantages for Mapping Subsurface Voids	14
3.2.3 Limitations for Mapping Subsurface Voids.....	15
3.2.4 Case Studies for Mapping Subsurface Voids.....	15
3.2.5 Application of the GPR Method at LBNM.....	16
3.3 Magnetic Method.....	16
3.3.1 General Background and Data Acquisition	16
3.3.2 Advantages for Mapping Subsurface Voids	17
3.3.3 Limitations for Mapping Subsurface Voids.....	17
3.3.4 Case Studies for Mapping Subsurface Voids.....	17
3.3.5 Application of the Magnetic Method at LBNM	17
3.4 Electrical Conductivity	18
3.4.1 General Background and Data Acquisition	18
3.4.2 Advantages for Mapping Subsurface Voids	18
3.4.3 Limitations for Mapping Subsurface Voids.....	18
3.4.4 Case Studies for Mapping Subsurface Voids.....	19
3.4.5 Application of the Conductivity Method at LBNM.....	19
3.5 Seismic Refraction.....	19
3.5.1 General Background and Data Acquisition	19
3.5.2 Advantages for Mapping Subsurface Voids	21
3.5.3 Limitations for Mapping Subsurface Voids.....	21
3.5.4 Case Studies for Mapping Subsurface Voids.....	21
3.5.5 Application of Seismic Refraction at LBNM	22
3.6 Seismic Reflection.....	22
3.6.1 General Background and Data Acquisition	22
3.6.2 Advantages for Mapping Subsurface Voids	22
3.6.3 Limitations for Mapping Subsurface Voids.....	22
3.6.4 Case Studies for Mapping Subsurface Voids.....	24

3.6.5 Application of the Seismic Reflection Method at LBNM	24
3.7 Gravity Method.....	24
3.7.1 General Background and Data Acquisition	24
3.7.2 Advantages for Mapping Subsurface Voids	26
3.7.3 Limitations for Mapping Subsurface Voids.....	26
3.7.4 Case Studies for Mapping Subsurface Voids.....	26
3.7.5 Application of the Gravity Method at LBNM	26
CHAPTER 4.0. GEOPHYSICAL MAPPING OF VOIDS AT LBNM.....	27
4.1 General Information	27
4.2 Golden Dome Cave	30
4.2.1 Site Description.....	30
4.2.2 Data Analysis and Interpretation	31
4.2.3 Comparisons	39
4.3 Indian Well Cave	40
4.3.1 Site Description.....	40
4.3.2 Data Analysis and Interpretation	41
4.3.3 Comparisons	49
4.4 Monument Road Cave	50
4.4.1 Site Description.....	50
4.4.2 Data Analysis and Interpretation	52
4.4.3 Comparisons	60
4.5 Bearpaw Bridge	60
4.5.1 Site Description.....	60
4.5.2 Data Analysis and Interpretation	63
4.5.3 Comparisons	63
4.6 Hercules Leg Cave – Known and Unknown Sections.....	64
4.6.1 Site Description.....	64
4.6.2 Data Analysis and Interpretation	65
4.6.3 Comparisons	77
CHAPTER 5.0. DISCUSSION OF RESULTS.....	79
5.1 Survey Method Evaluation	81
CHAPTER 6.0. QUALITY ASSURANCE AND QUALITY CONTROL	85
CHAPTER 7.0. CONCLUSIONS AND RECOMMENDATIONS	87
7.1 Conclusion.....	87
7.2 Recommendations	87
CERTIFICATION AND DISCLAIMER	89
ACKNOWLEDGEMENT.....	91
REFERENCES.....	93
APPENDIX A - PHOTOGRAPHS FROM LBNM	95
APPENDIX B - SURVEY PARAMETERS	99

APPENDIX C - GPR CROSS SECTIONS.....102
APPENDIX D - HIGH RESOLUTION SHEAR WAVE CROSS SECTIONS123
APPENDIX E - ELECTRICAL RESISTIVITY CROSS SECTIONS.....125

LIST OF FIGURES

Figure 1. Map. Site Map of Lava Beds National Monument. ⁽⁴⁾	7
Figure 2. Drawing. Electrode array for measuring ground resistivities. ⁽⁷⁾	10
Figure 3. Cross Section. Data collected over a void plotted as a pseudosection. ⁽⁹⁾	11
Figure 4. Photo. Data collection with the OhmMapper.	13
Figure 5. Drawing. Ground Penetrating Radar system over a void. ⁽⁷⁾	14
Figure 6. Screen Capture. Ground Penetrating Radar data over interpreted voids. ⁽⁷⁾	14
Figure 7. Photo. GPR data collection with the 400 MHz antenna at LBNM.	16
Figure 8. Photo. Data collection with the Geometrics G-858 Magnetometer at LBNM.	18
Figure 9. Photo. Data collection with the EM31 at LBNM.	20
Figure 10. Drawing. Seismic refraction data across a fracture zone. ⁽⁵⁾	20
Figure 11. Drawing. Shear waves over an air/water-filled void. ⁽⁷⁾	23
Figure 12. Cross Section. Voids interpreted from shear wave seismic data. ⁽⁷⁾	23
Figure 13. Photo. Data collection with the MicroVibrator and the Land Streamer at LBNM. ...	25
Figure 14. Drawing. Gravity field over a void. ⁽⁷⁾	25
Figure 15. Map. Cave Loop Road site (survey locations outlined in red). ⁽⁶⁾	28
Figure 16. Photo. Land Streamer deployed above Golden Dome Cave.	31
Figure 17. Map. GPR survey lines over Golden Dome Cave. ⁽⁶⁾	32
Figure 18. Profile. GPR cross section collected over Golden Dome Cave.....	33
Figure 19. Map. Plan and profile view of magnetic data collected over Golden Dome Cave	35
Figure 20. Map. HRSW survey line over Golden Dome Cave. ⁽⁶⁾	37
Figure 21. Cross Section. HRSW data collected over Golden Dome Cave.	39
Figure 22. Map. Comparison of anomalous zones at Golden Dome Cave.....	40
Figure 23. Photo. The entrance of Indian Well Cave.	41
Figure 24. Map. GPR survey line over Indian Well Cave. ⁽⁶⁾	41
Figure 25. Cross Section. GPR data collected over Indian Well Cave.....	42
Figure 26. Map. Plan and profile view of magnetic data collected over Indian Well Cave.	44
Figure 27. Map. Electrical Resistivity survey line over Indian Well Cave. ⁽⁶⁾	46
Figure 28. Cross Section. Electrical Resistivity data collected over Indian Well Cave.	47
Figure 29. Map. HRSW survey line over Indian Well Cave. ⁽⁶⁾	48

Figure 30. Cross Section. HRSW data collected over Indian Well Cave.....	49
Figure 31. Map. Comparison of anomalous zones at Indian Well Cave.	51
Figure 32. Photo. Monument Road Cave.....	52
Figure 33. Map. GPR survey lines at Monument Road Cave. ⁽¹⁷⁾	53
Figure 34. Profile. GPR data collected along Line 3 at Monument Road Cave.	54
Figure 35. Map. Plan and profile view of magnetic data collected over Monument Road Cave.....	55
Figure 36. Map. Electrical resistivity survey line at Monument Road Cave. ⁽¹⁷⁾	56
Figure 37. Cross Section. Electrical resistivity data collected over Monument Road Cave.	57
Figure 38. Map. HRSW survey line at Monument Road Cave. ⁽¹⁷⁾	58
Figure 39. Cross Section. HRSW data collected over Monument Road Cave.....	59
Figure 40. Map. Comparison of anomalous zones at Monument Road Cave.	61
Figure 41. Map. Electrical resistivity survey line on Bearpaw Bridge. ⁽⁶⁾	62
Figure 42. Photo. Bearpaw Bridge.....	62
Figure 43. Cross Section. Electrical resistivity data collected on Bearpaw Bridge.....	63
Figure 44. Photo. Entrance at Hercules Leg Cave.....	64
Figure 45. Map. Plan view index map of Hercules Leg Cave. ⁽⁶⁾	65
Figure 46. Map. GPR survey line over Hercules Leg Cave. ⁽⁶⁾	66
Figure 47. Cross Section. GPR data over the known section of Hercules Leg Cave.	67
Figure 48. Cross Section. GPR data over the unknown section of Hercules Leg Cave.	68
Figure 49. Map. Magnetic data collected over the known section of Hercules Leg Cave.	69
Figure 50. Map. Magnetic data collected over the unknown section of Hercules Leg Cave.	70
Figure 51. Drawing. Electrical resistivity survey line over Hercules Leg Cave. ⁽⁶⁾	71
Figure 52. Cross Section. Electrical resistivity data collected over Hercules Leg Cave.....	72
Figure 53. Map. Electrical conductivity data collected over Hercules Leg Cave.....	74
Figure 54. Map. HRSW survey line over Hercules Leg Cave. ⁽⁶⁾	75
Figure 55. Cross Section. HRSW data collected over Hercules Leg Cave.....	76
Figure 56. Map. Comparison of anomalous zones over Hercules Leg Cave.....	78
Figure 57. Photos. Site conditions.	95
Figure 58. Photos. Site conditions.	96
Figure 59. Photos. Site conditions.	97

Figure 60. Photos. Site conditions.....	98
Figure 61. Cross Section. GPR data.....	102
Figure 62. Cross Section. GPR data.....	103
Figure 63. Cross Section. GPR data.....	104
Figure 64. Cross Section. GPR data.....	104
Figure 65. Cross Section. GPR data.....	105
Figure 66. Cross Section. GPR data.....	106
Figure 67. Cross Section. GPR data.....	106
Figure 68. Cross Section. GPR data.....	107
Figure 69. Cross Section. GPR data.....	108
Figure 70. Cross Section. GPR data.....	108
Figure 71. Cross Section. GPR data.....	109
Figure 72. Cross Section. GPR data.....	109
Figure 73. Cross Section. GPR data.....	110
Figure 74. Cross Section. GPR data.....	110
Figure 75. Cross Section. GPR data.....	111
Figure 76. Cross Section. GPR data.....	111
Figure 77. Cross Section. GPR data.....	112
Figure 78. Cross Section. GPR data.....	112
Figure 79. Cross Section. GPR data.....	113
Figure 80. Cross Section. GPR data.....	113
Figure 81. Cross Section. GPR data.....	114
Figure 82. Cross Section. GPR data.....	114
Figure 83. Cross Section. GPR data.....	115
Figure 84. Cross Section. GPR data.....	115
Figure 85. Cross Section. GPR data.....	116
Figure 86. Cross Section. GPR data.....	116
Figure 87. Cross Section. GPR data.....	117
Figure 88. Cross Section. GPR data.....	117
Figure 89. Cross Section. GPR data.....	118

Figure 90. Cross Section. GPR data.....	118
Figure 91. Cross Section. GPR data.....	119
Figure 92. Cross Section. GPR data.....	119
Figure 93. Cross Section. GPR data.....	120
Figure 94. Cross Section. GPR data.....	120
Figure 95. Cross Section. GPR data.....	121
Figure 96. Cross Section. GPR data.....	121
Figure 97. Cross Section. GPR data.....	122
Figure 98. Cross Section. Uninterpreted HRSW data.....	123
Figure 99. Cross Section. Uninterpreted HRSW data.....	123
Figure 100. Cross Section. Uninterpreted HRSW data.....	124
Figure 101. Cross Section. Uninterpreted HRSW data.....	124
Figure 102. Cross Section. Electrical Resistivity Vertical 2-D.	125
Figure 103. Cross Section. Electrical Resistivity Vertical 2-D.	126
Figure 104. Cross Section. Electrical Resistivity Vertical 2-D.	127
Figure 105. Cross Section. Electrical Resistivity Vertical 2-D.	127
Figure 106. Cross Section. Electrical Resistivity Vertical 2-D.	128
Figure 107. Cross Section. Electrical Resistivity Vertical 2-D.	129
Figure 108. Cross Section. Electrical Resistivity Vertical 2-D.	130
Figure 109. Cross Section. Electrical Resistivity Vertical 2-D.	131
Figure 110. Cross Section. Electrical Resistivity Interpretation.....	132
Figure 111. Cross Section. Electrical Resistivity Interpretation.....	132
Figure 112. Cross Section. Electrical Resistivity Comparison.....	133
Figure 113. Cross Section. Electrical Resistivity Interpretation.....	133
Figure 114. Cross Section. Electrical Resistivity Interpretation.....	134
Figure 115. Cross Section. Electrical Resistivity Comparison.....	134
Figure 116. Cross Section. Electrical Resistivity Interpretation.....	135
Figure 117. Cross Section. Electrical Resistivity Interpretation.....	135
Figure 118. Cross Section. Electrical Resistivity Comparison.....	136
Figure 119. Cross Section. Electrical Resistivity Interpretation.....	136

Figure 120. Cross Section. Electrical Resistivity Interpretation.....137
Figure 121. Cross Section. Electrical Resistivity Comparison.....137

LIST OF TABLES

Table 1. Geophysical methods used for mapping subsurface voids at LBNM.....28
Table 2. DGPS base station coordinates.....29
Table 3. Cave parameters determined through surveying.30
Table 4. GPR survey line coordinates over Golden Dome Cave.....33
Table 5. Geophone coordinate locations at Golden Dome Cave.38
Table 6. GPR survey line coordinates over Indian Well Cave.42
Table 7. Electrical resistivity survey line coordinates over Indian Well Cave.....46
Table 8. Geophone coordinate locations over Indian Well Cave.48
Table 9. GPR survey line coordinates over Monument Road Cave.53
Table 10. Electrical resistivity line survey coordinates over Monument Road Cave.....56
Table 11. Geophone coordinate locations over Monument Road Cave.59
Table 12. GPR survey line coordinates over Hercules Leg Cave.....66
Table 13. Electrical resistivity survey line coordinates over Hercules Leg Cave.71
Table 14. Geophone coordinate locations over Hercules Leg Cave.....75
Table 15. Reference guide of the final results from the geophysical surveys at LBNM.....82
Table 16. Geophysical survey methods’ capabilities, production rates, and cost effectiveness for
lava tube detection.83
Table 17. GPR survey parameters.99
Table 18. Geometrics OhmMapper TR2 array parameters.....100
Table 19. High Resolution Shear Wave reflection survey parameters.101

EXECUTIVE SUMMARY

The purpose of this report is to provide information on geophysical techniques to detect the presence of shallow-subsurface voids where road projects are planned. Determining subsurface conditions for road projects will significantly reduce the risk to roadway construction activities, provide improved long-term stability and maintenance of the roadway, and improve public safety. Identifying these voids will potentially preserve them from damage. It will also provide planners with information on corridor alignment to mitigate impacts.

In order to accurately and economically locate near-surface voids that may affect roadway stability, the FHWA-CFLHD in coordination with Blackhawk investigated a variety of geophysical techniques at Lava Beds National Monument (LBNM) in northern California. The main objectives were to: (a) detect the presence of subsurface voids under specific geologic settings, (b) detect and characterize the vertical/horizontal extent of the voids, (c) determine the most economical and efficient (time effective) geophysical method(s) to use during roadway site investigations, and (d) identify the range of applications of such methods nationwide.

Geophysical techniques were chosen for near-surface void detection because they are non-intrusive and cost- and time-effective methods. In general, their accuracy and resolution depend on the depth of investigation and geological factors (for most geophysical methods, resolution decreases as depth increases).

The LBNM area was chosen as the site for these investigations for the following reasons: (a) the existence of many well-mapped caves that vary both in size and depth beneath the ground surface and (b) future roadwork is planned in LBNM and the results may be beneficial to this work.

Geophysical data were collected at the site using Ground Penetrating Radar (GPR), Magnetics, High Resolution Shear Wave Seismic Reflection (HRSW), Electrical Resistivity (ER), and Electrical Conductivity methods. Each site has known underground void geometries and locations. This information was used to assess the accuracy of each applied geophysical method for void detection at LBNM.

The results of the investigation indicated that some of the geophysical methods were effective in detecting voids, while other methods were limited due to the localized geological setting and void geometries. Depending on site conditions, such as subsurface geology or void size and depth, when a combination of methods were used, there was a greater chance of effectively delineating the location and orientation of the voids. The combined GPR and magnetic methods were the most economical and least time consuming for detecting voids whose depths range between 0 to 9 m (0 to 30 ft). Magnetic surveys should be performed first as a reconnaissance tool in order to locate the position of magnetic anomalies that may indicate the presence of potential voids. A focused GPR survey would then be conducted to evaluate each magnetic anomaly and to determine the depth and lateral extent of the features.

This study includes information about the site geology, survey site descriptions, overview of the geophysical methods used, data acquisition parameters, and interpretations. The results of this study will be of interest to federal land managers who protect these types of features, highway designers, maintenance crews, geotechnical engineers, owners of roads constructed over old mine works, and utility crews; in general, whoever is interested in locating voids beneath roadways.

REPORT ORGANIZATION

The Executive Summary provides a summary of the geophysical study, results, and recommendations.

Chapter 1 provides a brief background on engineering problems related to the presence of voids beneath roadways and the geophysical methods used during the study.

Chapter 2 outlines the regional location of the LBNM area and its geological background. The geological setting of investigative area is important when planning a geophysical survey.

Chapter 3 describes the geophysical methods/techniques available to meet the study's objectives. Five geophysical methods were used at the LBNM site. The general background of the methods, data acquisition, advantages and limitations for mapping subsurface voids, and case studies for mapping subsurface voids are discussed.

Chapter 4 details the geophysical surveys at LBNM. This chapter includes individual site descriptions, data analysis and interpretation, and comparisons of each method used at each site.

Chapter 5 lists the results from the geophysical surveys at LBNM.

Chapter 6 details the Quality Assurance and Quality Control activities performed in order to provide quality products and services.

Chapter 7 states the conclusions and recommendations derived from this report.

The certification and disclaimer, the acknowledgement, and references are listed at the end of the text.

Appendix A contains photographs from LBNM.

Appendix B lists survey parameters used at LBNM.

Appendix C contains GPR cross sections from the data collected at LBNM.

Appendix D contains electrical resistivity cross sections from the data collected at LBNM.

Appendix E contains high resolution shear wave cross sections from the data collected at LBNM.

CHAPTER 1.0. INTRODUCTION

Lava tubes are used by many people for recreational purposes such as spelunking or cave exploration. Scientists use lava tubes for research of lava flow mechanisms and evolution. In the past, lava tubes have been used for dwellings and burial sites. On the other hand, lava tubes may pose a threat to roadway construction activities, long-term road stability, road maintenance, and public safety. Therefore, locating and imaging subsurface lava tubes will reduce a risk of collapse of roadways and improve lava tube preservation.

This study describes the procedures and results of recent surface geophysical surveys performed at the Lava Beds National Monument (LBNM) located in Siskiyou County, California over several known lava tubes. The main objective of this comprehensive geophysical program was to determine the most effective geophysical imaging technology for delineating voids that may pose a threat to road construction and heavy equipment working above them.

To address the requirements of this study, the Central Federal Lands Highway Division (CFLHD), Federal Highway Administration (FHWA) in coordination with Blackhawk investigated a variety of geophysical techniques at LBNM. Data were collected using Ground Penetrating Radar (GPR), Magnetics, High Resolution Shear Wave Seismic Reflection (HRSW), Electrical Resistivity and Electrical Conductivity methods.

The results of this program will support a planned road reconstruction effort in LBNM and in Hawaii as well as to support FHWA's more comprehensive initiatives concerning void detection.

CHAPTER 2.0. LOCATION AND GEOLOGICAL BACKGROUND

LBNM was established in 1925 with assistance from cave enthusiast J.D. Howard. Much of the park was developed through the hard work of the Civilian Conservation Corps ⁽¹⁾. “As part of the National Park System, Lava Bed’s mandate includes the protection and preservation of natural and cultural resources. This mandate is derived from the National Park Services Organic Act of 1916 which outlines the fundamental purposes of the National Park System ⁽²⁾.”

Previously, adventurers used the area unimpeded, leading to unnatural damage of many exhibit areas. The goal of this study is to apply non-destructive and non-invasive geophysical methods for locating lava tubes and to continue the preservation of these protected unique geological features.

The LBNM area contains several hundred known lava tubes from over 30 separate flows making it the largest concentration of lava tubes in the continental United States ⁽³⁾. LBNM resides within the extensive flood basalts of the Modoc Plateau in northern California. The area is bounded by the Cascade Mountain Range, which contains extensive dormant volcanoes, to the west and the northern extremes of the Sierra Nevada to the south. This broad volcanic plateau extends northward across Oregon, and fades eastward into the Basin and Range of northern Nevada (Figure 1).

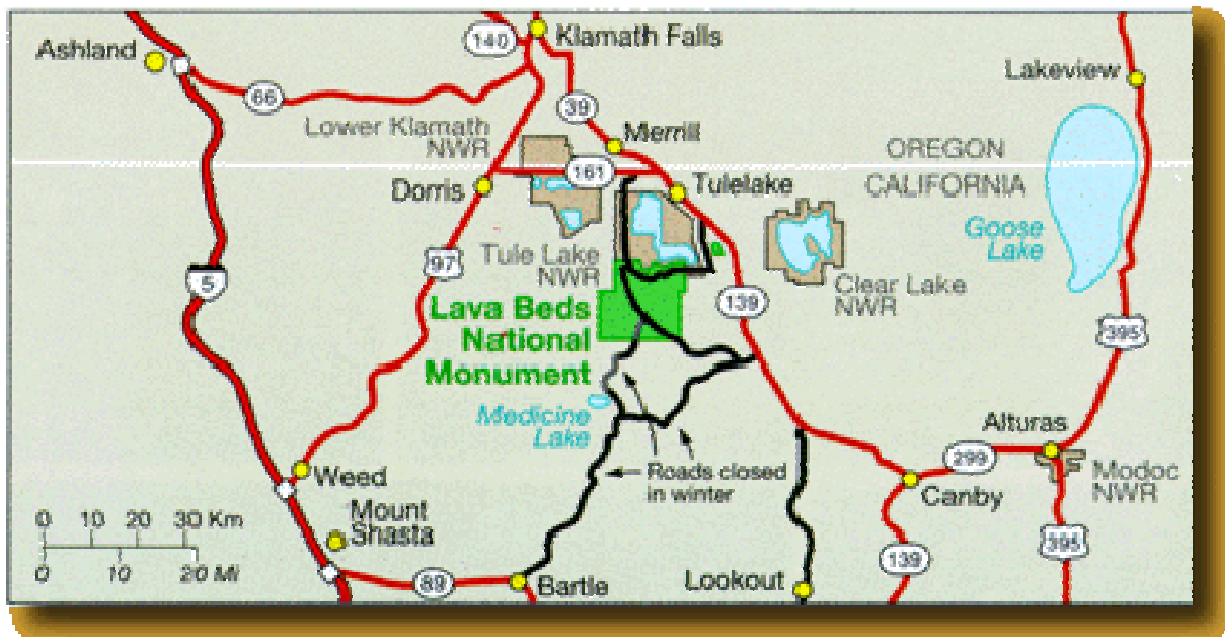


Figure 1. Map. Site Map of Lava Beds National Monument. ⁽⁴⁾

The flood basalts of the Modoc Plateau, covering hundreds of square miles, are among the youngest of the immense flows occurring globally in the past 250 million years. Locally, LBNM is located on the northeast side of Medicine Lake Volcano, an enormous shield volcano that

initially erupted nearly two million years ago, with at least six different eruptions from four distinct events occurring in the last 2,000 years ⁽⁵⁾.

Basically, there are two different types of lava tubes in LBNM. First, “surface tubes” are created when the top and sides of the lava flow cool due to their exposure to the air. This cooled lava solidifies creating a hard cast surrounding the flowing lava, which may then be covered by subsequent flows. Generally, surface tubes that are only a few meters in diameter are abundant at the LBNM. The second type of lava tube is formed when lava flows down a pre-existing channel, such as riverbed or a depression. The roof of the lava, being exposed to air, cools and hardens forming the eventual tube roof. Such tubes can be quite large, with some at LBNM exceeding 15 m (50 ft) in diameter. In both cases, the lava tube eventually drains to become a subsurface void, filled with air, water, or collapsed overburden. It is also common for tubes to be stacked on top of each other, often connected by intervening “skylights” ⁽⁶⁾.

Geophysical surveys were conducted in the vicinity of Cave Loop Road in the southern end of LBNM at three locations: Indian Well Cave, Golden Dome Cave, and Hercules Leg. Two other locations, Merrill Cave, approximately 3 km (1.86 mi) northwest of the Visitor’s Center, and Monument Road Cave along Hill Road near Devil’s Homestead Flow were also investigated.

CHAPTER 3.0. GEOPHYSICAL METHODS FOR MAPPING VOIDS

A variety of geophysical techniques exist with the capability of locating near-surface voids. Each method has limitations in depth of exploration and resolution depending on the geological settings, target (void) size and orientation.

The general background of the methods, data acquisition, and the capabilities of these methods for mapping near-surface voids are based on the results of previous work and will be explained in more detail later in this report. The capabilities of the proposed methods for mapping near-surface voids within the particular geological settings at LBNM will also be addressed.

The geophysical methods described in this Chapter include:

- Electrical Resistivity.
- Ground Penetrating Radar.
- Magnetic Method.
- Electrical Conductivity.
- Seismic Refraction.
- Seismic Reflection.
- Gravity Method.

However, only the following geophysical methods were used at LBNM:

- Electrical Resistivity.
- Ground Penetrating Radar.
- Magnetic Method.
- Electrical Conductivity.
- Seismic Reflection.

The seismic refraction method was not selected because no specific refractors are expected to occur at the depth of interest. The gravity method, although potentially useful for locating voids, is slow and therefore expensive in the field, since great care has to be taken with each reading and all of the stations need accurate elevation control. In addition, significant processing may be required to account for all of the factors that can influence the gravity readings.

3.1 ELECTRICAL RESISTIVITY

3.1.1 General Background and Data Acquisition

Electrical Resistivity methods measure the apparent resistivity of the subsurface. Apparent resistivity is the term used for the field measurements since, without interpretation, the resistivity measurement does not refer to any particular geologic layer. Graphs of apparent resistivity against electrode separation are used to model the subsurface, thereby providing the vertical distribution layer thicknesses, depths and resistivities. The electrical resistivity equipment

consists of a transmitter and a receiver along with the electrodes and wires. The transmitter passes low frequency square wave current into the ground using two electrodes inserted into the ground. The receiver measures the resulting voltage using two different electrodes. The measured apparent resistivity of the ground is found by dividing the measured voltage by the amount of current injected into the ground and multiplying this by a geometric factor that is derived from the geometry of the electrode array. The depth of investigation is a function of the array type and the electrode spacing. As the distance increases between the current and the potential electrodes, the depth of investigation increases. Figure 2 shows an electrode array with electrical current flow lines.

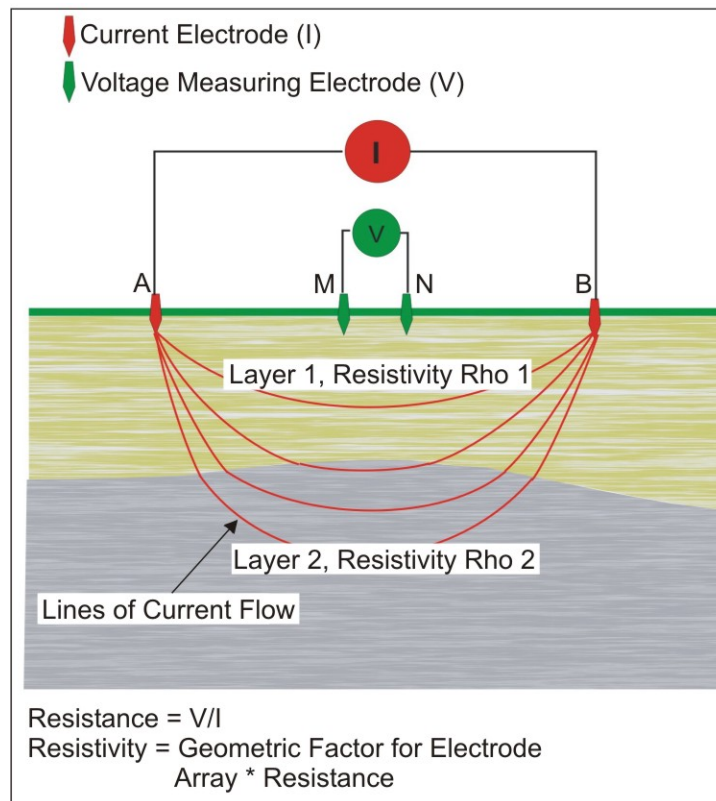


Figure 2. Drawing. Electrode array for measuring ground resistivities. ⁽⁷⁾

There are basically two different types of electrical resistivity methods: the profile, or traverse, method and the sounding method. In electrical profiling, where the electrode separation is fixed, information concerning lateral variations in resistivity is obtained. In the electrical sounding method, the center of the electrode spread is maintained at a fixed location and the electrode spacing is gradually increased. Sounding arrays provide information about the subsurface at increasing depths; however, they give limited information about lateral changes. Electrical soundings and profiles (traverses) are now often combined for relatively shallow surveys. In these cases, a series of electrodes are positioned at regular intervals and all connected to the transmitter and receiver using cables. Using an automated switching mechanism, the transmitter and receiver collect data using the positioned electrodes by automatically selecting the

appropriate electrodes. This procedure is repeated for different electrode sets until the whole line has been recorded.

The common unit for electrical resistivity is ohm-m.

3.1.2 Advantages for Mapping Subsurface Voids

Resistivity methods have been successful in locating voids providing there is a resistivity contrast between the void and the surrounding host rock. Water filled voids, depending on salt content and acidity, have a resistivity range between 40 and 500 ohm-m⁽⁸⁾, whereas air filled voids are considered infinitely resistive. Figure 3 is an example of a geoelectric cross-section showing an air filled void.

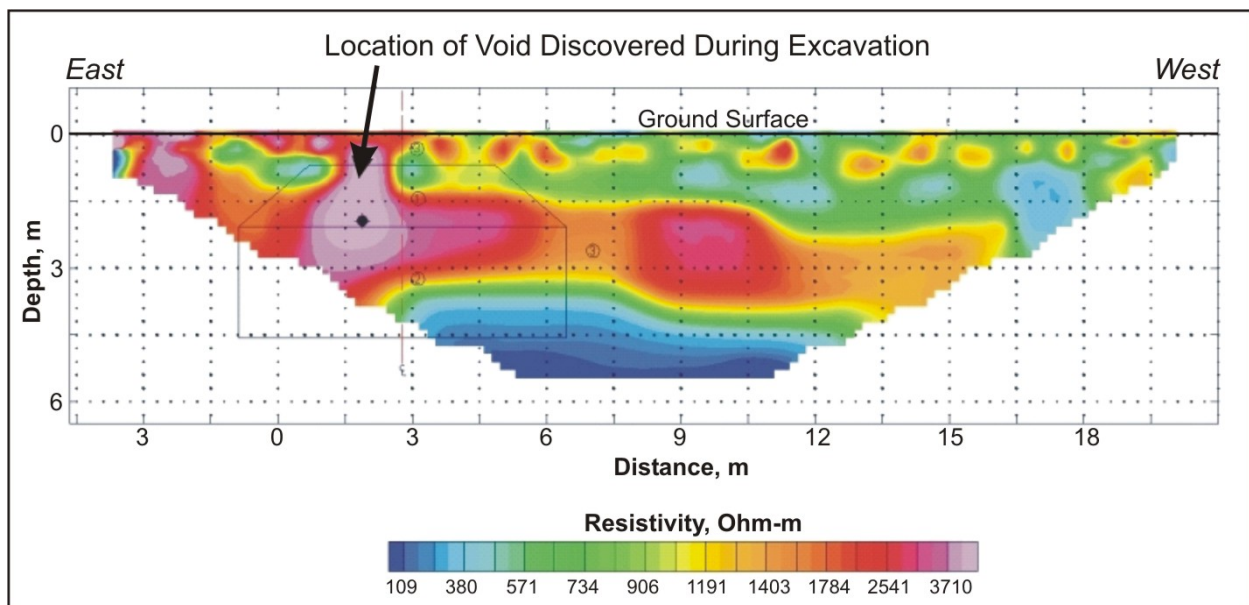


Figure 3. Cross Section. Data collected over a void plotted as a pseudosection.⁽⁹⁾

3.1.3 Limitations for Mapping Subsurface Voids

Electrical resistivity methods are usually quite labor intensive and time consuming in the field, especially in areas of hard rock where electrodes may need to be pounded into the ground. Also, it is often difficult to lower the contact resistance, or the ability for current to pass from the electrode into the subsurface, in resistive ground. Advances in technology have generated electrodes that inject current into the ground using capacitive methods and arrays have been developed that are towed along the ground by a single operator. However, these are only effective in resistive conditions and at fairly shallow depths. Finally, if a lava tube is filled with water, data interpretation searching for voids may be difficult because the difference between the resistivity of the host rock and that of the water-filled void may not vary enough to generate an interpretable anomaly.

3.1.4 Case Studies for Mapping Subsurface Voids

Electrical resistivity has been used to identify voids in several cases. “In eastern Ohio, subsidence features were identified on Interstate 70” (9). It was determined that they were caused by collapsed mines found beneath the highways. Since the mines were not adequately mapped and drilling was a costly investigative tool, it was imperative to know if a geophysical method was capable of locating potential collapse zones. The resulting research was a joint effort between the Wright State University and the Ohio Department of Transportation and is summarized in a report titled *Identifying Potential Collapse Features Under Highways* (9).

In phase I, several geophysical methods were applied over an area with known subsidence to determine the method, or combination of methods, that would be most viable at detecting subsurface cavities. At the Jackson County, Ohio site in phase I, electrical resistivity data were collected using a dipole-dipole electrode array with Advanced GeoSciences, Inc. (AGI) Sting/Swift R1 resistivity meter to locate voids in a coal seam that was located 1.5 to 6.1 m (4.9 to 20.0 ft) below the subsurface. Data were collected on both the north and south sides of the road. Data from the north side of the road was recorded using an electrode spacing of 1.5 m (4.9 ft) whereas that along the south side of the road had an electrode spacing of 3 m. The resistivity data were modeled with RES2DINV software written by Geotomo Software. From ground truth information, it was discovered that areas of low resistivity (0.6 to 5.5 ohm-m) corresponded well with voids. This information suggested that the voids were saturated with electrically conductive moisture. After extensive excavations were performed on the area, it was determined that the resistivity data accurately mapped the voids (Figure 3).

Electrical resistivity was also used in the Pellissippi Parkway Study, showcased on the AGI website (10). After numerous “cave-ins” occurred near a highway, a dipole-dipole electrical resistivity survey was conducted to determine if there were other voids that could lead to future cave-ins. The Sting/Swift system was utilized for data collection. The survey line consisted of 56 electrodes with 3 m (9.8 ft) electrode spacing and was established parallel to the highway. The data were interpreted using the RES2DINV program. The results showed two air filled voids with high resistivity values (over 20,000 ohm-m) and one void filled with water or mud with a resistivity value less than 200 ohm-m. The voids were located between 5 and 20 m (16.4 and 65.6 ft) below the subsurface.

3.1.5 Application of the Electrical Resistivity at LBNM

The resistive nature of the basalt that comprises much of the subsurface at LBNM provides an ideal setting for using the capacitive electrode system mentioned previously in this report. Since electrical resistivity methods have proven successful in detecting voids, a Geometrics OhmMapper TR2 system was used to detect lava tubes at LBNM. The OhmMapper is pictured in Figure 4. The OhmMapper is a capacitively-coupled resistivity meter that measures the electrical resistivity of the ground without grounded electrodes. It is a towed, non-invasive instrument that is both quick to deploy and easy to use under the right survey conditions. The electrodes are configured in a dipole-dipole array, which allows for good lateral resolution at different depths.



Figure 4. Photo. Data collection with the OhmMapper.

3.2 GROUND PENETRATING RADAR

3.2.1 General Background and Data Acquisition

Ground Penetrating Radar (GPR) is a non-invasive geophysical method that uses electromagnetic waves to map boundaries between lithologies or objects that have different electrical properties. As the GPR system is towed along a surface, pulses of electromagnetic energy penetrate the subsurface. A fraction of the wave is reflected back to the surface when it encounters a boundary where there is a change in electrical properties (commonly referred to as relative dielectric constant). The relative dielectric constant of a material is the ratio of the permittivity of that material to the permittivity of free space. A receiver records the reflected waves.

A variety of frequencies are used depending on the survey target and geologic setting. Higher frequencies are able to provide more detail of the subsurface structure; however, high frequency signals attenuate rapidly as they propagate into the subsurface, thus limiting the depth of exploration. Lower frequencies provide less resolution but are capable of obtaining information to greater depths. A schematic showing a GPR system, and associated waves, over a void is

shown in Figure 5. Figure 6 shows a GPR cross section where two voids have been interpreted to exist in the subsurface.

3.2.2 Advantages for Mapping Subsurface Voids

GPR is advantageous for mapping relatively shallow subsurface voids. This method can provide good depth estimates if the dielectric constant is known, along with the lateral extent of subsurface features.

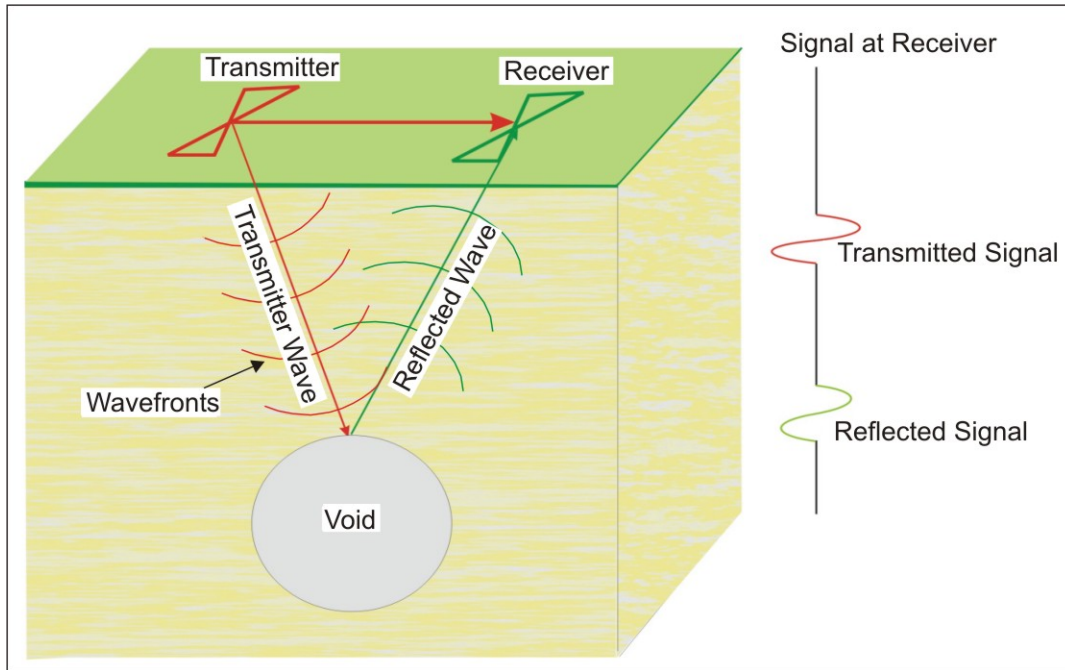


Figure 5. Drawing. Ground Penetrating Radar system over a void. ⁽⁷⁾

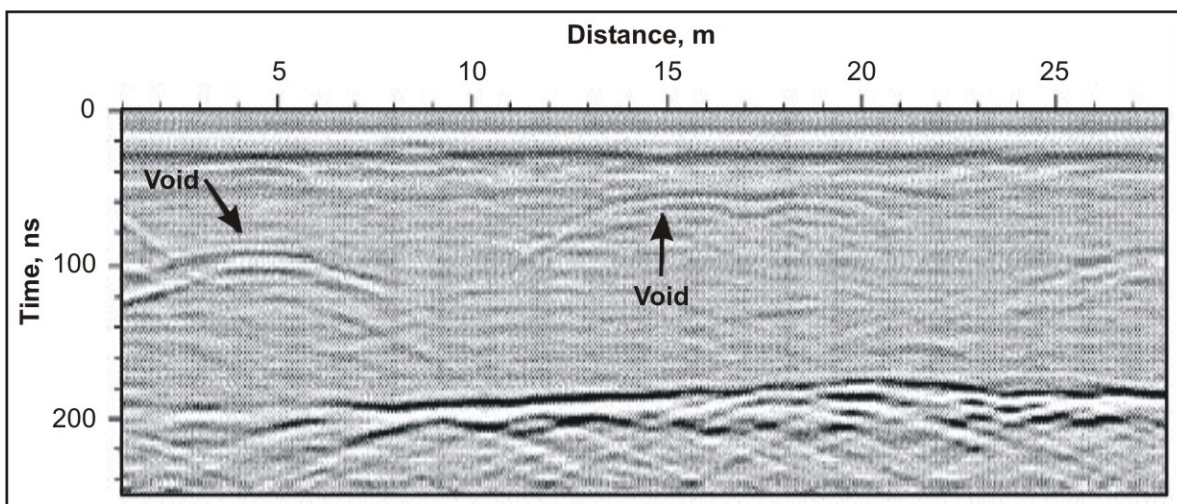


Figure 6. Screen Capture. Ground Penetrating Radar data over interpreted voids. ⁽⁷⁾

3.2.3 Limitations for Mapping Subsurface Voids

Many factors limit the success of GPR during field surveys with local geology playing a significant role. Electromagnetic waves attenuate rapidly in soils that are electrically conductive (i.e. high in clay content or saline conditions), making GPR an ineffective method in these areas when the target lies within or below clay layers. If saline conditions occur, thus making the subsurface electrically conductive, then penetration depths will be severely limited. If the dielectric constant between the layers is similar, insufficient energy may be reflected at the boundary and the receiver will not detect the boundary change. Cultural noise such as radio towers, power lines, and cellular phones may also lower the quality of data.

3.2.4 Case Studies for Mapping Subsurface Voids

The use of GPR to locate lava tubes has already occurred worldwide. In a case study titled *Ground Penetrating Radar to detect lava tubes: preliminary results of a GPR application to Fuji volcano, Japan (11)*, a GPR survey was conducted over a paved road that bisects a well mapped lava tube, the Komoriana cave in the Aokigahara flow. The subsurface consisted of a basaltic lava flow. A Subsurface Interface Radar (SIR) 2 was utilized in the survey coupled with a 200 MHz antenna produced by Geophysical Survey Systems, Inc (GSSI). One two-dimensional profile was collected approximately perpendicular to the cave orientation. The raw data showed two distinct anomalies in the data that were interpreted to be the top and the bottom of the cave. The report did not list the extent, depth, and size of the cave. The preliminary results, however, suggests that GPR is an effective method in locating lava tubes.

Hot and Cold Lava Tube Characterization with Ground Penetrating Radar (12) is an additional study involving lava tube detection performed by the Department of Geophysics, Colorado School of Mines. The study was conducted on the island of Hawaii in Hawaii Volcanoes National Park. Two types of GPR equipment were utilized during this survey: the Sensors and Software PulseEKKO 1000 and the GSSI SIR-8 radar systems. The data were processed and modeled using GRORADAR and custom software written by M. Lagmanson. The results from two locations were discussed in the paper.

The first location was the south side of the Kilauea volcano over an active lava tube in a shatter ring. Data were collected at multiple frequencies with both systems, with the purpose of locating structural defects around the lava tubes. It was determined that GPR could detect, but not characterize, the hot lava tubes due to the fact that "...molten lava is conductive and makes the surrounding material highly lossy (producing an attenuation shadow in the image). There is not a clear image from a hot tube as the temperature gradient produces a gradual dielectric contrast gradient."

The second site was located south of the Mauna Ulu crater near Chain of Craters Road. The surveys were conducted over cold lava tubes. Data were collected over an area with two known lava tubes. The first time the data were collected, the ground was dry and the tubes were not located. After a night of rain, the data were recollected and the lava tubes were easily identified because the lava tubes were draining water, which has a high dielectric contrast with basalt.

In general, lava tubes as deep as 6 m (19.7 ft) were interpreted in the data. In addition to the 2 known tubes, many lava tubes less than 1.5 m (4.9 ft) in diameter and less than 0.4 m (1.3 ft) in depth were located. Although not presented in the referenced paper, processing and modeling successfully derived the size, shape and orientation of the lava tubes.

3.2.5 Application of the GPR Method at LBNM

Based on the previous successes of GPR applications, the GPR method was selected as one of the methods to be tested at LBNM. The GSSI SIR-2000 instrument was selected along with the 100 MHz, 200MHz, and 400 MHz antennas. A photograph of the 400 MHz antenna and the 100 MHz antenna (shown in the background) utilized during the LBNM survey is illustrated in Figure 7.



Figure 7. Photo. GPR data collection with the 400 MHz antenna at LBNM.

3.3 MAGNETIC METHOD

3.3.1 General Background and Data Acquisition

Measurements of the natural magnetic field strength can be used to interpret the subsurface distribution of magnetic minerals, usually magnetite. If a lava tube occurs near the ground surface, it may be detected using the magnetic method because it provides a region in the subsurface where no magnetic minerals are present. If the host rocks contain magnetite, then the lava tube may create an anomaly that can be measured by a magnetometer on the ground surface.

The Earth's magnetic field is often thought of as similar to that which would result from a large magnet placed in the interior of the Earth. The magnetic north pole is close to, but not coincident with, the geographic North Pole. Thus, the lines of force due to the Earth's magnetic field can be thought of as emanating from the magnetic South Pole and "returning" to the magnetic North

Pole. This field is a vector and has a direction and a magnitude. The field is thought to result from large-scale movements of magma within the earth. Superimposed on top of this field are time varying pulsations caused by the movement of electrical charges at distances of many km above the earth. One of the causes of these charge movements is sun spot activity. These time varying fields have a wide range of periods (or frequencies) varying from fractions of a second to hours. Generally, however, the amplitude of these variations has a daily cycle, and they are therefore called Diurnal variations. During magnetic surveys, the Diurnal variations in the magnetic field are accounted for by having a base station collect data at a fixed location as the survey progresses. During processing, the Diurnal variations are removed from the survey data.

When the Earth's magnetic field interacts with magnetic mineral in a rock, a "secondary" magnetic field is created. It is these secondary magnetic fields that give rise to anomalies that can be detected with a magnetometer.

3.3.2 Advantages for Mapping Subsurface Voids

The magnetic method was successful at detecting the presence of lava tubes. The field data acquisition is rapid and therefore large areas can be efficiently surveyed, thus making it a good reconnaissance method. Although magnetic anomalies are seen over most of the known lava tubes, their shapes are complex. However, detailed computer modeling may be used to obtain more information about the lava tube, such as the depth to its top and possibly its dimensions.

3.3.3 Limitations for Mapping Subsurface Voids

The complexity of the geologic setting of most lava tubes makes anomaly prediction and interpretation difficult. The basalt surrounding the lava tube is often comprised of lava from different flows, cooling over different periods of time and at different rates. Thus, the magnetic properties of the basalt could vary greatly from flow to flow, causing the magnetic properties of the basalt to vary greatly. Interpretation of magnetic data can be ambiguous, in that several different geologic and dimensional models can be constructed, each of which may produce a similar anomaly. Therefore, magnetic data interpretation is usually verified with the results from other geophysical methods.

3.3.4 Case Studies for Mapping Subsurface Voids

No publicly published work related to the detection of lava tubes exists for review.

3.3.5 Application of the Magnetic Method at LBNM

Although magnetic methods were not initially proposed for this project, the Geometrics G-858 cesium-vapor magnetometer system was tested at LBNM. This instrument is carried manually, with the magnetometer strapped to a harness worn around the shoulders and the control panel worn around the waist of the operator. Data were collected at walking speed, with sensor positioning accomplished with a Differential Global Positioning System (DGPS) unit also worn by the operator. Figure 8 is a photograph of the magnetometer system and DGPS system in use at LBNM.

3.4 ELECTRICAL CONDUCTIVITY

3.4.1 General Background and Data Acquisition

Electrical conductivity is the ability of a material to transport electrical charge. Conductivity is the inverse of resistivity, although some geophysical instruments are designed to specifically measure conductivity, rather than resistivity. The conductivity, or resistivity, of rocks spans a wide range, and depends significantly on the degree of rock pore saturation and the conductivity of the saturating fluids. There are various types of instruments that measure the bulk conductivity of the subsurface down to a particular depth, depending on the instrument and its mode of use. In the case of lava tubes, the air within a lava tube will have a very low electrical conductivity. The conductivity of the surrounding lava will depend on the fluids, if any, within the pore spaces of the lava. If the pore spaces are filled with air then the lava will have a low conductivity, although probably not as low as that of air.



Figure 8. Photo. Data collection with the Geometrics G-858 Magnetometer at LBNM.

3.4.2 Advantages for Mapping Subsurface Voids

Instruments using inductive techniques to measure electrical conductivity do not require ground contact. Thus, data can be recorded quickly. In addition, different instruments could be used in different modes allowing different depths of investigation.

3.4.3 Limitations for Mapping Subsurface Voids

The instruments used to measure electrical conductivity produce better results in fairly conductive conditions. This is because they need to generate electrical currents (called secondary currents) in the ground inductively. When the ground has a very low conductivity,

only very small secondary currents are generated. Therefore, the secondary electromagnetic fields, which these secondary currents generate and which are sensed by the instrument, are also very small. In these cases there is very little signal to measure and the instrument becomes ineffective. This may be the case at LBNM. It is possible that instruments, which inductively measure electrical conductivity, could locate lava tubes filled with salt water or in areas where conductive clays are associated with the lava tubes.

3.4.4 Case Studies for Mapping Subsurface Voids

No publicly published work related to the detection of lava tubes exists for review.

3.4.5 Application of the Conductivity Method at LBNM

Prior to mobilization to the survey site, it was recognized that inductive measurements of electrical conductivity might not be successful. However, it was difficult to accurately estimate all of the possible geologic conditions without on site testing. Since measurements of electrical conductivity using inductive methods are rapidly acquired, this method has the potential to be very useful for locating lava tubes if the geologic conditions are appropriate. Thus the method was tested at the LBNM site. Data was recorded using the EM31, which generates electromagnetic waves oscillating at 9.8 KHz in order to measure bulk conductivity. The instrument was used with the plane of the coils (transmitter and receiver) parallel to the ground surface (Figure 9). In this mode the effective exploration depth is about 5 m (16.4 ft). The instrument outputs conductivity data in mmho/m to a data logger.

3.5 SEISMIC REFRACTION

3.5.1 General Background and Data Acquisition

Seismic refraction is a geophysical method that analyzes the time of the first arrival of energy at each geophone. A seismic line, consisting of an array of geophones, is laid out in a straight line. Generally, the length of a seismic refraction spread should be three or four times the expected depth of the refractor, although this depends on the particular geological conditions. Acoustic energy is injected into the subsurface by a seismic source such as explosives or a sledgehammer. The acoustic energy travels through the ground as a wave front of energy. When this wave front encounters a layer with a higher velocity, such as an alluvial/bedrock interface, a portion of the energy is refracted as a head wave along this interface. As this wave travels along this interface, waves are continuously refracted back to the ground surface where they are detected by geophones. Both compression (P-waves) and Shear (S-waves) waves are used in seismic refraction. P-waves and S-waves have different propagation characteristics. P-waves are longitudinal waves and medium displacements are in the direction of motion. S-waves are transverse waves and medium displacements are perpendicular to the direction of motion. Figure 10 is an illustration of the seismic refraction method over a void.



Figure 9. Photo. Data collection with the EM31 at LBNM.

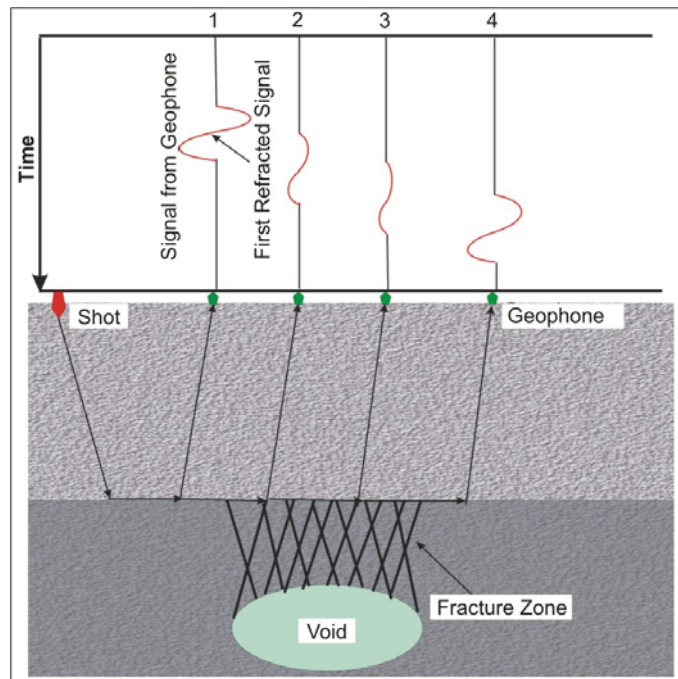


Figure 10. Drawing. Seismic refraction data across a fracture zone. ⁽⁵⁾

3.5.2 Advantages for Mapping Subsurface Voids

The refraction method can detect voids in multiple ways. First, in certain geologic settings, voids will induce fracturing in the overlying rock. The fractures result in a localized decrease in seismic velocity, which results in a delay of the travel time of the first arrival of energy. Second, if the void is near the seismic interface, a localized decrease in seismic amplitudes will occur on the refraction record. This method is also more cost effective than other seismic methods.

3.5.3 Limitations for Mapping Subsurface Voids

Seismic refraction is more cost effective than other seismic methods; however, the information gained from seismic refraction is limited. In the case illustrated in Figure 10, the seismic refraction method does not directly map the void. The amplitude attenuations and delayed travel times may also be caused by other geologic features. However, if the void were beneath a refractor then its existence may be more definitively identified. The fieldwork may also be time consuming.

3.5.4 Case Studies for Mapping Subsurface Voids

Seismic refraction was also used to locate subsurface voids at Jackson County, Ohio. The procedures and results for this survey are outlined in a report titled *Identifying Potential Collapse Features Under Highways*⁽⁹⁾. Both P-wave and S-wave data were collected parallel to the road over potential voids. A 36 channel seismograph with 30 Hz geophones was utilized in both surveys. Positioning was accomplished using a theodolite.

In phase I of the research project conducted at the Jackson County, Ohio site, drilling confirmed the presence of the Clarion coal seam at a depth of 1.5 m and 4.6 m (4.9 ft and 15.1 ft) below the subsurface. Variance in the depth is in part due to mining and possible collapse features. The overlying material consists of clay, limestone, and shale layers. P-wave refraction data were collected along two lines. The data were analyzed using two different software programs. The first program is SIP by Rimrock Geophysics. SIP models are generated from the first break times giving depth models for each profile. The depth profiles were in error due to the voids in the subsurface that decrease the velocity of the seismic wave. However, variations in the travel times of the first arrivals in seismic traces provided information about the location of the voids, since longer travel times were evident over the voids. The valleys in the data corresponded well with the locations of the voids mapped at a later date.

P-wave signal attenuation was also used to locate voids. The signal attenuations are possibly the result of wave scattering caused by the fracturing above a void or by the absorption of energy of the waves traveling from the bottom of the coal layer, through a mined area, and to the surface. Trace displays of the attenuation data were generated with Promax, a computer program for processing seismic data. P-wave attenuation was observed on both a north survey line and a south survey line. After ground truth was collected, it was shown that the areas of signal attenuation correlated with voids.

3.5.5 Application of Seismic Refraction at LBNM

Even though the seismic refraction method has successfully located voids, this method was not tested at LBNM. Since the geological setting consists of layers of basalts, it would be difficult to distinguish which fractures were caused by voids from fractures formed during lava's natural cooling process. Also, other seismic methods (e.g. high-resolution shear wave reflection) have proved more successful in mapping subsurface voids.

3.6 SEISMIC REFLECTION

3.6.1 General Background and Data Acquisition

When a seismic wave traveling into the subsurface encounters an interface providing an impedance contrast (change in velocity and/or density) part of the wave is reflected back to the ground surface, while the remainder propagates to greater depths where it may again encounter an impedance contrast repeating the phenomena described above. This phenomenon will continue to occur as the wave propagates deeper into the ground until the seismic energy dissipates. Producing the seismic waves and recording the reflected signals is the basis for the seismic reflection method. Both P-wave and S-wave data can be used in the seismic reflection method. Figure 11 is an illustration of the seismic reflection method.

3.6.2 Advantages for Mapping Subsurface Voids

In the case illustrated in Figure 11, the seismic waves are directly influenced by the void and its presence may be inferred, although probably not uniquely, from the seismic records. S-waves are usually used to locate voids since they cannot propagate through liquids or gases. Also, seismic reflection can provide information about the size of the void and the depth beneath ground surface.

3.6.3 Limitations for Mapping Subsurface Voids

Voids are interpreted in shear wave reflection data mostly from diffraction patterns and amplitude attenuation, which are sometimes caused by other features. Field data recording of reflection seismic data is fairly labor intensive. Processing of the data requires a significant amount of knowledge and specialized training. Likewise, interpretation of the data requires knowledge and experience, since the anomalies from lava tubes may not be obvious. Figure 12 is a seismic reflection cross section showing several voids, visible mostly because of amplitude attenuation and reflector discontinuities.

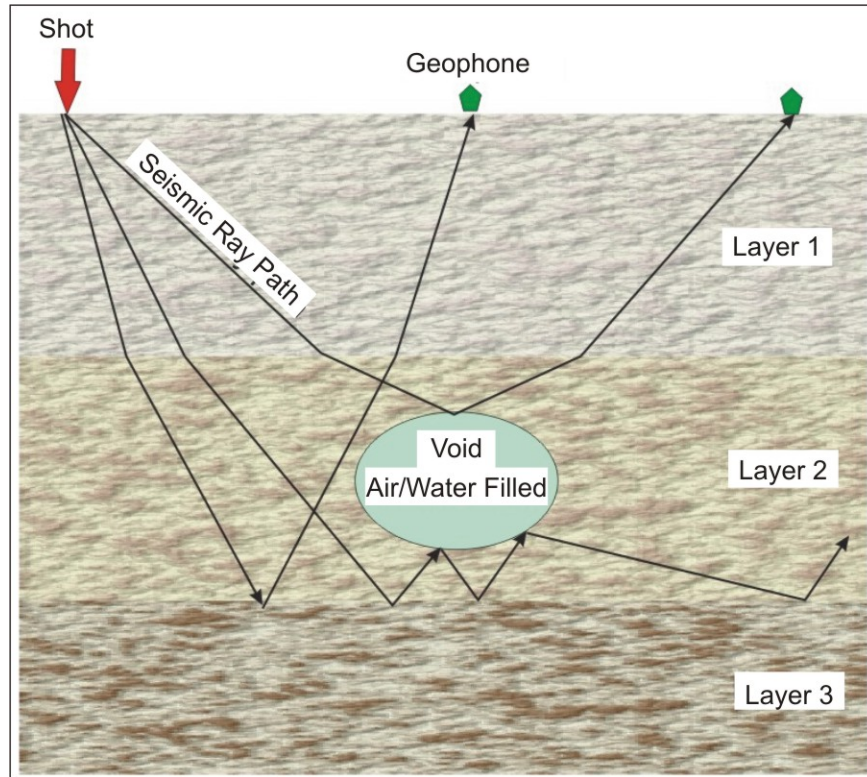


Figure 11. Drawing. Shear waves over an air/water-filled void. ⁽⁷⁾

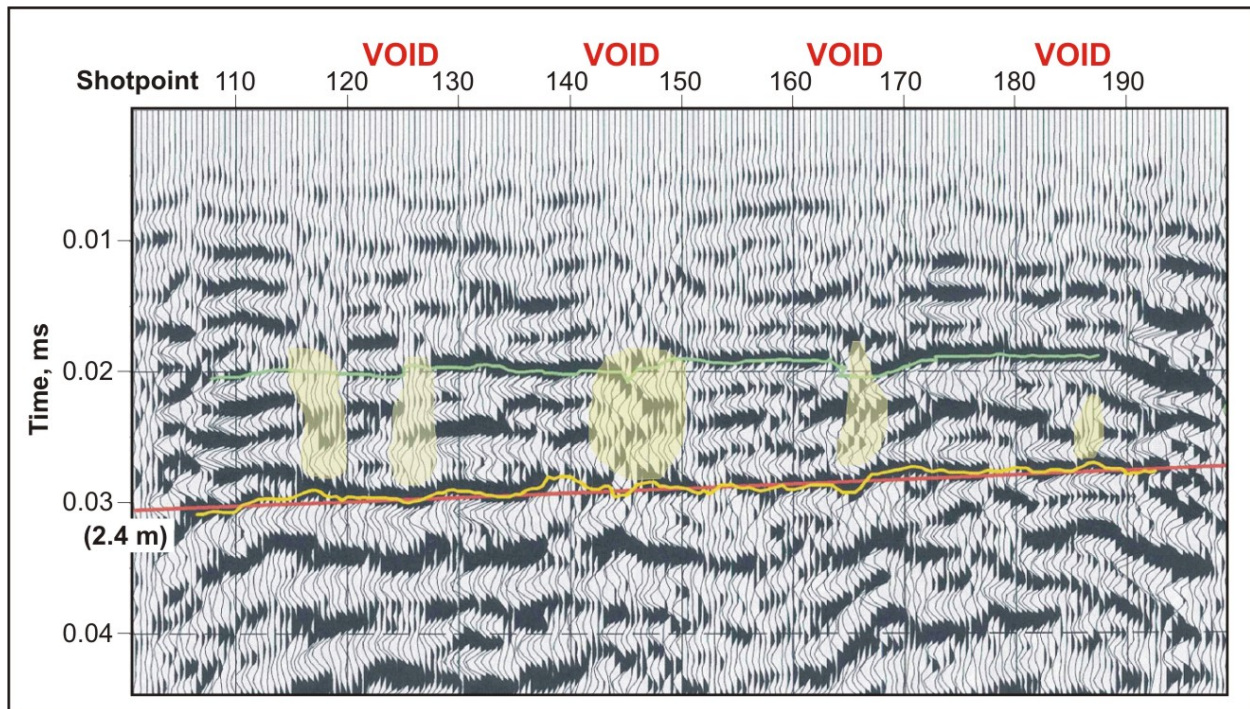


Figure 12. Cross Section. Voids interpreted from shear wave seismic data. ⁽⁷⁾

3.6.4 Case Studies for Mapping Subsurface Voids

Shear wave reflection has proven successful in the past for locating voids. In a paper titled *Double Feature at the Bijou: Shear Wave Reflection Seismic Acquired Within a Working Movie Theater*⁽¹²⁾, shear wave seismic data located an abandoned mine underneath a movie theater. A MicroVibrator was used as the seismic source because it is compact, portable, has controlled frequency output, and has improved ambient noise rejection. OYO 1x 40 Hz SMC-70 shear wave geophones were used. Three lines were laid out parallel to each other with a fourth line running perpendicular to the first three lines.

The geology in the area consists of 8.8 m (28.9 ft) of horizontally layered clays interlaced with layers of sands, overlaying weathered shale roughly 4.1 m (13.5 ft) thick. This sequence overlays a coal seam that is 1.7 m (5.6 ft) thick. The seismic data showed the coal seam dipping to the south and terminating against an erosional channel. A channel was also observed in each of the three parallel lines. Borings in the area confirmed the presence of a channel in the coal.

3.6.5 Application of the Seismic Reflection Method at LBNM

The high-resolution shear wave reflection method was tested at LBNM. The equipment included the MicroVibrator, a 96-channel OYO DAS-1 Seismograph, and a 96-channel Land Streamer configured with 40-Hz OYO SMC70 horizontal geophones. These particular geophones differ from classical geophones because they do not require insertion into the ground in order to record the signals. All 96 geophones are connected to a nylon strap that rests on the ground surface. The collection time with the Land Streamer is less when compared to other seismic setups. However, it is important to note that this method has a reduced signal to noise ratio due to the less effective ground coupling than with conventional geophones. The MicroVibrator and Land Streamer are shown in Figure 13. HRSW was originally proposed to investigate areas where cut bank operations were to take place. In these areas, CFLHD was interested in detecting voids to depths between 10 and 20 m.

3.7 GRAVITY METHOD

3.7.1 General Background and Data Acquisition

The gravitational method measures small spatial differences in the gravitational field of the Earth. The gravitational field of an object is directly related to its mass; therefore, the more mass that an object has, the higher the gravitational pull from that object. Likewise, if a mass deficit occurs, as with a lava tube, then this will result in a decrease in the gravitation pull close to this feature. Figure 14 illustrates this concept over a void. Geophysical gravity surveys do not measure the absolute gravitational pull; rather, they measure the gravitational pull relative to that at some known location, usually some point close to the site of interest. Since the gravitational pull from an object decreases as the inverse square of its distance from the measuring point, the anomaly from a void, or lava tube, decreases rapidly with depth. In order to observe the expected small anomalies from voids, accurate gravity reading would be required. Since the pull of gravity decreases with distance from the center of the earth, the elevations

(± 1 inch) of the gravity stations would also be required. Microgravity is the name given to surveys requiring the most accurate data, such as would be needed to locate lava tubes.



Figure 13. Photo. Data collection with the MicroVibrator and the Land Streamer at LBNM.

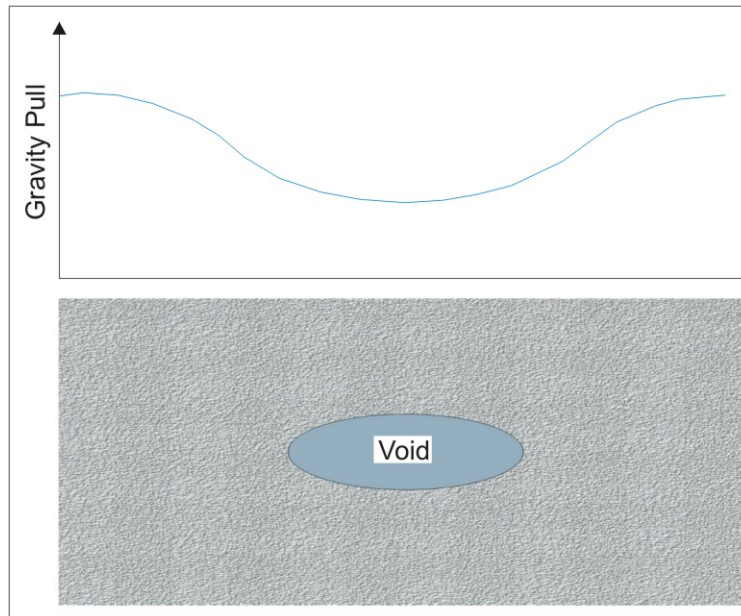


Figure 14. Drawing. Gravity field over a void. ⁽⁷⁾

3.7.2 Advantages for Mapping Subsurface Voids

The gravity method may be useful in that well defined “negative” anomalies are likely to be caused by some kind of local mass deficit, which in this area will probably be a near surface lava tube. Gravity is a good method at locating larger tubes, which should provide a significant mass deficit, thus producing a significant anomaly.

3.7.3 Limitations for Mapping Subsurface Voids

Since precise gravitational readings are required, gravitational data collection is tedious and time consuming. Field crews must level the instrument and accurate elevation and spatial control is essential. Also, interpretation of gravity data, like magnetic data, can be ambiguous. A larger, deeper anomaly may have the same signature in the gravity data as a smaller shallower anomaly. In addition, cultural noise such as traffic and wind can negatively affect the data.

3.7.4 Case Studies for Mapping Subsurface Voids

In a paper titled *Microgravity and Magnetic Investigations for Dikes, Fissures, and Lava Tubes* ⁽¹⁵⁾, microgravity data were acquired over the Kings Bowl lava field and other lava flows on the Eastern Snake River Plain (ESRP), Idaho. This location was chosen because it is a Holocene field with exposed eruptive and non-eruptive fissures. After collection and processing, maps were created showing both the magnetic and microgravity data. The microgravity data showed many anomalies that did not relate to lava tubes, dikes, or fissures. “This indicates that basalt flows along the ESRP display rapid horizontal changes in density and magnetization, that are in part likely related to near-surface basalt porosity variations.” It was determined that variances in the data collected over all but the larger fissures could be attributed to near surface density variations. In addition, gravitational data does not clearly show fissures. This is not surprising since fissures are not usually associated with significant mass changes. The microgravity data collected over Bear Trap Cave, however, showed a distinct anomaly, which decreased in amplitude as the cave depth increased.

3.7.5 Application of the Gravity Method at LBNM

Gravity data were not collected at LBNM. Because data acquisition with this method is slow, along with the need to record accurate elevations at each station, the method is quite expensive. Therefore, in view of the fact that several other methods were available, most of which were expected to be as effective as the gravity method, provide more rapid data acquisition and may be less costly, the gravity method was not used.

CHAPTER 4.0. GEOPHYSICAL MAPPING OF VOIDS AT LBNM

4.1 GENERAL INFORMATION

This chapter contains information describing each of the five individual sites where geophysical surveys were performed. Since many aspects of the surveys are similar at the other sites, only details that differ significantly are discussed at length.

The park consists of a variety of rock types such as basalt, andesite, dacite, and rhyolite ⁽¹⁵⁾. One unit, basalt of the Mammoth Crater, created the majority of the caves at LBNM, including the five caves selected for geophysical surveys. This unit is considered to have formed during the late Pleistocene epoch ⁽¹⁶⁾, and is comprised of several different flows. The silica values in the basalt range from 48.3 to 55.1%. The remnant paleomagnetization is consistent throughout this unit suggesting that this unit formed within a 100-year time span ⁽¹⁶⁾. In addition to lava tubes, this basalt unit also contains blisters, or small pockets of air ranging in size from a few cm to hundreds of cm. On top of the basaltic rock is a thin layer of pumice deposited during the last eruption ⁽⁶⁾. There are also layers of scoria visible in outcrops. The most observable attribute of the park is the large cinder cones that are located throughout the park. Photographs of LBNM recorded during the survey are shown in Appendix A.

The geophysical surveys were conducted over Monument Road Cave, Indian Well Cave, Golden Dome Cave, Hercules Leg Cave, and Bear Paw Bridge. Three locations (Golden Dome, Hercules Leg, and Indian Well Cave) are located in the Cave Loop vicinity at the southern end of LBNM. Figure 15 shows the location of the caves along Cave Loop Road. Surveys were also conducted at one location approximately 3.2 km (2.0 mi) northwest of the Visitor's Center (Bearpaw Bridge at Merrill Cave) and at one location (Monument Road Cave) along Hill Road near Devil's Homestead Flow (the location of this cave is not given per LBNM officials' request). Table 1 summarizes the geophysical methods used at each of the sites for determining cave locations.

All the selected caves differ in size and depth below the ground surface and were chosen in order to test the capabilities of the geophysical systems under different circumstances. Information regarding these caves comes from multiple resources including the book Lava Beds Caves by Charlie and Jo Larson ⁽⁶⁾, cave maps provided by LBNM personnel, personal observations made by the field personnel, and survey information obtained in the field.

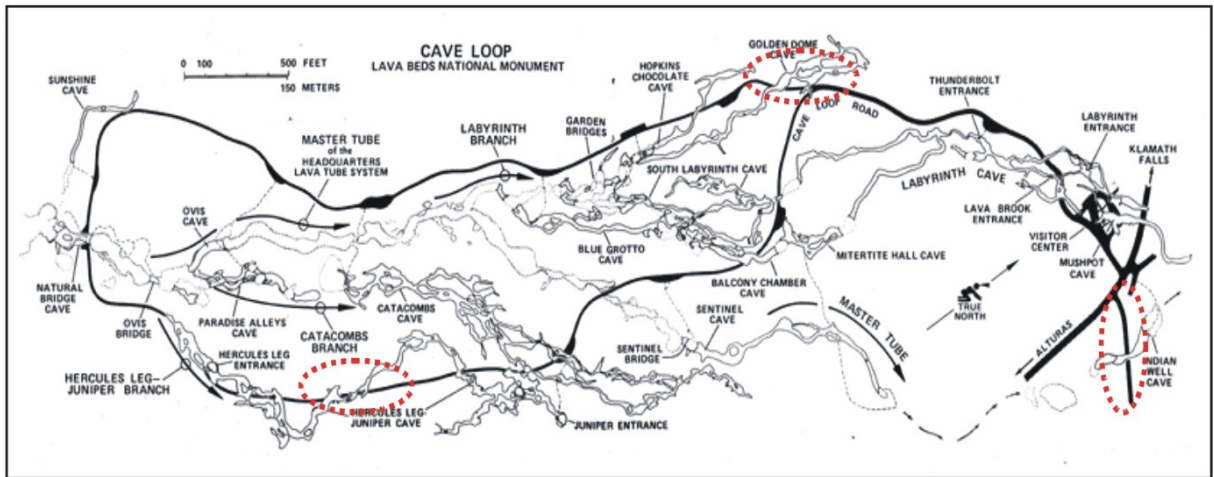


Figure 15. Map. Cave Loop Road site (survey locations outlined in red). ⁽⁶⁾

Table 1. Geophysical methods used for mapping subsurface voids at LBNM.

Site/Method	Golden Dome Cave	Indian Well Cave	Monument Road Cave	Bear Paw Bridge	Hercules Leg Cave
GPR	•	•	•		•
Magnetic	•	•	•		•
HRSW	•	•	•		•
Electrical Resistivity		•	•	•	•
Electrical Conductivity					•

All above ground topographic and spatial surveying was accomplished with the Trimble 4700 Real Time Kinematic Differential Global Positioning System (DGPS). Geophysical survey points (i.e. geophone locations and survey line start and end points) as well as points of interest (i.e. cave openings, estimated cave location, and road locations) were surveyed. These points have been positioned on many of the figures. Additionally, DGPS data were coupled with magnetic and electrical conductivity data for sensor positioning purposes. Table 2 lists the base station coordinates used to acquire the DGPS data.

Table 2. DGPS base station coordinates.

ID	Coordinates (NAD 83/UTM Zone 10)		
	Easting (m)	Northing (m)	Elevation (m)
4770 USFS	624064.33	4619061.79	1430.3
Description	A metal cap marked 4770 USFS is located approximately 1.5 m north of the entrance to Mushpot Cave on a small rock		
640 LABE	NA	NA	1300.19
Description	A metal cap marked 640 LABE is located approximately 1.2 m south of the entrance to Monument Road Cave on a large rock. (Note: exact coordinates are not listed at the request of LBNM officials)		

A compass and chain surveying method was used to find the approximate location where the cave passed beneath the road. In addition, both the height and the width of the cave underneath the road and the thickness of overburden between the road and the roof of the cave were obtained. The equipment utilized in the survey included a compass, measuring tape, hand-level, and stadia rod.

In order to find the location of the cave under the road, a point was selected at the entrance to the cave that could be accurately compared to a known point on the surface. The directional trend of the cave was then ascertained using a compass and measuring tape. A stadia rod and level were used to obtain elevation changes. The path of the cave on the ground surface was then found along with the approximate position where it crossed the road. These points were surveyed using the DGPS and are listed above. Table 3 shows the cave parameters that were determined through compass and chain surveying and differential global positioning system surveying. Two separate caves at the Hercules Leg Cave site were surveyed. No survey information was collected at Bear Paw Bridge; however, information was obtained through other sources and is discussed later. Please note that all measurements are approximate. There are small discrepancies in the location and size of lava tubes when the survey information is compared to those locations listed in the book *Lava Beds Caves* (6). The lava tubes were surveyed at the end of the field project. Geophysical survey lines were situated with respect to the cave locations using the *Lava Beds Caves* (6) book. Cave locations displayed on geophysical data figures are those obtained through the compass and chain method.

The interpretations of the geophysical methods provide, where feasible, the depths and dimensions of the sources of the anomalies. These factors (depths and dimensions) are given to the greatest accuracy possible, sometimes to within 0.1 meter (.33 ft). However, each geophysical method provides different accuracies for these factors. It should be noted that providing these factors to the accuracy presented does not necessarily imply that the method is accurate to this degree.

Table 3. Cave parameters determined through surveying.

Location	Overburden Thickness (m) ¹	Width of Cave Under Road (m)	Height of Cave Under Road (m)	Point on Road Above Cave		
				Easting (m)	Northing (m)	Elevation (m)
Monument Road Cave	5.5	12.2	5.5	619712.33	4625420.4	1302.4
Indian Well Cave	8.8	7.9	8.5	624226.29	4618993.32	1428.6
Golden Dome Cave	4.0	4.0	2.7	623650.26	4618743.77	1467.8
Hercules Leg Cave – North	3.4	9.8	.91	623652.55	4618028.22	1499.7
Hercules Leg Cave – South	2.7	22.3	2.4	623645.36	4618011.38	1501.0

All coordinates are listed in NAD 83/ UTM Zone 10
 1-Overburden thickness is measured from the road to the top of the cave.

4.2 GOLDEN DOME CAVE

4.2.1 Site Description

Golden Dome Cave is located at the north end of Cave Loop Road. The cave is oriented generally in a north-south direction. Lava tube slime, a type of mold found in humid microclimates, is found on the ceiling in this cave. This mold is hydrophobic and beads of water rest on its surface. The reflection of light off the beads is golden in color, hence the name Golden Dome. Other types of lava tube characteristics found in this cave include cupolas, cutbanks, lava flowstones, and “aa” lava floors⁽⁶⁾. There has been little collapse of the overburden into this cave. Through simple surveying techniques and maps, it has been determined that the cave has a height of approximately 2.7 m (8.9 ft) under the road and the overburden is approximately 4 m thick (13.1 ft). The width of the cave varies underneath the road, but at one point it is 9.8 m (32.2 ft) wide. This cave was selected because it would test the ability of the geophysical methods to detect a cave whose depth is greater than its width. Figure 16 is a picture showing the Land Streamer deployed along the road at Golden Dome Cave.



Figure 16. Photo. Land Streamer deployed above Golden Dome Cave.

4.2.2 Data Analysis and Interpretation

Ground Penetrating Radar

In general, voids in the subsurface are visible in the GPR cross sections in the form of reflection and diffraction hyperbolae. In the case of lava tube detection at LBNM, the voids are irregularly shaped with a highly uneven rock-air boundary. This will cause the lava tubes to produce diffraction hyperbolae at the rock-air interface in the GPR cross sections. Analyses of raw and processed profiles collected at LBNM show numerous diffractions and diffraction hyperbolae. GPR signals are scattered by voids, fracturing, inclusions, and other inhomogeneous features in the subsurface and provide a detailed but difficult section to interpret.

At each site, the GPR data were collected with the SIR-2000 system using two or three different antennae (100 MHz, 200 MHz, and 400 MHz) in two directions along each survey line. The length of the lines and distance between the lines varied at each site. Both wheel mode and automatic mode were used during this survey. The GPR data acquisition parameters for each site are listed in Appendix B.

The GPR data were processed using RADAN, written by GSSI. During processing, the profiles were corrected for distance; the time range was limited to enhance near surface features and remove noise; the data were stretched to enhance details; a background filter was used to remove

noise, and a deconvolution filter was applied to attenuate multiples and improve the quality of reflections. The data files were then exported figures were created.

Processed GPR cross sections are shown throughout this chapter. The sections are displayed with the horizontal (length) and vertical (depth) scales in ft and m using a velocity calculated with the dielectric constant, ϵ_r , equal to 8. Note the slight exaggeration in the vertical scale. The sections are displayed in a line scan format using a grayscale palette. Interpreted figures, shown in this section, are provided with known caves highlighted in blue, and suspected caves highlighted in red. Uninterrupted GPR figures are included in Appendix C. The 200 MHz data, rather than the 400 MHz data, has been selected for interpretation because it provides a greater depth of penetration although resolution is less than that which can be obtained with the 400 MHz data. In addition, because the 200 MHz antenna provides a longer wavelength than the 400 MHz antenna, the signal is less susceptible to scattering.

The descriptions of the GPR data acquisition, processing, and interpretation procedures apply to all of the cave sites in this report.

To maximize coverage at Golden Dome Cave, three profiles were collected at different angles and different lengths with each of the GPR antennae. Figure 17 shows the approximate location of the survey lines superimposed on a plan map obtained from The Lava Beds Caves book. It appears that the survey lines cross the cave; however, after surveying with a compass and chain, it was determined that the cave is actually further west than is shown in the figure. Therefore, the GPR survey was not conducted over the cave. Table 4 gives the coordinates of the start and end point of each GPR line at this site.

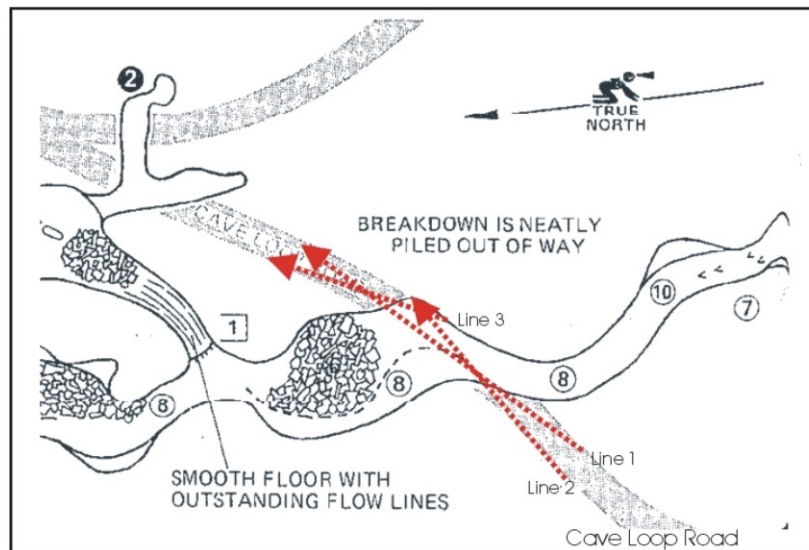


Figure 17. Map. GPR survey lines over Golden Dome Cave. ⁽⁶⁾

Table 4. GPR survey line coordinates over Golden Dome Cave.

Line #	Southwest End Point		Northeast End Point	
	Easting (m)	Northing (m)	Easting (m)	Northing (m)
Line 1	623654.38	4618750.3	623685.26	4618788.08
Line 2	623654.45	4618750.33	623676.13	4618767.79
Line 3	623672.37	4618762.61	623681.54	4618788.15

All coordinates are listed in NAD 83/UTM Zone 10

Figure 18 displays the 200 MHz antenna data collected at the Golden Dome Cave survey site. Since GPR data were not collected over the known cave, the known cave is not outlined on the GPR cross section. All measurements discussed are from the start of the profile (0 m), unless otherwise noted. Multiple anomalies (hyperbolae) are visible in the first 10.7 m (35.1 ft) of the profile. Of these, three have been outlined in red as possible lava tubes. Two of the hyperbolae are centered at 7.6 m (24.9 ft), and almost completely overlap, although they are interpreted to lie at different depths, 3.4 m and 2.1 m (11.2 ft and 6.9 ft), and have slightly different widths, 4.9 m and 5.8 m (16.1 ft and 19 ft), respectively. Widths of GPR anomalies are estimates based on analysis of the width of the diffraction hyperbolae. The third hyperbola is centered at 9.8 m (32.2 ft) at a depth of 2.7 m (8.9 ft) with a width of 4.3 m (14.1 ft). These anomalies are small and may represent very small lava tubes, blisters, or fracturing in the rock. Two high amplitude anomalies are outlined in the data as well. A small hyperbola is visible at 31.7 m (104.0 ft). It is characterized by a high amplitude response at its apex and along the right tail while the left tail is lost in an area of multiple diffractions. The last area outlined, between 38.1 and 48.8 m (125.0 and 160.1 ft), is comprised of a possible layer as well as a high amplitude hyperbola. The hyperbola is less than 3.0 m (9.8 ft) in width but has a very high amplitude response. These anomalies may be caused by small lava tubes, blisters, or fracturing.

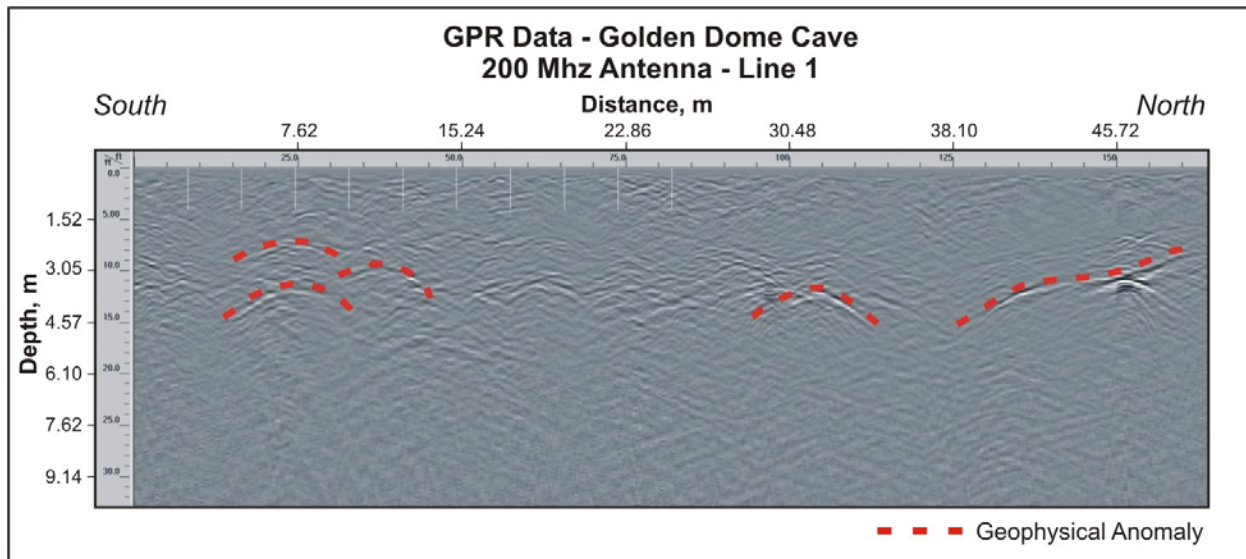


Figure 18. Profile. GPR cross section collected over Golden Dome Cave.

Magnetic Method

Three lines of magnetic data were collected along the road section at each site. One line was collected down either side of the road and one line was collected in the middle of the road. The line spacing was between 1.5 and 2.2 m (4.9 and 7.2 ft). The magnetic data was collected with a Geometrics G-858 magnetometer, which measures the magnitude of the magnetic field vector, at a rate of 10 measurements per second. The data were coupled with DGPS for positioning. A base station magnetometer was recorded during the magnetic survey.

The magnetic data was processed in MagMap2000. In this program, data files were inspected for data spikes, a diurnal correction was applied to the data, DGPS antenna offset corrections were applied, the diurnal magnetic field was removed, and the data were exported with spatial coordinates associated with each magnetic field data point (*.xyz ASCII format). The ASCII files were then read into Oasis montaj where the data from each line were shifted slightly to compensate for spatial errors in the GPS data and figures were created.

The descriptions of the magnetic data acquisition, processing, and interpretation procedures apply to all of the cave sites in this report.

Figure 19 shows the magnetic data collected over Golden Dome Cave. The top of the figure shows gridded data from all three lines along the road. The bottom of the figure shows magnetic profiles from all three survey lines. The direction of the magnetic profile is SW-NE.

The interpretation of magnetic anomalies for lava tubes in this environment is quite challenging. The feature of interest is a void, and is therefore a non-magnetic source. This contrasts with the usual magnetic anomaly interpretations where magnetic sources are interpreted. In addition, it is possible that remnant magnetization exists whose direction is different from that of any induced magnetization. The basalts and other rocks may have different concentrations of magnetite in different locations, thus forming anomalies unrelated to voids. However, a simple visual analysis of the type of anomaly that can be expected over a void suggests that if the anomaly results from induced magnetization alone then a bipolar anomaly should be seen with the negative part of the anomaly occurring to the south of the void and the positive part to the north. However, it should be kept in mind that this simple shape may be significantly modified if the factors described above become prominent.

The response of the void in magnetic data will vary from site to site. Magnetic data interpretation requires information on the site's location, including the inclination and declination of the survey, the geologic conditions, and the survey's orientation. Because of the large number of factors that may be involved in the production of anomalies, it is not possible in this report to ascribe a physical explanation to every anomaly. Thus, for each of the sites where magnetic data were acquired, only a brief discussion is provided, mostly pointing out the anomalies and their association with known caves, or their potential to indicate unknown caves.

Figure 19 shows that the largest anomaly correlates well, spatially, with the known cave location. The survey width of the cave is approximately 3.8 m (12.5 ft) and the surveyed depth to its top is 4.0 m (13.1 ft). Two other anomalies located northeast of the known cave were selected as a possible cave location along the survey lines. Both anomalies have characteristics similar to the anomaly over the lava tube. It may be possible to model these anomalies using computer software, possibly providing more details about the geometry of the lava tube. Although brief attempts at modeling have been made, much more analysis needs to be done and no conclusions are currently drawn from the modeling.

Seismic Reflection

High Resolution Shear Wave reflection data were collected along 57.9 m (190 ft) profiles at most sites (a longer profile line was collected at Hercules Leg). The Land Streamer consists of 96 geophones at 0.61 m (2 ft) intervals. The first geophone on the Land Streamer was designated as geophone 101 and the last geophone as 196. The MicroVibrator was positioned adjacent to the Land Streamer and between two geophones, called half stations. Data collection began at shot point 101.5 and continued through shot point 195.5. Data acquisition parameters are included in Appendix B.

The S-wave data were processed using the UNIX-based ProMax® software. The processing flow is based on a standard common midpoint (CMP) reflection processing sequence with modification for specific conditions at the survey site. Each line was processed individually while all area-based parameters were kept constant.

Since the MicroVibrator is a frequency domain seismic source, rather than a shot source, the data is processed so that the final data traces from each geophone are similar to that observed with explosives or other impulsive sources. In order to process the data, the geometry and coordinates of the source and receiver positions along the seismic profile are transferred to a computer. An attempt was made to reverse the localized filtering effects that near surface materials have on the seismic signal using a process called deconvolution and amplitude recovery.

The effects of the surface topography and variations in the upper layer of the ground are substantially removed using techniques called datum and static shift removal. Nonlinear effects of the data acquisition geometry (velocity analysis and normal move-out correction) are accounted for and removed in order to correctly image subsurface features. Directional filters are applied to the source (shot) records to eliminate unwanted signals generated by the seismic source (surface wave / linear noise attenuation). The data, which were recorded in shot point mode, were sorted to produce CMP gathers. All of the traces in each gather were then summed to produce a CMP stack. This process significantly improves the signal to noise ratio. The data were spectrally whitened to adjust the amplitudes of all frequency components and filtered to keep those reflection frequencies with the best signal to noise ratios (spectral balance).

The descriptions of the HRSW reflection data acquisition, processing, and interpretation procedures apply to all of the cave sites in this report.

Figure 20 is a plan map (6) that shows the approximate location of the survey line and direction of data collection with respect to the Golden Dome Cave. Table 5 provides locations of every tenth geophone over Golden Dome Cave.

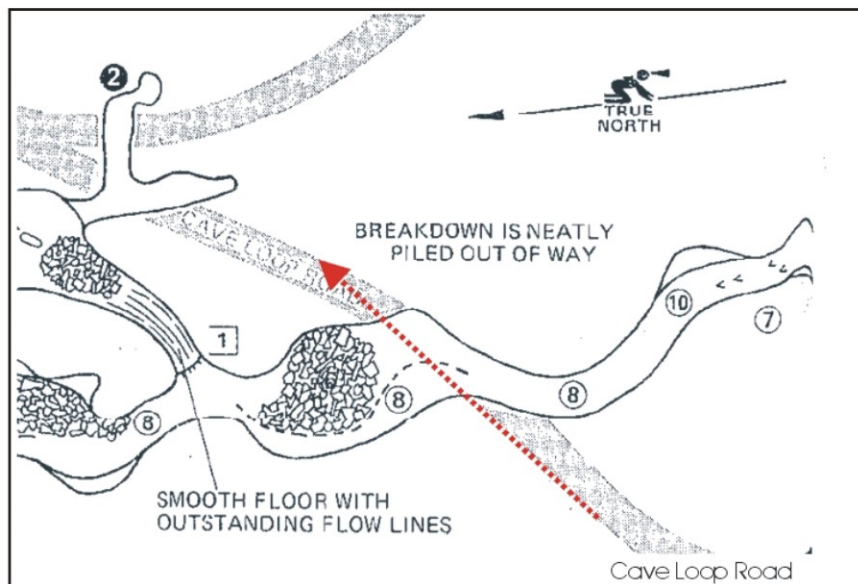


Figure 20. Map. HRSW survey line over Golden Dome Cave. ⁽⁶⁾

Table 5. Geophone coordinate locations at Golden Dome Cave.

ID	Easting (m)	Northing (m)	Elevation (m)
Geophone 101	623636.5	4618729.71	1468.7
Geophone 111	623640.7	4618733.97	1468.3
Geophone 121	623644.92	4618738.25	1468
Geophone 131	623649.15	4618742.54	1467.8
Geophone 141	623653.33	4618746.83	1467.6
Geophone 151	623657.55	4618751.11	1467.3
Geophone 161	623661.76	4618755.4	1467
Geophone 171	623665.97	4618759.7	1466.7
Geophone 181	623670.18	4618764	1466.4
Geophone 191	623674.38	4618768.27	1466.1
Geophone 196	623676.47	4618770.43	1465.9
All coordinates are listed in NAD 83/UTM Zone 10			

The data collected over Golden Dome Cave is shown in Figure 21. The HRSW data is displayed in two different ways to aid interpretation. The top cross section in each of the HRSW figures is comprised of an amplitude envelope display with wiggle traces superimposed for interpretation purposes. The horizontal scale is in m but also shows the shotpoint numbers. The distance between each of the traces is half that of the shot points. The shot records start at number 101. The vertical scale is displayed in time (ms). The same field data, shown in the lower section, is presented using an amplitude envelope with a 140/150 Hz lowcut filter, a different color scale, and no superimposed wiggle traces. There is no depth scale on the figures because the only rock velocities are those obtained for stacking the traces in the gathers (stacking velocities). Although this velocity can be used to provide depth estimates, it has to be accepted that this may not be the “true” velocity of the seismic wave within the rock layers and significant depth errors can occur. Figures displaying the uninterpreted HRSW data are available in Appendix D.

Zero time on the section is at an elevation of 1475.2 m (4839.9 ft). The known cave on this profile is centered at shot point 132, based on surveying measurements, and is thought to extend approximately 1.8 m (5.9 ft) on either side of the shot point location. On this line, reverberating reflections indicate the presence of a shallow layer with a high velocity contrast, possibly a thin, shallow scoria bed.

The stacking velocity in the vicinity of the known cave is approximately 1585 m/sec (5200 ft/sec), and the interpreted depth is 4.0 m (13.1 ft) using this velocity. The ground surface corresponds to about 12.5 ms on this section; therefore, the reflection from the top of the cave should occur at about 17 ms on this profile. An arcuate (hyperbolic) reflection can be seen at the calculated point, shown in blue, although this event does not stand out against the background. Faint diffractions extend from both edges of the location of the lava tube, although they are more evident on the deeper part of the section (below 40 ms). The interpreted width of the lava tube

measures some 3.5 m (11.5 ft) across on the seismic section based on analysis of the tails of the reflection patterns.

Two suspected lava tubes are interpreted on this profile, both highlighted in red. The first is centered at shot point 160, and, using the stacking velocity given earlier, appears to be approximately 4.9 m (16.1 ft) deep and 4.2 m (13.8 ft) across. The second is centered on shot point 188, is approximately 4.6 m (15.1 ft) across and occurs at a depth of about 6.1 m (20.2 ft). Both are manifested on the data by arcuate reflection events and faint diffractions.

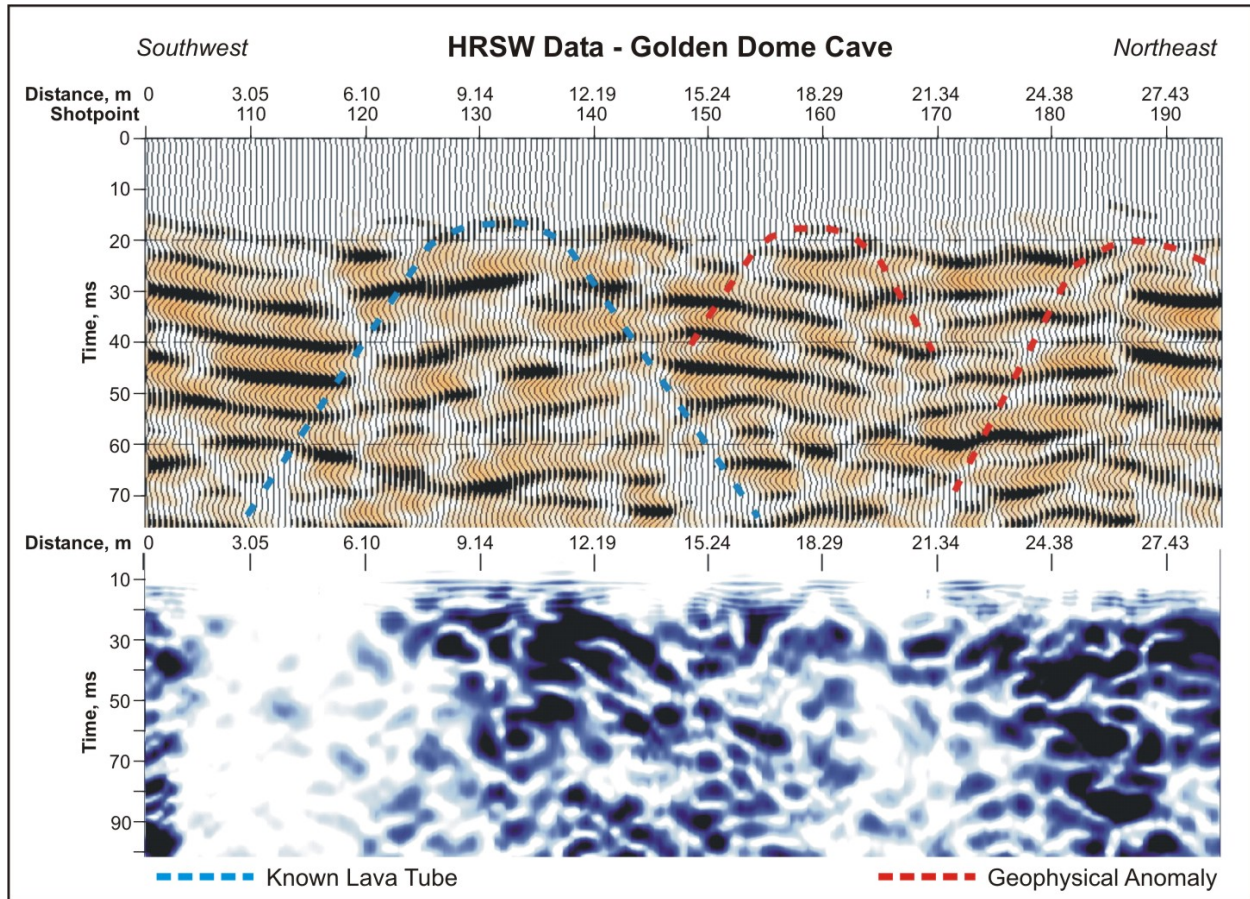


Figure 21. Cross Section. HRSW data collected over Golden Dome Cave.

4.2.3 Comparisons

Figure 22 shows an individual map for each geophysical method tested at Golden Dome Cave with anomalous zones shown as colored blocks. The anomalous zones indicate areas with a high probability of containing an anomaly. Since GPR data was not collected over the Golden Dome Cave, it was not seen in the data. However, both the magnetic and the HRSW data located the cave. An anomaly just northeast of Golden Dome Cave was interpreted using the HRSW reflection data and the GPR data. These anomalies correspond well in location and approximate size. The middle magnetic anomalous zone corresponds to the most northern anomalous zone in

the HRSW data and the most northern magnetic anomalous zone corresponds to the most northern GPR anomalous zone. All anomalous zones at this site were identified with at least two different methods.

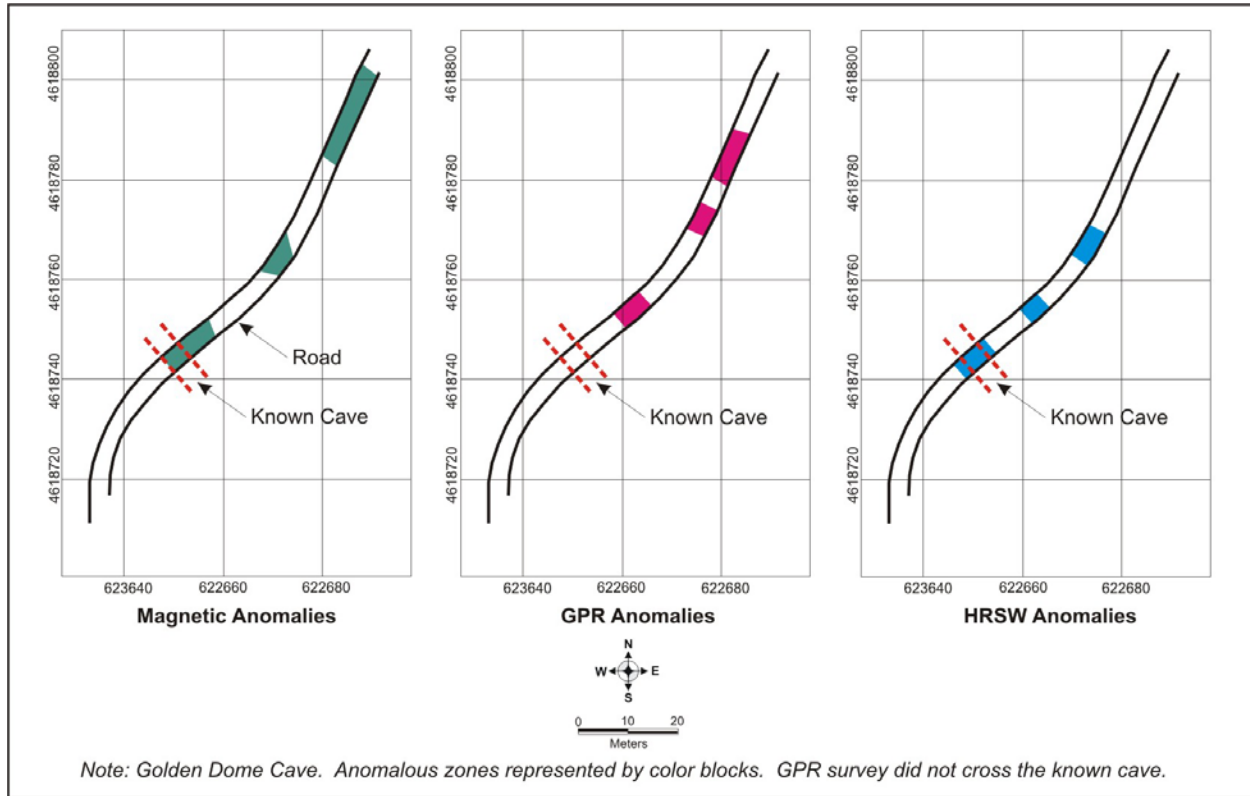


Figure 22. Map. Comparison of anomalous zones at Golden Dome Cave.

4.3 INDIAN WELL CAVE

4.3.1 Site Description

Indian Well Cave, pictured in Figure 23, is located under the service road that leads to the LBNM Headquarters. The cave received its name from the well in the bottom of an alcove located in the cave’s deepest spot. The well is replenished each year from melting ice and snow. Inside the cave there are numerous boulders and large rocks resulting from the collapse of the lining of the cave⁽⁶⁾. The depth to the roof of the cave, and the overburden thickness, vary greatly with location. Under the service road, the suspected height of the cave is approximately 7.6 to 11.3 m (24.9 to 37.1 ft), with the overburden thickness being approximately 9.7 m (31.8 ft). This cave was selected as a survey site because it is a rather large cave and it is located approximately 10 m (32.8 ft) below the subsurface. This will test the ability of the geophysical methods abilities to detect large voids at this depth.



Figure 23. Photo. The entrance of Indian Well Cave.

4.3.2 Data Analysis and Interpretation

Ground Penetrating Radar

Figure 24 is a plan view map ⁽⁶⁾ that illustrates the approximate location of the GPR survey lines over Indian Well Cave. The exact coordinates of the three GPR lines are listed in Table 6.

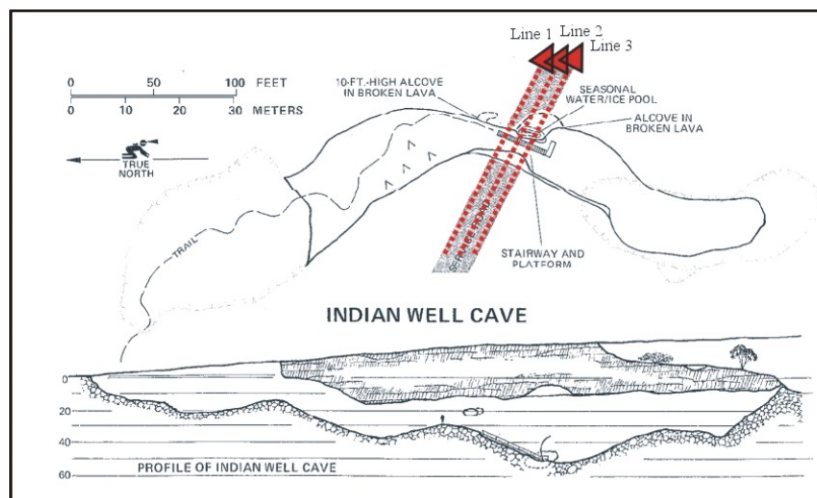


Figure 24. Map. GPR survey line over Indian Well Cave. ⁽⁶⁾

Table 6. GPR survey line coordinates over Indian Well Cave.

Line #	Northwest End Point		Southeast End Point	
	Easting (m)	Northing (m)	Easting (m)	Northing (m)
Line 1	624182.01	4619014.98	624230.48	4618991.35
Line 2	624181.94	4619012.17	624229.39	4618988.42
Line 3	624182.77	4619009.44	624228.24	4618985.81

All coordinates are listed in NAD 83/UTM Zone 10

Approximately 53.3 m (174.9 ft) of data were collected along each of three profiles (two profiles for the 100 MHz antenna) at Indian Well Cave. In general all profiles correlate well with another and show many of the same characteristics. To simplify the discussion, only the 200 MHz data, shown in Figure 25, which was collected along Line 3 is discussed. Although the 200 MHz antenna does not have the resolution of the 400 MHz antenna, the lack of resolution and increased depth of investigation provided an interpretable GPR cross section. Due to a possible wiring problem the 100 MHz antenna produced no interpretable profiles.

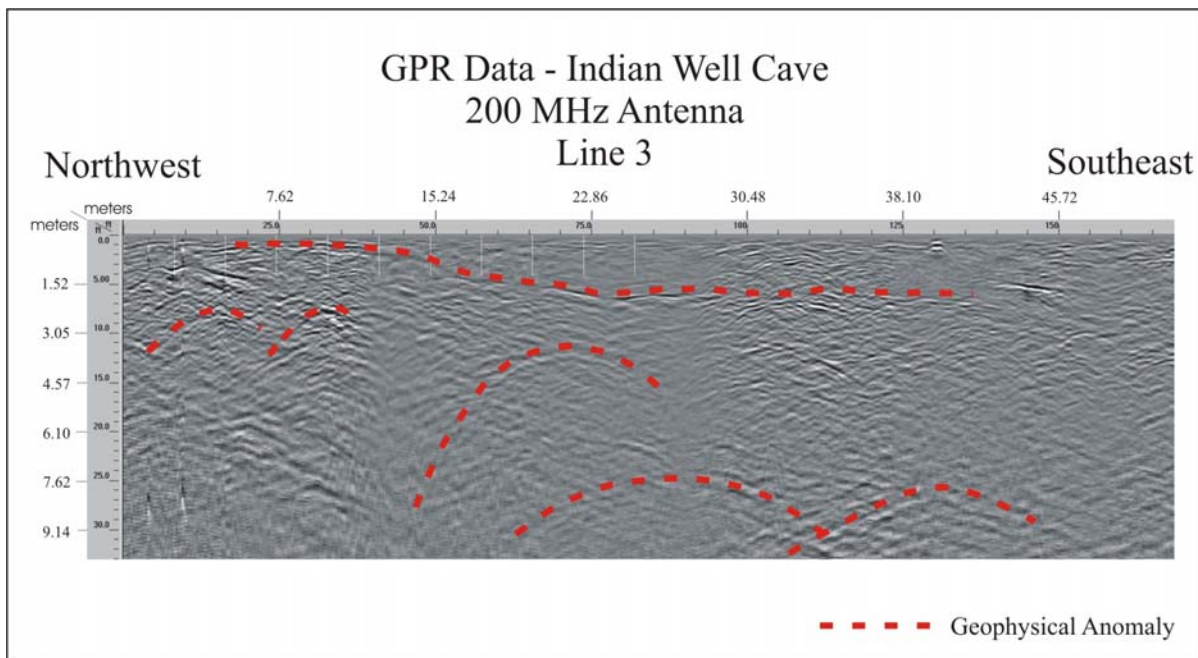


Figure 25. Cross Section. GPR data collected over Indian Well Cave.

Generally, the data quality is good and shows numerous anomalies. The profile shows areas of low amplitude response from 11.6 to 14.3 m (38.1 to 46.9 ft) and from 22.9 to 28.3 m (75.1 to 92.8 ft) and areas with multiple diffractions from 0 to 11.6 m (0 to 38.1 ft) and from 28.4 to 37.5 m (93.2 to 123.0 ft). The low amplitude areas might be the result of little or no fracturing in the basalt since, in this case, there would be no boundaries to reflect the EM waves. Areas with numerous diffractions may indicate areas of severe fracturing resulting in multiple rock-void boundaries. Although many anomalies exist in the data, only the six most prominent features

were selected from the GPR data collected along Line 3. The remaining features are not likely to represent caves. The anomalies have been marked on Figure 25. These were selected based on shape, depth and estimated size (width of anomaly) and are the most likely to be associated with caves.

The Indian Well lava tube was expected to cross Line 3 at approximately 44.2 to 45.7 m (145.0 to 149.9 ft) from the start of the line. A selected anomaly, outlined in red to denote an interpreted lava tube, is centered at approximately 39.6 m (129.9 ft). This anomaly is located at an estimated depth of 7.6 m (24.9 ft) using a dielectric constant $\epsilon_r = 8$ and produces a broad hyperbolic shape measuring approximately 13.7 m (44.9 ft) wide. Another large hyperbola is centered from 26.5 to 26.8 m (86.9 to 87.9 ft) and measures approximately 15.2 m (49.9 ft) wide. These hyperbolae were difficult to interpret because of the low amplitudes associated with them. Three other anomalies, two diffraction hyperbolae and one interpreted layer, are visible at shallower depths along the profile. A low amplitude hyperbola is centered at 21.9 m (71.9 ft) and has a depth of 3.4 m (11.2 ft) and a width of 10.7 m (35.1 ft). The interpreted layer is characterized by regions of high amplitude response (dark black color) from 20.4 to 23.2 m (66.9 to 76.1 ft) and 23.7 to 27.4 m (77.8 to 89.9 ft) and extends for a total length of 35.7 m (117.1 ft). An anomaly having a partial hyperbolic shape is centered at 10.4 m (34.1 ft) at a depth of 3.0 m (9.8 ft). Both the left side and right side of the hyperbola are still evident in spite of being in an area of muted response. Another hyperbolic anomaly is centered at approximately 4.3 m (14.1 ft) and is at a depth of 2.1 m (6.9 ft). The apex of the hyperbola is much more visible (higher amplitude values) than the tails, as is the case with the previous hyperbola discussed. The tails of the diffraction hyperbolae are lost in the interference resulting from multiple diffractions in this area. GPR data collected over Lines 1 and 2 are shown in Appendix C. These profiles show the same basic characteristics and were not interpreted individually.

Magnetic Method

The magnetic data collected over Indian Well Cave is displayed in Figure 26. The top of the figure shows gridded data from all three lines along the road. The bottom of the figure shows profiles from all three lines along which data was recorded. The direction of the magnetic profile is SE-NW. Three main magnetic anomalies are observed, and are shown outlined on the plan map of the site. The highest amplitude anomaly correlates spatially with the known cave location. The anomalies from all of the lines are similar at this location, although the amplitude of one of the lines is less.

Two other significant anomalies are seen to the northwest of the known cave location. The shape of the magnetic anomalies slightly differs from the magnetic anomaly over the known cave location. In both of these anomalies, one of the three survey lines indicates a magnetic high while the other two survey lines indicate a magnetic low. These anomalies may indicate unknown caves.

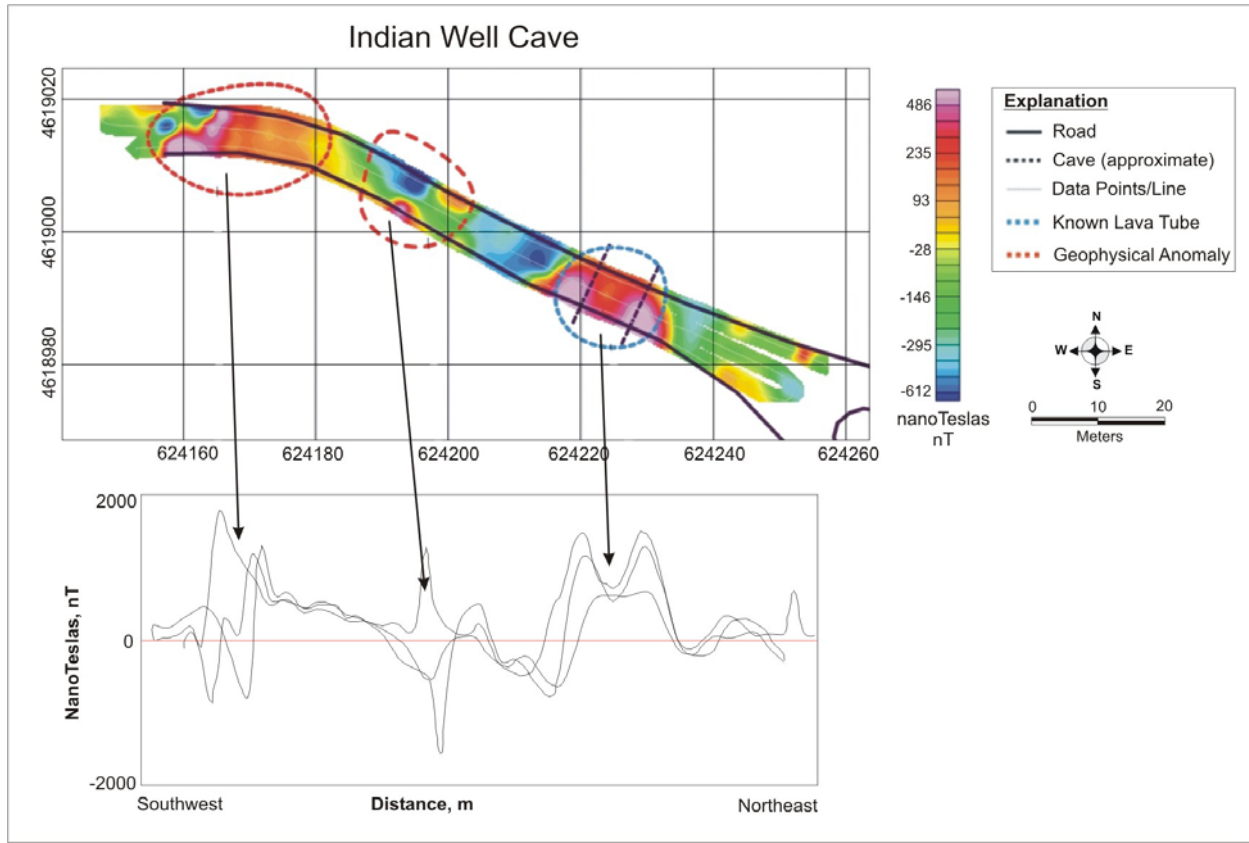


Figure 26. Map. Plan and profile view of magnetic data collected over Indian Well Cave.

Electrical Resistivity

A single line of electrical resistivity data was collected with the OhmMapper TR2 along the roads at each of the four sites. The OhmMapper TR2 array consisted of two receiver dipoles and one transmitter dipole. A non-conductive rope separates the 10 meter (32.8 ft) dipole transmitter and 15 meter (49.2 ft) dipole receivers. The length of the non-conductive rope along with the dipole lengths determines the depth of investigation. At LBNM, two different non-conductive rope lengths, 5 and 10 m, were used giving three different ‘n’ spacings of 0.5, 1.0, and 1.5 m (1.6, 3.3, and 4.9 ft). The data acquisition parameters are listed in Appendix B.

A survey line was marked along the road and the location of the line was surveyed with DGPS. A person manually towed the system along the ground surface, recording data at a rate of 2 hertz. Marks were placed in the data for positioning.

During data collection, an additional dipole cable was placed between the two receivers (a total of two dipole cables instead of one). The additional dipole cable resulted in an asymmetric 15 meter (49.2 ft) dipole receiver for both receivers.

The OhmMapper TR2 data was first imported into MagMap2000, where the data quality was checked and the array parameters were verified. A despiking filter was applied to the data to

remove abnormal spikes in the data. The position of the data was corrected using the marks in the data and the surveyed locations. The corrected data were then exported from MagMap2000 and imported into RES2DINV where the data was inverse modeled using a robust, 2-D finite-difference method. The inversion performed in RES2DINV is based on the smoothness-constrained least squares method. The 2-D model used in the inversion process divided the subsurface into a fine mesh of rectangular blocks from shallow to deep that are limited at depth by the approximate depth of investigation provided by the largest electrode spacing. The program iteratively determines the resistivities of the model blocks that will produce an apparent resistivity pseudosection that matches the field data. Through inversions, the electrical resistivity method produces a geoelectric cross-section. The cross section is developed by gridding the resistivity as a function of depth. The cross section does not show the exact structural characteristics of the subsurface. Instead, it shows a cross section with exemplified areas of extremely high or low resistivities compared to the bulk resistivity of the entire cross section.

The final RMS error, which is the difference between the successive 2-D model inversions and the measured data, was less than 5% for all sites. Fortunately, there were very few bad data points. These are usually caused by ambient noise, poor coupling, or system problems. Those that did occur were removed from the data. The final results are bitmaps displaying the measured apparent resistivity pseudosection, a calculated apparent resistivity pseudosection, and an inverse model resistivity section. These bitmaps are shown in Appendix E. Only the inverse model resistivity section is shown in the following figures.

It is important to note that an extra dipole cable used during data collection influenced the data in three ways. Due to this cable, multiple position corrections, and gridding factors, the position of the data is only approximate. The extra dipole cable caused the geoelectric cross-section to have generally higher resistivity values; however, the overall pattern of the geoelectric cross-section will remain constant. Finally, the extra cable made anomalies' location in the data shallower than its actual depth. These three factors were considered during data interpretation.

Areas of high resistivity, compared to the average for that particular geoelectric cross section, were selected as possible cave locations since the caves in this area are filled with air (infinitely resistive). This method does not show accurate boundaries of voids or any other subsurface features; however, it does give an approximate location of the middle of the void. A hole drilled into the center of the highly resistive area would verify if an anomaly exists. The dashed outlines on the geoelectric cross sections are only outlines of highly resistive areas and do not necessarily represent the true size or existence of the void. The approximate depth and size of the voids were estimated from the edges of highly resistive areas in the inverse resistivity section. Where the highly resistive area is near an edge of the geoelectric cross section, more data is needed to characterize the anomaly.

The descriptions of the procedures for the data acquisition, processing, and interpretation for the electrical resistivity method apply to all cave sites in this report.

Figure 27 displays a segment of the electrical resistivity survey line where it travels over Indian Well Cave ⁽⁶⁾ and Table 7 gives the coordinates of the end points and center point used as

markers along the survey line. Figure 28 displays the resistivity data collected at Indian Well Cave. This data was recorded from northwest to southeast. A blue arrow indicates the known cave. The anomalies are circled in red. The background resistivity values for this site lie between 1,500 ohm-m and 5,000 ohm-m, which is high for basalt, whose resistivity often ranges from 100 to 1000 ohm-m. The maximum resistivity value, 48,100 ohm-m over known cave, is located at 32.0 m (105.0 ft) at an interpreted depth of 5.5 m (18.0 ft). Since the cave appears as a half circle, with the other half of the circle below the collected data, we are unable to predict the true depth or height of the cave. The interpreted width of the cave is 6.1 m (20.0 ft), which is reasonably close to the surveyed width of the cave, which is 7.9 m (25.9 ft).

Table 7. Electrical resistivity survey line coordinates over Indian Well Cave.

ID	Easting (m)	Northing (m)
Point 1 (SE end point)	624252.03	4618976.38
Point 2	624147.62	4619017.32
Point 3	624206.04	4619000.05
Point 4	624206.04	4619000.05
Point 5 (NW end point)	624147.62	4619017.32
All coordinates are listed in NAD 83/UTM Zone 10		

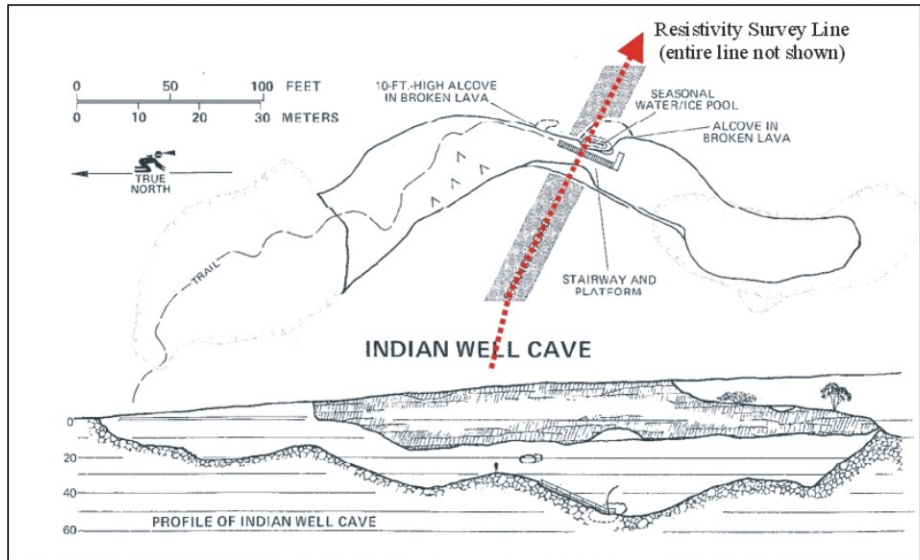


Figure 27. Map. Electrical Resistivity survey line over Indian Well Cave. ⁽⁶⁾

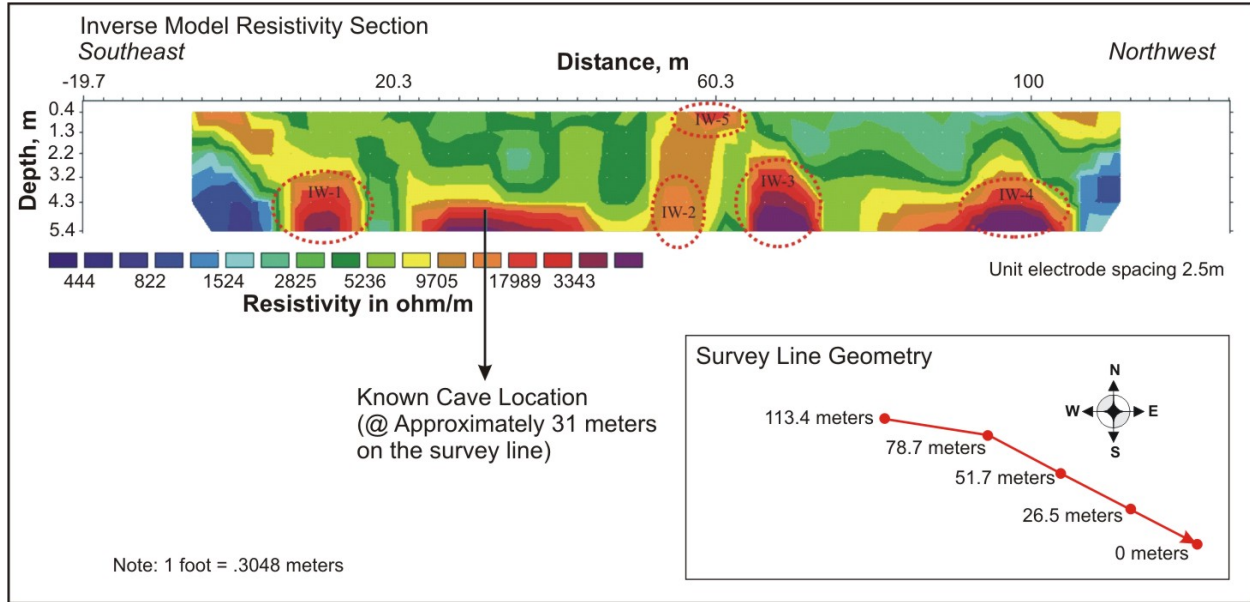


Figure 28. Cross Section. Electrical Resistivity data collected over Indian Well Cave.

There are five other areas of high resistivity at the Indian Well Cave site. Anomalies IW-1, IW-2, IW-3, and IW-4 all have peak resistivities of 28,000 ohm-m, 17,500 ohm-m, 32,600 ohm-m, and 72,100 ohm-m, respectively. These four anomalies appear as half circles along the bottom edge of the cross-section. To identify the true characteristics of these anomalies, it would be advantageous to survey to greater depths. One additional anomaly, IW-5, located at 24.4 m (80.1 ft) from the southeast and located very close to the surface, has a maximum resistivity of 18,800 ohm-m. The width of the small anomaly appears to be approximately 2.4 m (7.9 ft). The larger anomalies, namely IW-1, IW-3 and IW-4, may represent unknown caves. While the smaller anomalies could represent very small caves, they could also represent normal resistivity variations within the basalt.

Seismic Reflection

Figure 29 displays the approximate location of the HRSW survey line as it passed over Indian Well Cave ⁽⁶⁾ and Table 8 gives the location of every tenth geophone along the line. Interpreted and uninterpreted sections are provided on Figure 30 and in Appendix D, respectively. Zero time is at an elevation of 1435 m (4708.0 ft). Reverberations are minimal on this line, indicating that the basalt in this area has minimal velocity changes with depth.

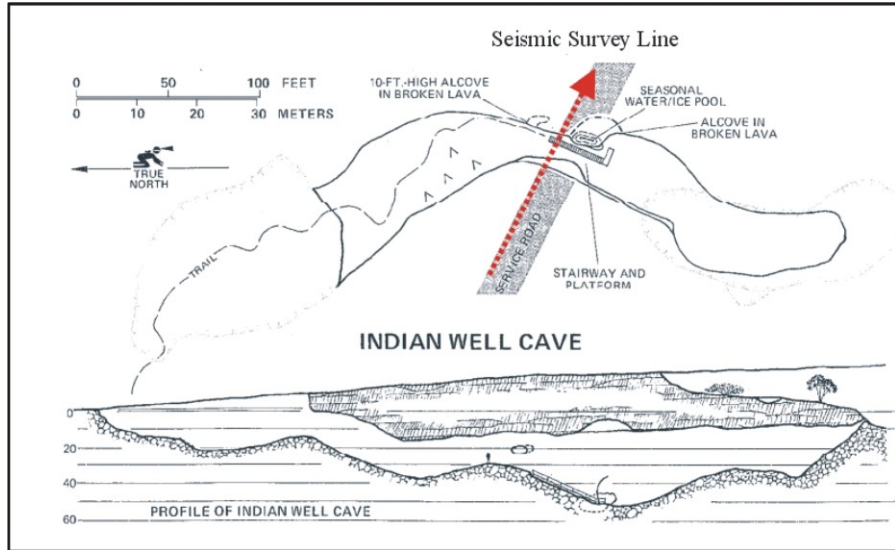


Figure 29. Map. HRSW survey line over Indian Well Cave. ⁽⁶⁾

Table 8. Geophone coordinate locations over Indian Well Cave.

ID	Easting (m)	Northing (m)	Elevation (m)
Geophone 101	624183.36	4619014.2	1428.40
Geophone 111	624188.69	4619011.36	1428.51
Geophone 121	624194.07	4619008.55	1428.63
Geophone 131	624199.42	4619005.77	1428.69
Geophone 141	624204.77	4619002.99	1428.75
Geophone 151	624210.11	4619000.2	1428.83
Geophone 161	624215.45	4618997.43	1428.89
Geophone 171	624220.81	4618994.76	1428.94
Geophone 181	624226.22	4618992.17	1428.97
Geophone 191	624231.64	4618989.56	1429.04
Geophone 196	624234.34	4618988.25	1429.08

All coordinates are listed in NAD 83/UTM Zone 10.

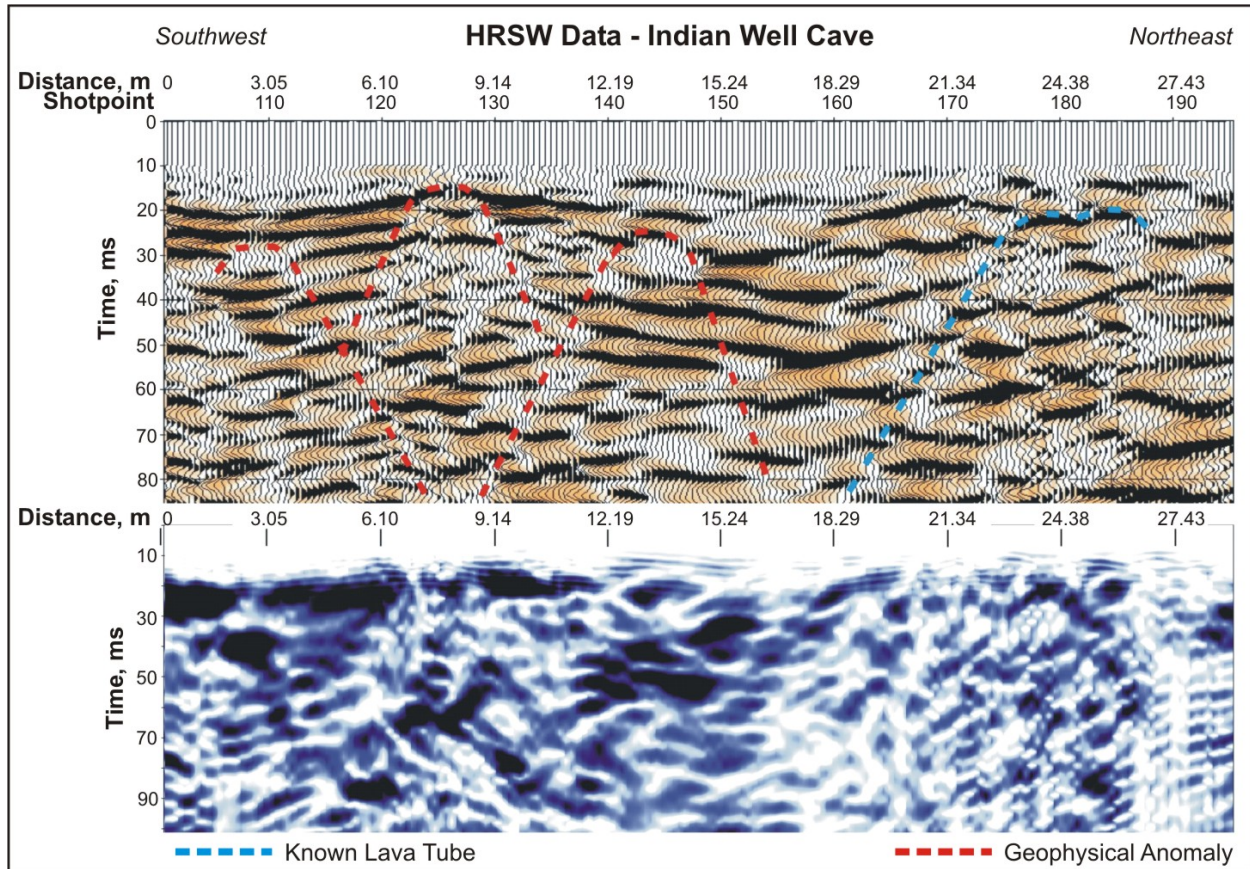


Figure 30. Cross Section. HRSW data collected over Indian Well Cave.

The known cave beneath this profile is centered at shot point 180 and extends about 4.0 m (13.1 ft) on either side of this point. The stacking velocity in the vicinity of the known cave is approximately 1,356 m/sec (4449 ft/sec), and the expected overburden is approximately 8.8 m (28.9 ft) thick. The reflection from the top of this lava tube should then occur 13 ms below the start of the data (the ground surface is at 10 ms on this line). A reflection event is evident at this level, with a zone of incoherent seismic reflectors underneath it. The lava tube is evident from a destructive interference diffraction pattern that extends down to the left from the west (left) edge of the cave resulting in a linear region where the seismic reflectors are disjointed and have lower amplitudes. This zone is outlined in blue.

A suspected lava tube occurs at shot point 126, and appears to be approximately 3.7 m (12.1 ft) across. This anomaly originates about 4.0 m (13.1 ft) below the ground surface, and is evidenced by an arcuate reflection event overlying a zone of low amplitudes bounded on either side by diffractions. The diffractions on either side are located at shot points 109 and 144.

4.3.3 Comparisons

Figure 31 displays the anomalous zones at the Indian Well Cave site. Indian Well Cave was detected in the HRSW reflection, magnetics, and electrical resistivity data sets. All interpreted

locations correspond well with each other. Additional anomalies were selected along the entire length of the road with each of the methods, although the locations and size interpretations varied widely. Of the methods used, the electrical resistivity and magnetic methods provided the most spatially consistent locations. The GPR method did not, in this case, show anomalies over the known cave site.

4.4 MONUMENT ROAD CAVE

4.4.1 Site Description

LBNM officials suggested that this cave might be appropriate for geophysical testing. The shadowed area shown at the bottom of Figure 32 is one of the entrances to Monument Road Cave. It has two large openings that are located on either side of the road. The cave is 76.8 m (252.0 ft) in length and is oriented northeast to southwest ⁽¹⁷⁾. The depth from the road surface to the roof of the cave is 5.5 m (18.0 ft). The cave has a width of 12.2 m (40.0 ft) and a height of 5.5 m (18.0 ft) underneath the road. The entire floor of the cave is covered with debris ranging in size from pebbles to boulders. Some areas in the cave contain coralloid on the walls, a type of mineral deposit left by evaporation of mineral rich groundwater ⁽¹⁷⁾. This site was selected because it is a large cave beneath thin overburden.

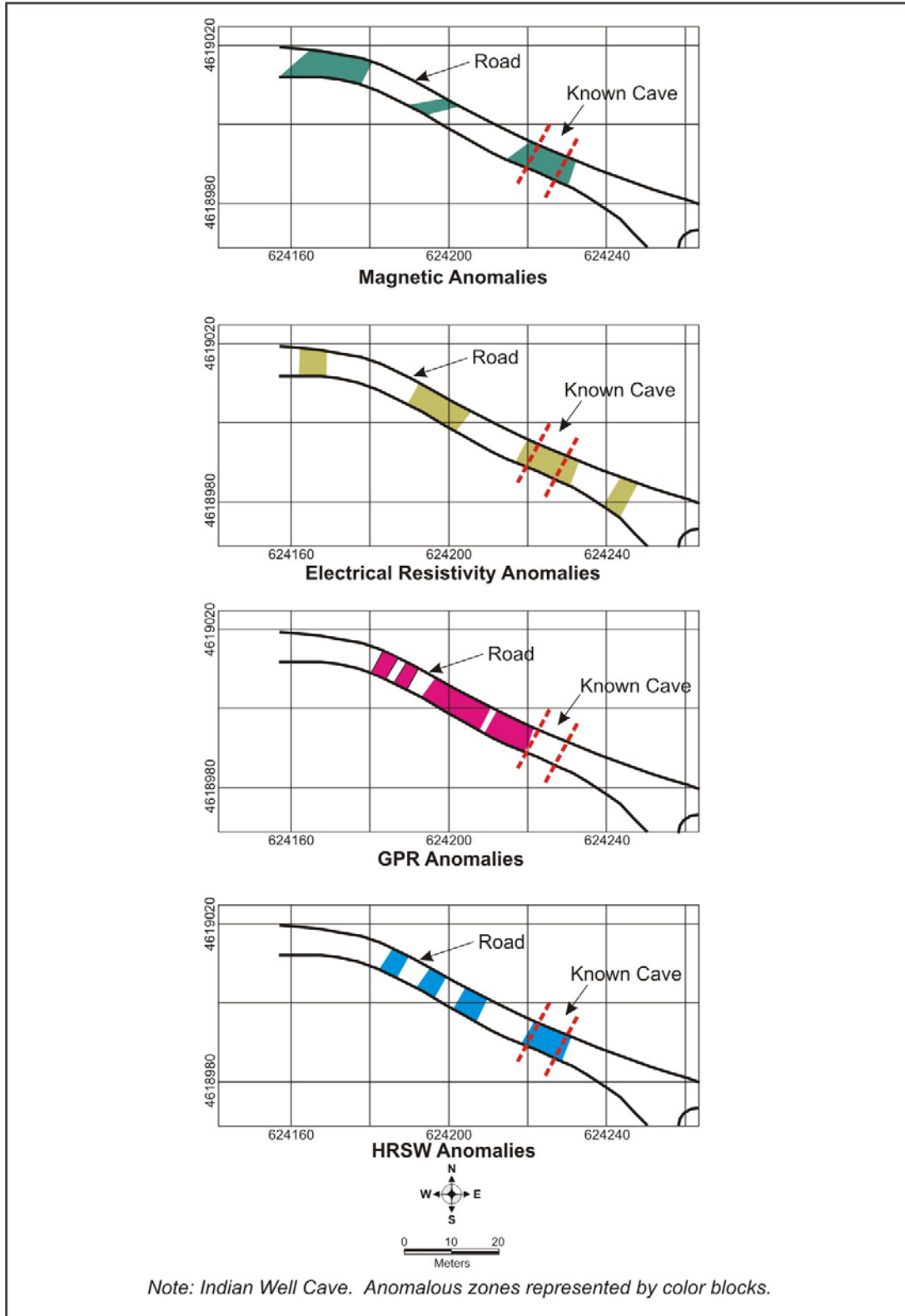


Figure 31. Map. Comparison of anomalous zones at Indian Well Cave.

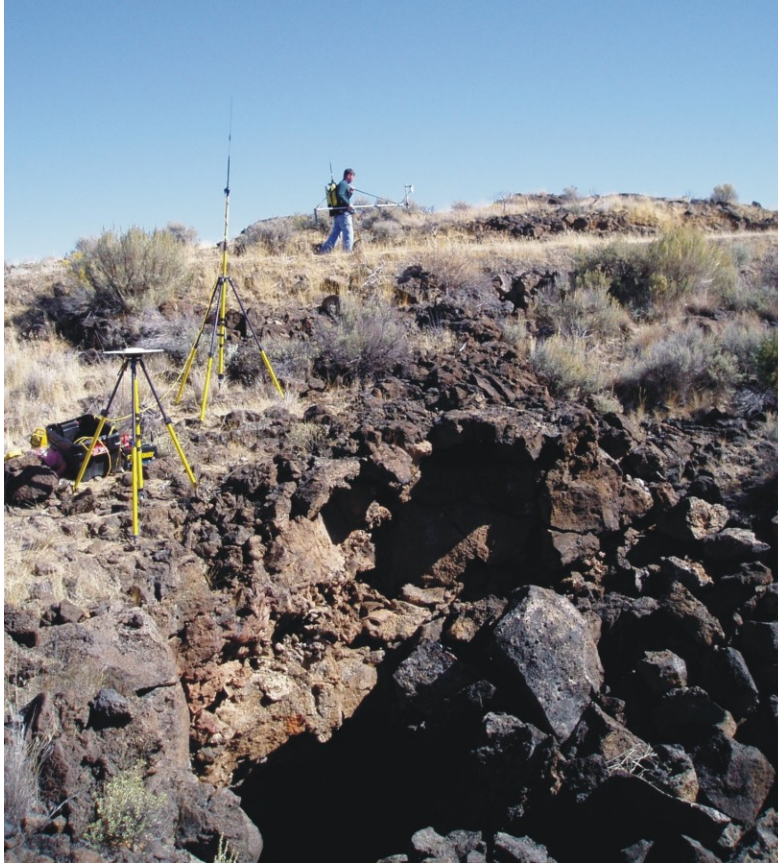


Figure 32. Photo. Monument Road Cave.

4.4.2 Data Analysis and Interpretation

Ground Penetrating Radar

Figure 33 is a plan view map, obtained from LBNM officials, that illustrates the approximate location of the GPR survey lines over Monument Road Cave. Exact coordinates of the starting and ending points of the three GPR lines are listed in Table 9. Approximately 53.3 m (174.9 ft) of data were collected along each of three profiles at Monument Road Cave using the 200 and 400 MHz antennae. In general all profiles correlate well with each other and show many of the same characteristics. There is a distinct difference in the amplitudes evident in the three profiles for both the 200 and 400 MHz antennae. Although the same patterns are detected along the profile from line to line there is a decrease in the amplitude of the events from Line 3 to Line 1. It is unclear what may be causing this but it may be related to the material used to construct the road or road base. Figure 34 displays the GPR data.

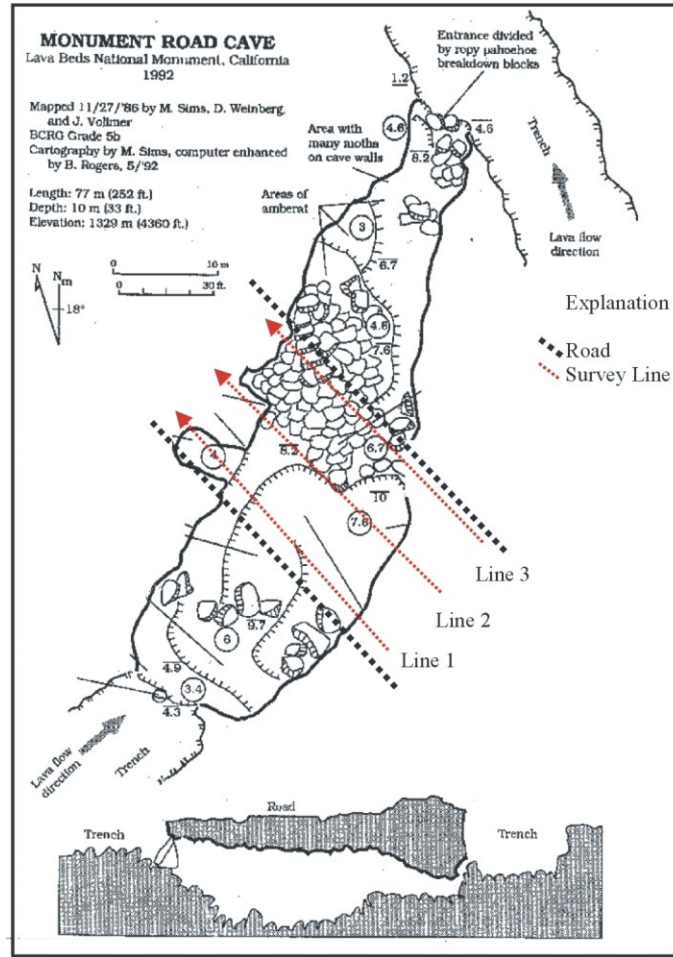


Figure 33. Map. GPR survey lines at Monument Road Cave. ⁽¹⁷⁾

Table 9. GPR survey line coordinates over Monument Road Cave.

Line #	North End Point		South End Point	
	Easting (m)	Northing (m)	Easting (m)	Northing (m)
Line 1	619707.33	4625439.54	619722.25	4625386.67
Line 2	619711.69	4625439.04	619725.24	4625386.82
Line 3	619715.83	4625439.19	619728.64	4625386.73

All coordinates are listed in NAD 83/UTM Zone 10

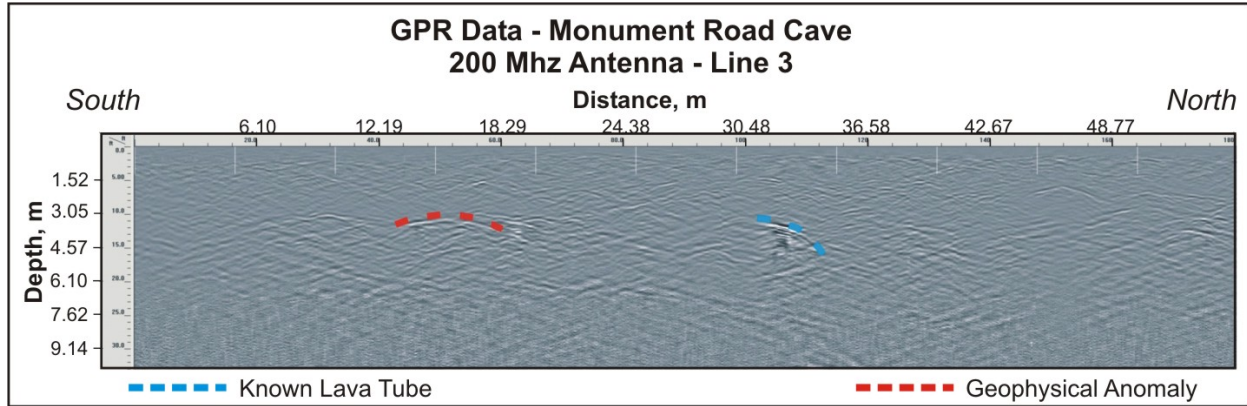


Figure 34. Profile. GPR data collected along Line 3 at Monument Road Cave.

The GPR data collected at Monument Road Cave shows the same types of features as the data collected at the other three sites. Multiple diffractions are present with areas of concentrated high amplitude diffractions and other areas having low amplitude diffractions. From the data collected over Line 1, two anomalies were selected. An interpreted unknown lava tube is outlined in red at approximately 15.2 m (49.9 ft) along the profile. The second anomaly is outlined in blue, which is the approximate known location of the cave, at 32.6 m (107.0 ft) along the profile.

Magnetic Method

The magnetic data showed a large positive anomaly coincident with the known cave location. Figure 35 displays the magnetic data in both plan and profile view. A second large anomaly, as indicated by the positive amplitude magnetic field, is located 45.7 m (150.0 ft) south of the known cave and may represent an unknown cave.

Electrical Resistivity

Figure 36 displays the segment of the electrical resistivity survey line where it passes over Monument Road Cave ⁽¹⁷⁾ and Table 10 gives the coordinates of the end points and center points of the survey line. Figure 37 shows the electrical resistivity profile collected over Monument Road Cave plotted from south to north. The data collected at Monument Road Cave has unique characteristics when compared to the data collected at the other sites. A highly resistive band of material occurs in the center of the section that encompasses five possible voids, including the known cave. A less resistive layer, approximately 1.2 m (3.9 ft) in depth, rests on top of this layer. The overall resistivities for this site appear lower than the resistivities obtained at the other sites, although, being generally over 600 ohm-m, they are still quite high. The lower resistivity strip near the surface may result from fill material deposited when the road was created, or possibly weathered material.

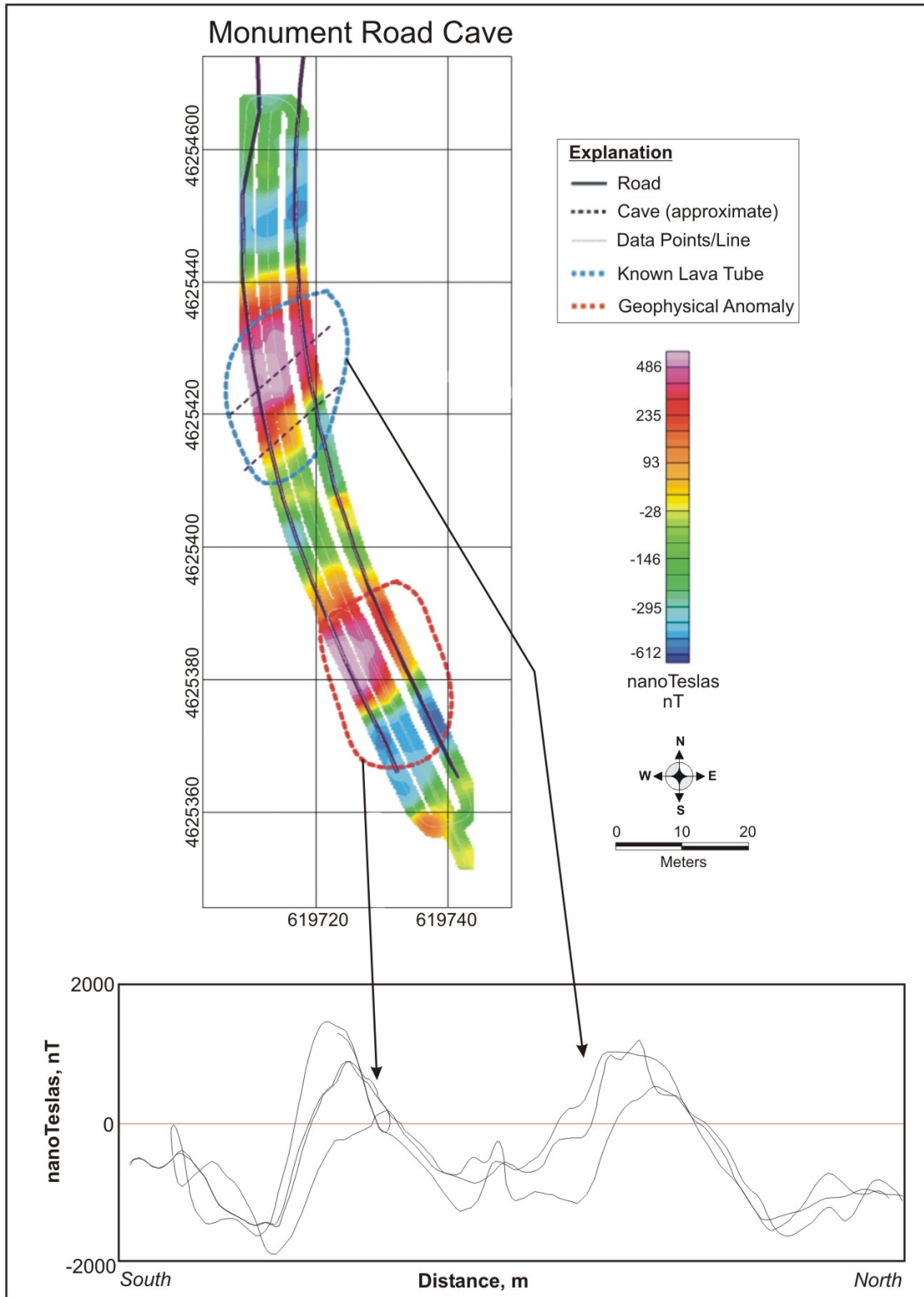


Figure 35. Map. Plan and profile view of magnetic data collected over Monument Road Cave.

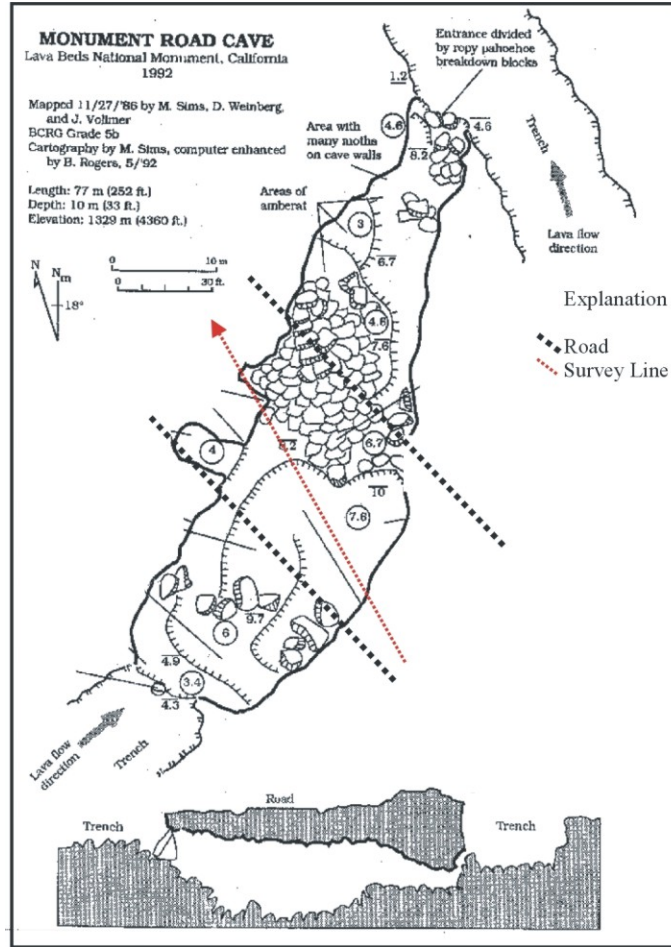


Figure 36. Map. Electrical resistivity survey line at Monument Road Cave. ⁽¹⁷⁾

Table 10. Electrical resistivity line survey coordinates over Monument Road Cave.

ID	Easting (m)	Northing (m)
Point 1 (south end point)	619737.25	4625369.32
Point 2	619725.24	4625386.82
Point 3	619714.86	4625407.23
Point 4	619711.69	4625439.04
Point 5 (north end point)	619711.43	4625465.65
All coordinates are listed in NAD 83/UTM Zone 10		

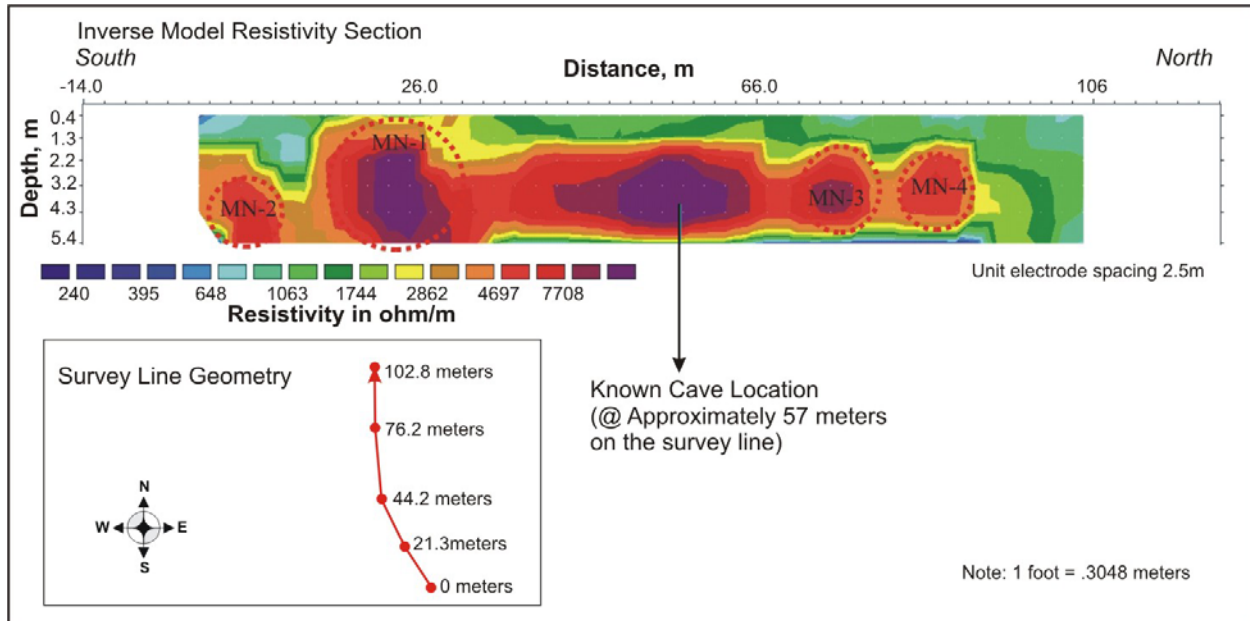


Figure 37. Cross Section. Electrical resistivity data collected over Monument Road Cave.

There is an anomalous resistivity high of 14,300 ohm-m at the location of the known cave, and it is likely that this results from the void space in the cave. The interpreted depth to the top of the void is 3.0 m (9.8 ft). The width of the cave is interpreted to be approximately 12.5 m (41.0 ft), which agrees with survey data. The interpreted height of the cave, at only 2.4 m (7.9 ft), is much less than the measured height of 5.4 m (17.7 ft). However, more information at greater depths is needed to fully characterize the cave

MN-1 is a large anomaly with a maximum value of 12,000 ohm-m at a depth of 3.0 m (9.8 ft). The interpretation section (Figure 37) suggests that the depth to the top of this feature is about 2.2 m (7.2 ft) and the depth to its bottom is about 5.5 m (18.0 ft); however, more information at greater depths is needed to characterize the bottom of this anomaly. The interpretation of the anomaly over the cave showed that the interpreted depth was too shallow. Based on these results it is possible that the interpreted depth to the source of this anomaly, which may be an unknown cave, may be too shallow and the depth to its bottom may be too small.

MN-2 is located on the southern side of the traverse and appears slightly deeper than the other anomalies. More survey information at a greater depth is needed to fully characterize this anomaly. MN-3 and MN-4 have maximum values of 8,300 ohm-m and 6,459 ohm-m, respectively. It is possible that each of these anomalies represents small cavities.

Seismic Reflection

Figure 38 displays the approximate location of the HRSW survey line as it passed over Monument Road Cave⁽¹⁷⁾ and Table 11 gives the location of every tenth geophone along the geophysical survey line. The Monument Road Cave profiles are included as Figure 39 and in Appendix D.

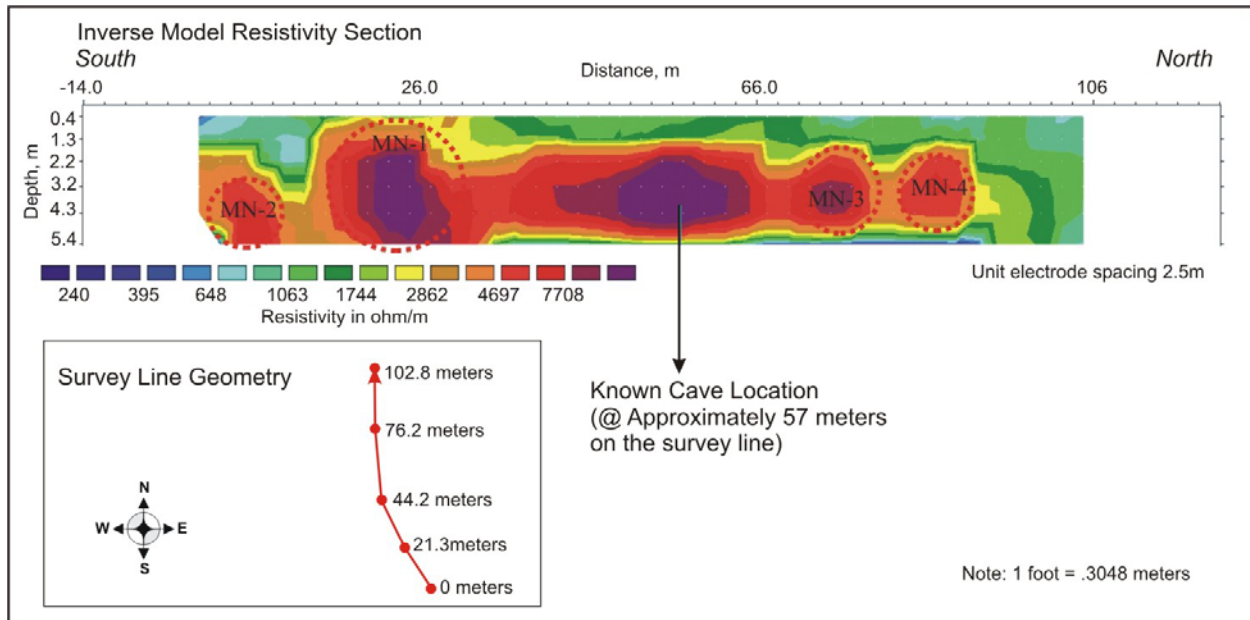


Figure 38. Map. HRSW survey line at Monument Road Cave.⁽¹⁷⁾

The seismic data is dominated by reverberating reflection events, indicating the presence of a shallow subsurface layer with a high velocity contrast. A scoria bed between lava flows could produce such an effect. The known cave is centered on shot point 165, extending 6.1 m (20.0 ft) on either side of this point. Zero time on the section is at an elevation of 1311.0 m (4301 ft).

Table 11. Geophone coordinate locations over Monument Road Cave.

ID	Easting (m)	Northing (m)	Elevation (m)
Geophone 101	619724.00	4625386.98	1303.24
Geophone 111	619722.34	4625392.77	1303.06
Geophone 121	619720.66	4625398.60	1302.85
Geophone 131	619719.05	4625404.42	1302.64
Geophone 141	619717.48	4625410.20	1302.44
Geophone 151	619715.91	4625415.97	1302.25
Geophone 161	619714.34	4625421.73	1302.07
Geophone 171	619712.93	4625427.58	1301.85
Geophone 181	619711.45	4625433.40	1301.63
Geophone 191	619710.08	4625439.25	1301.42
Geophone 196	619709.43	4625442.19	1301.31

All coordinates are listed in NAD 83/UTM Zone 10.

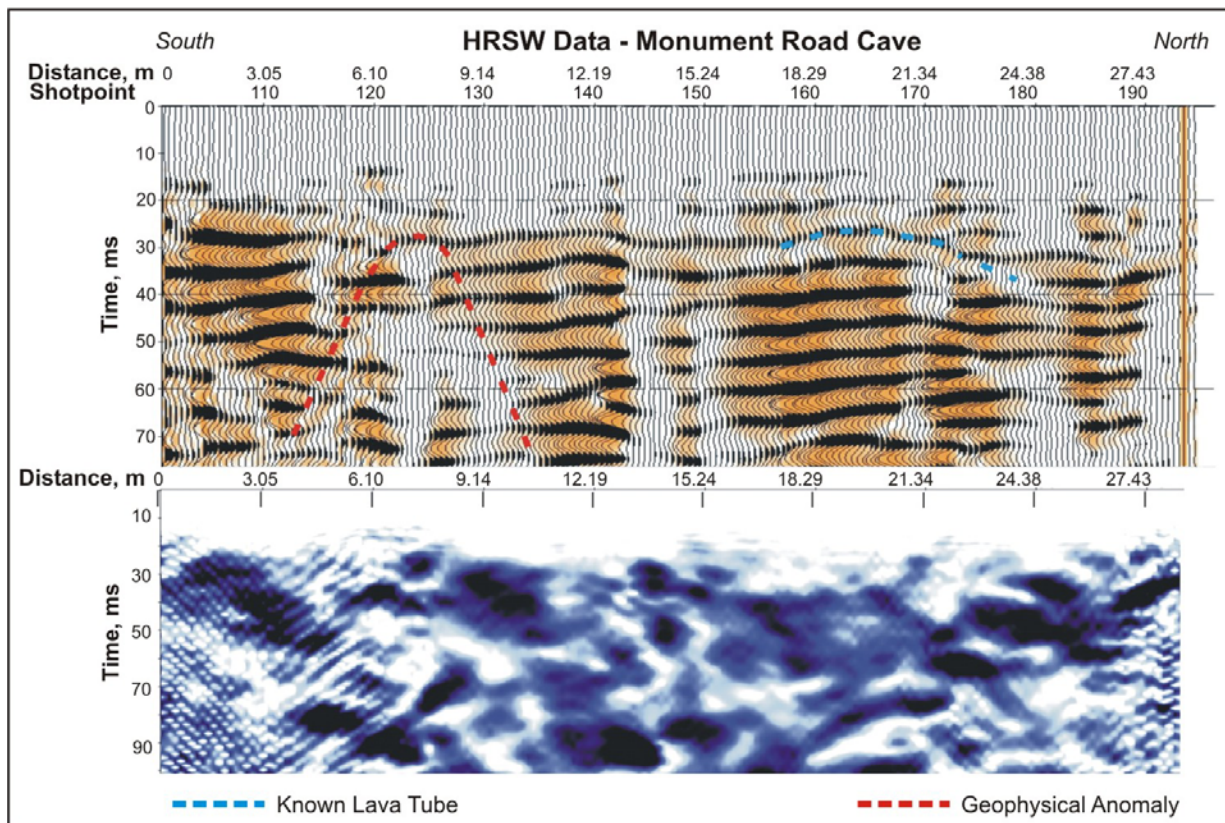


Figure 39. Cross Section. HRSW data collected over Monument Road Cave.

The stacking velocity in the vicinity of the known cave is 914 m/sec (2999 ft/sec), which is considerably slower than velocities seen at the other lava tube sites. As a result, the anomaly from the known cave should occur 12 ms below the ground surface. The ground surface is at 14 ms on this line. An arcuate reflector can be seen at this point, but diffractions are not clearly evident. Strong reverberations occur beneath this anomaly, but they do not retain the arcuate shape of the top of the cave reflector. This indicates that the shallow layering causing the reverberations lies between the ground surface and the top of the cave.

A suspected lava tube is interpreted as being centered on shot point 123 and highlighted in red. The interpretation is based on an arcuate reflector over a disturbed zone. This anomaly occurs at 13 ms below the ground surface and is about 2.4 m (7.9 ft) across.

4.4.3 Comparisons

Figure 40 shows the anomalous zones interpreted from the different data sets recorded at this site. Monument Road Cave was detected with the HRSW, electrical resistivity, and magnetic data sets. All of the interpreted locations and dimensions correspond well with each other and with the surveyed location of the cave. Additional anomalies were selected to the south of the known cave in each of the methods. As with some of the other sites, there appears to be better correlation between the electrical resistivity and magnetic data sets, rather than the HRSW and the GPR data sets. However, at this site, all of the methods apart from GPR show anomalies coincident with the known cave. In addition to identifying the correct location of the cave, the magnetic method also appeared to predict its trend.

4.5 BEARPAW BRIDGE

4.5.1 Site Description

Bearpaw Bridge is located between Merrill Cave and Bearpaw Cave. The bridge is oriented in an east to west direction. On either side of the bridge, the roof of the cave has collapsed leaving large amounts of rubble consisting of volcanic boulders in huge pits. The cave dimensions were obtained from a plan map from The Lava Beds Book. The depth from the road surface to the bottom of the cave is approximately 10.5 m (34.4 ft) with the maximum overburden thickness of approximately 6.4 m. The cave is approximately 15.2 m (49.9 ft) wide with a height of 3.0 m (9.8 ft) below the road surface. Electrical resistivity data were collected along the road at this location. Figure 41 shows both a plan and profile view of the Bearpaw Bridge ⁽⁶⁾ with the approximate location of the electrical resistivity line superimposed on the plan map. Figure 42 is a photo of Bearpaw Bridge. Only electrical resistivity data were collected over Bearpaw Bridge.

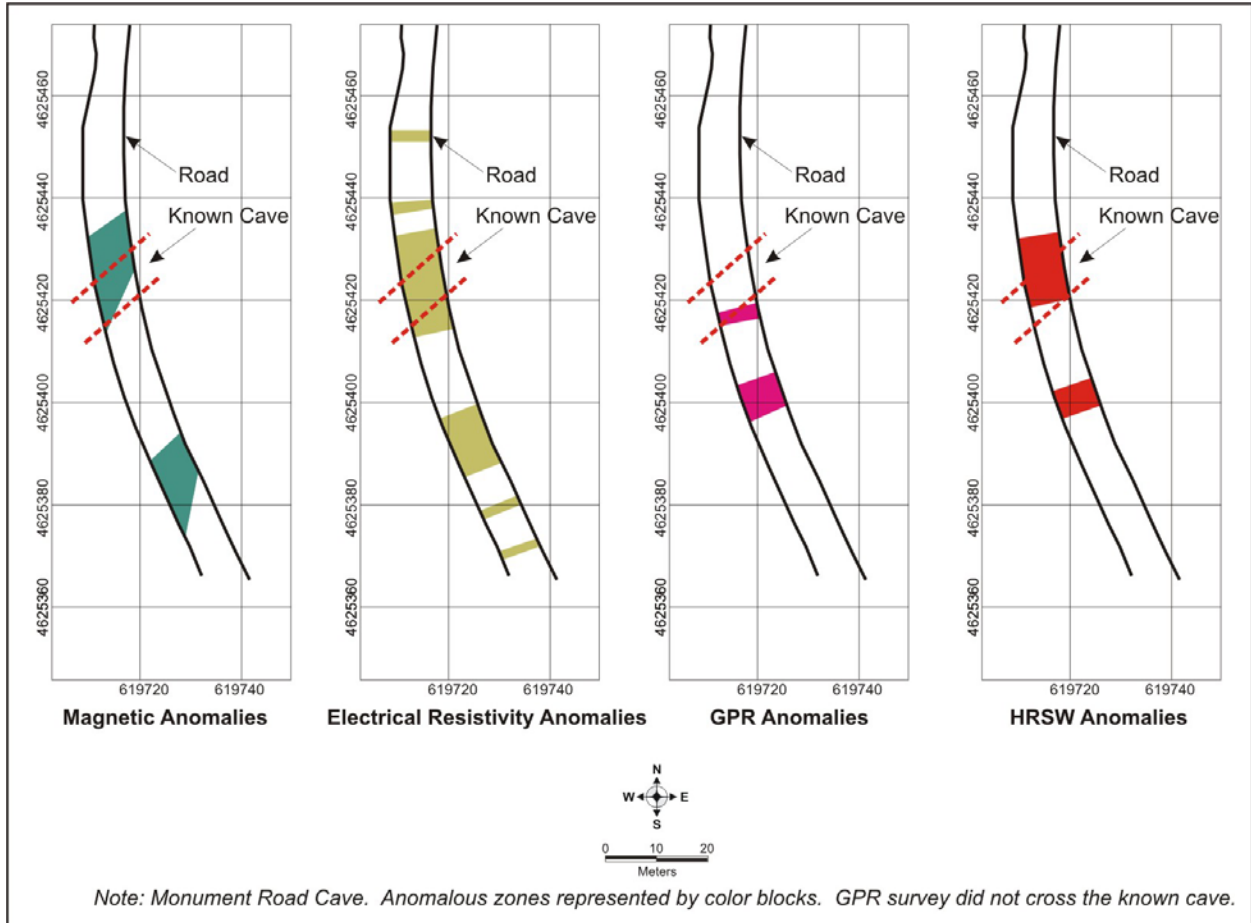


Figure 40. Map. Comparison of anomalous zones at Monument Road Cave.

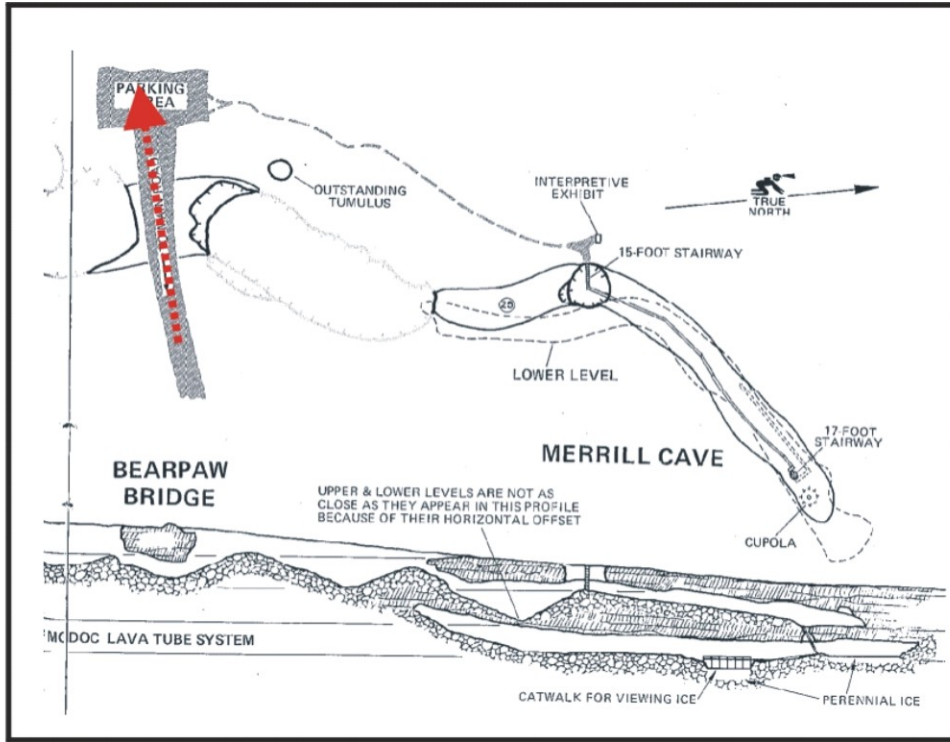


Figure 41. Map. Electrical resistivity survey line on Bearpaw Bridge. ⁽⁶⁾



Figure 42. Photo. Bearpaw Bridge.

4.5.2 Data Analysis and Interpretation

Electrical Resistivity

The interpreted resistivity data is shown in Figure 43. Three resistive anomalies are observed, labeled BP-1, BP-2 and the large resistive anomaly coincident with the cave location. The center of this anomaly is located at approximately 41.2 m (135.2 ft) along the survey line. The maximum resistivity value at the cave location, located at 40.9 m (134.2 ft) to the east and along the bottom edge of the data, is 84,400 ohm-m. More information at greater depths is needed to fully characterize this anomaly.

BP-1 is a large anomaly located along the lower western (left) portion of the geoelectric cross section. This anomaly has a large lateral extent, approximately 15 m (49.2 ft). Resistivity data at greater depths are needed to fully characterize this anomaly. BP-2 is a small anomaly located near the surface at approximately 30 m (98.4 ft) along the survey line. It has a maximum resistivity value of 64,439 ohm-m and is located less than a meter below the surface. The diameter of this anomaly is approximately 2.5 m (8.2 ft).

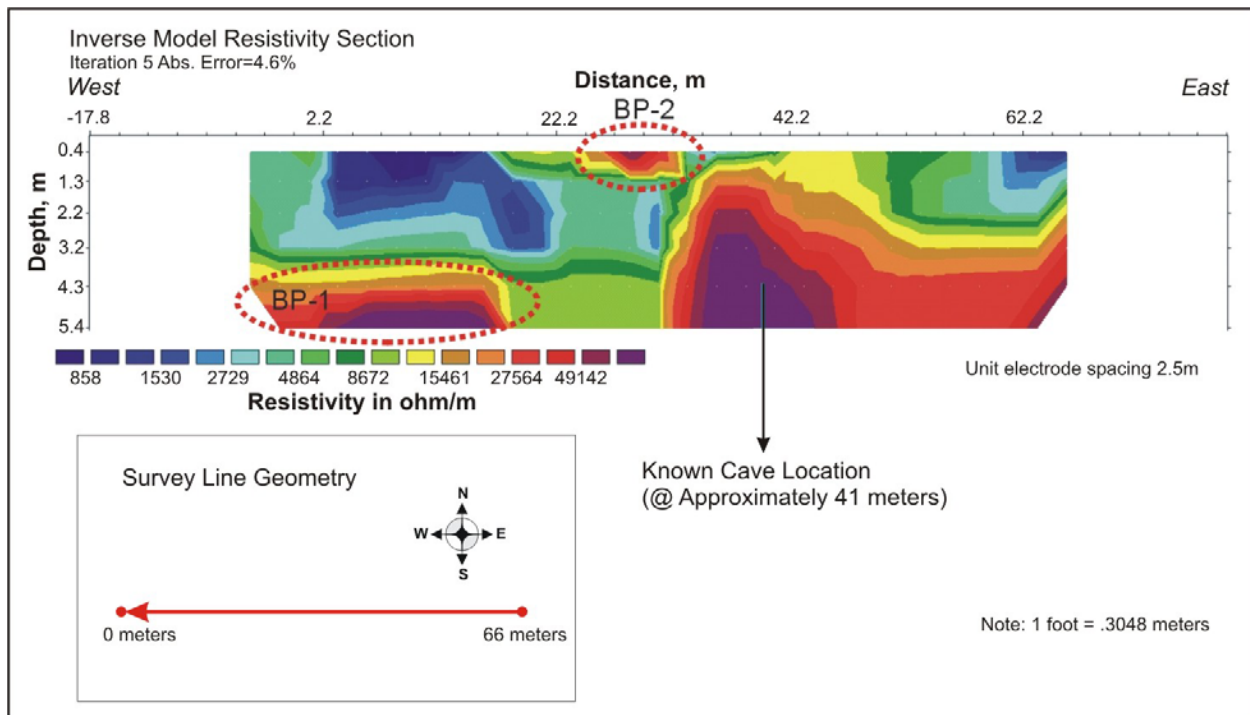


Figure 43. Cross Section. Electrical resistivity data collected on Bearpaw Bridge.

4.5.3 Comparisons

Only electrical resistivity data were collected over Bearpaw Bridge. Therefore, no comparisons are possible at this site.

4.6 HERCULES LEG CAVE – KNOWN AND UNKNOWN SECTIONS

4.6.1 Site Description

The Hercules Leg Cave, pictured in Figure 44, is part of a cave system located on the southern end of Cave Loop Road and to the east of the Master Tube. Hercules Leg Cave meanders across the area and passes under the road several times. The cave contains many geological features including copulas, overburden collapse, “aa” cauliflower, lava waves, skylights, and some of the finest lava ribs in the park ⁽⁶⁾. The overburden thickness in this area varies between approximately 2.7 m to 3.4 m (8.9 ft to 11.2 ft). Figure 45 shows two plan view maps of this cave. The first part is considered a “known” area, outlined in blue, where the cave travels underneath the road at least twice. For this report, different names are given to each individual section of the Hercules Leg Cave that passes underneath the road in order to allow clearer descriptions. The “Hercules Leg Cave – North” refers to the northernmost part of Hercules Leg Cave that passes underneath the road. At this location the cave has a width of 9.8 m (32.2 ft) and a height of 0.91 m (3.0 ft) at one point underneath the road. The southern portion of the cave, named “Hercules Leg Cave – South” in this report, has a width of 22.3 m (73.2 ft) and a height of 2.4 m (7.9 ft). The second part of this survey site is considered an “unknown” area and is located just north of the known area, outlined in red.

The Hercules Leg Cave was chosen as a survey site because the cave passes underneath the road twice. This will test the capability of the geophysical methods to distinguish multiple caves close to one another. Also, it will test the capabilities of the methods to find shallow voids.



Figure 44. Photo. Entrance at Hercules Leg Cave.

4.6.2 Data Analysis and Interpretation

Ground Penetrating Radar

Figure 46 is a plan view map ⁽⁶⁾ that illustrates the approximate location of the GPR survey lines over the known and suspected locations of Hercules Leg Cave. The exact coordinates of the starting and ending points of the three GPR lines are listed in Table 12.

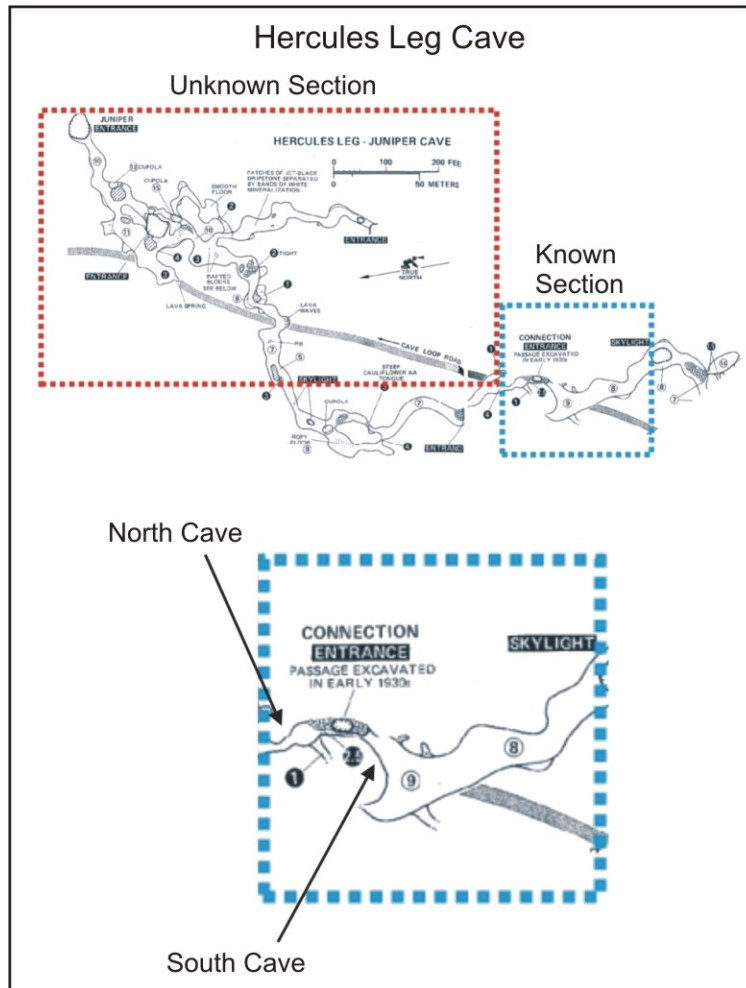


Figure 45. Map. Plan view index map of Hercules Leg Cave. ⁽⁶⁾

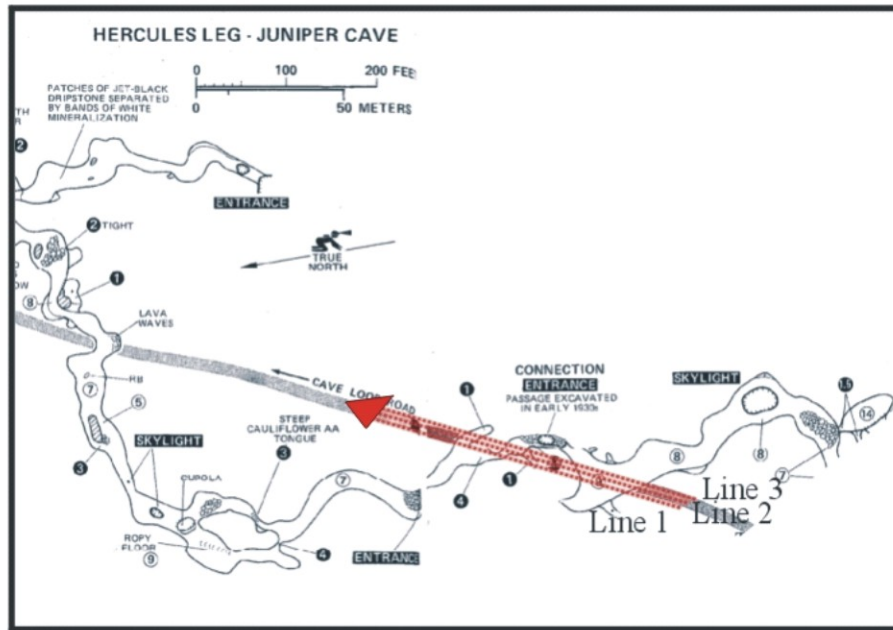


Figure 46. Map. GPR survey line over Hercules Leg Cave. ⁽⁶⁾

Table 12. GPR survey line coordinates over Hercules Leg Cave.

Line #	North End Point		Mid Point		South End Point	
	Easting (m)	Northing (m)	Easting (m)	Northing (m)	Easting (m)	Northing (m)
Line 1	623679.67	4618090.99	623659.54	4618045.37	623637.36	4617996.32
Line 2	623680.86	4618090.54	623660.73	4618044.87	623639.05	4617995.62
Line 3	623681.81	4618090.14	623661.67	4618044.53	623639.96	4617995.28

All coordinates are listed in NAD 83/UTM Zone 10

Approximately 106.7 m (350.1 ft) of data were collected along each of three profiles at Hercules Leg Cave with both the 200 and 400 MHz antennae. Two profiles were collected measuring approximately 53.3 m (174.9 ft) using the 100 MHz antenna. In general, the data from each of the profiles correlate well with each other and show many of the same characteristics. The known lava tubes at Hercules Leg Cave were the most readily identifiable lava tubes in all of the GPR cross sections collected at LBNM. Figures 47 and 48 display the 200 MHz data collected along Line 1, which crosses the region of known caves along with the area where caves are suspected to occur, respectively. Anomalies coincident with the known caves are clearly evident in the processed data. The clarity of the anomalies is probably due to the small amount of overburden present and possible lack of fracturing and blistering in the area. Tape and compass surveying estimated 2.7 m (8.9 ft) of overburden at Hercules Leg South Cave and 3.4 m (11.2 ft) of overburden at Hercules Leg North Cave, compared to 2.1 and 1.8 m (6.9 and 5.9 ft),

respectively, of interpreted overburden from the GPR Line 1 profile. Thus, the interpreted and measured depths are reasonably comparable. Surveying methods provided width estimates of 22.3 m (73.2 ft) for the Hercules South Cave and 9.8 m (32.2 ft) for the Hercules North Cave. Width estimates using the GPR data indicated 21.3 m (69.9 ft) for the Hercules South Cave and 12.2 m (40.0 ft) for the Hercules North Cave. A third lava tube has been interpreted from the data and outlined in red at approximately 55.8 m (183.1 ft). This anomaly is slightly deeper, approximately 2.4 m (7.9 ft), and smaller in width than the two known tubes. No other anomalies were selected in this data.

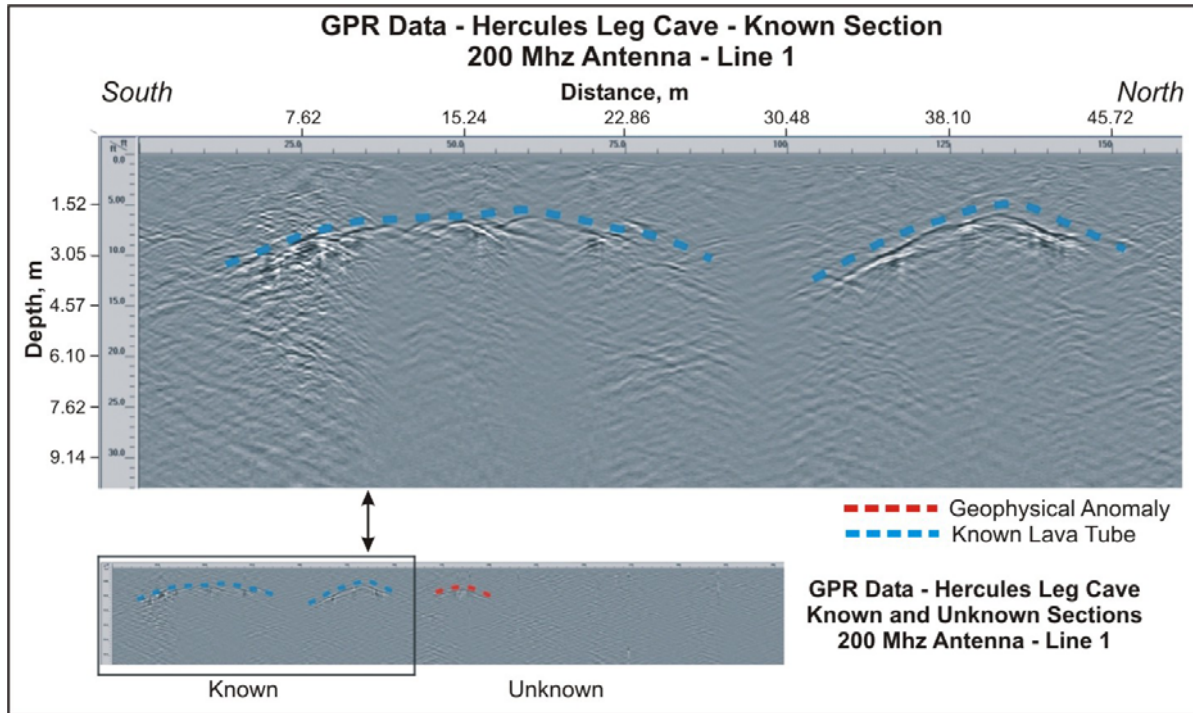


Figure 47. Cross Section. GPR data over the known section of Hercules Leg Cave.

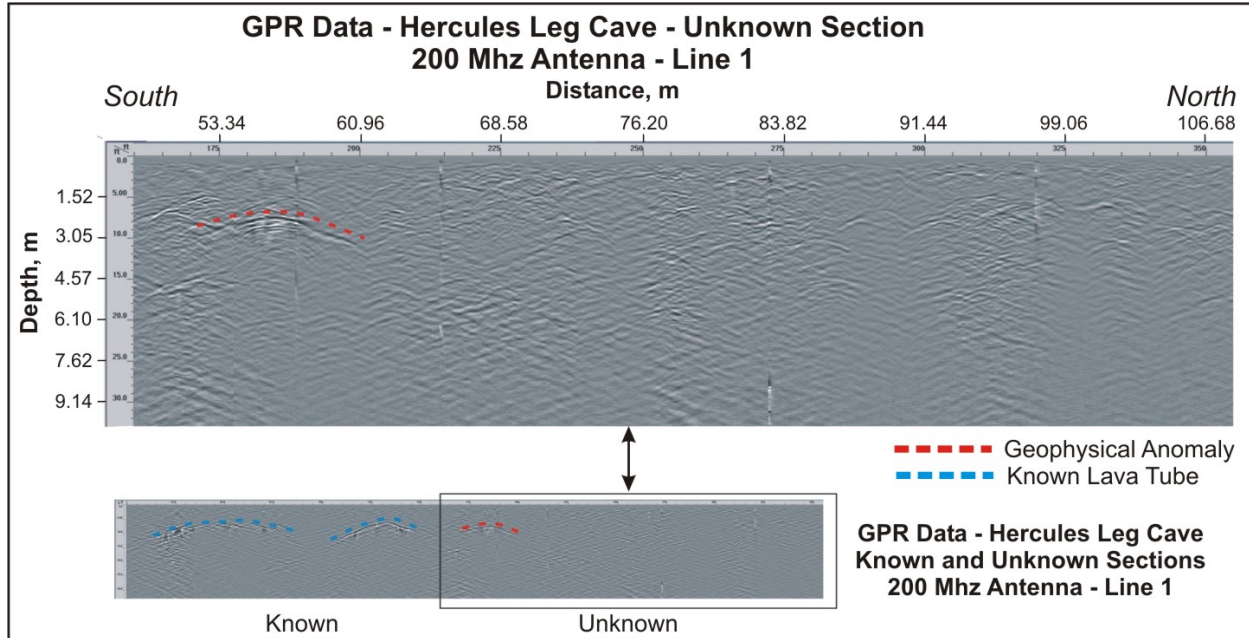


Figure 48. Cross Section. GPR data over the unknown section of Hercules Leg Cave.

Figure 50 shows the magnetic data collected over the section where there are no known lava tubes at Hercules Leg Cave. The magnetic profile illustrates three or four anomalies having amplitudes of a few hundred nanoTeslas superimposed on a more “regional” trend. Although their amplitudes are small, four of these anomalies were selected from the data as the most likely to represent cave locations. The best defined anomaly is located in the middle of the line, and shows a magnetic trough on all three survey lines. The anomaly indicated on the southwestern portion of the line is also fairly well defined and could result from a cave. The remaining two anomalies are less defined and have smaller amplitudes.

Electrical Resistivity

Figure 51 displays the segment of the electrical resistivity survey line where it crosses Hercules Leg Cave⁽⁶⁾ and Table 13 gives the coordinates of the end points and some points internal to the survey line. The resistivity data collected at Hercules Leg Cave are shown in Figure 52. This geoelectric cross section is much longer than those over the other cave sites in order to cross an area where potential, undocumented caves may exist.

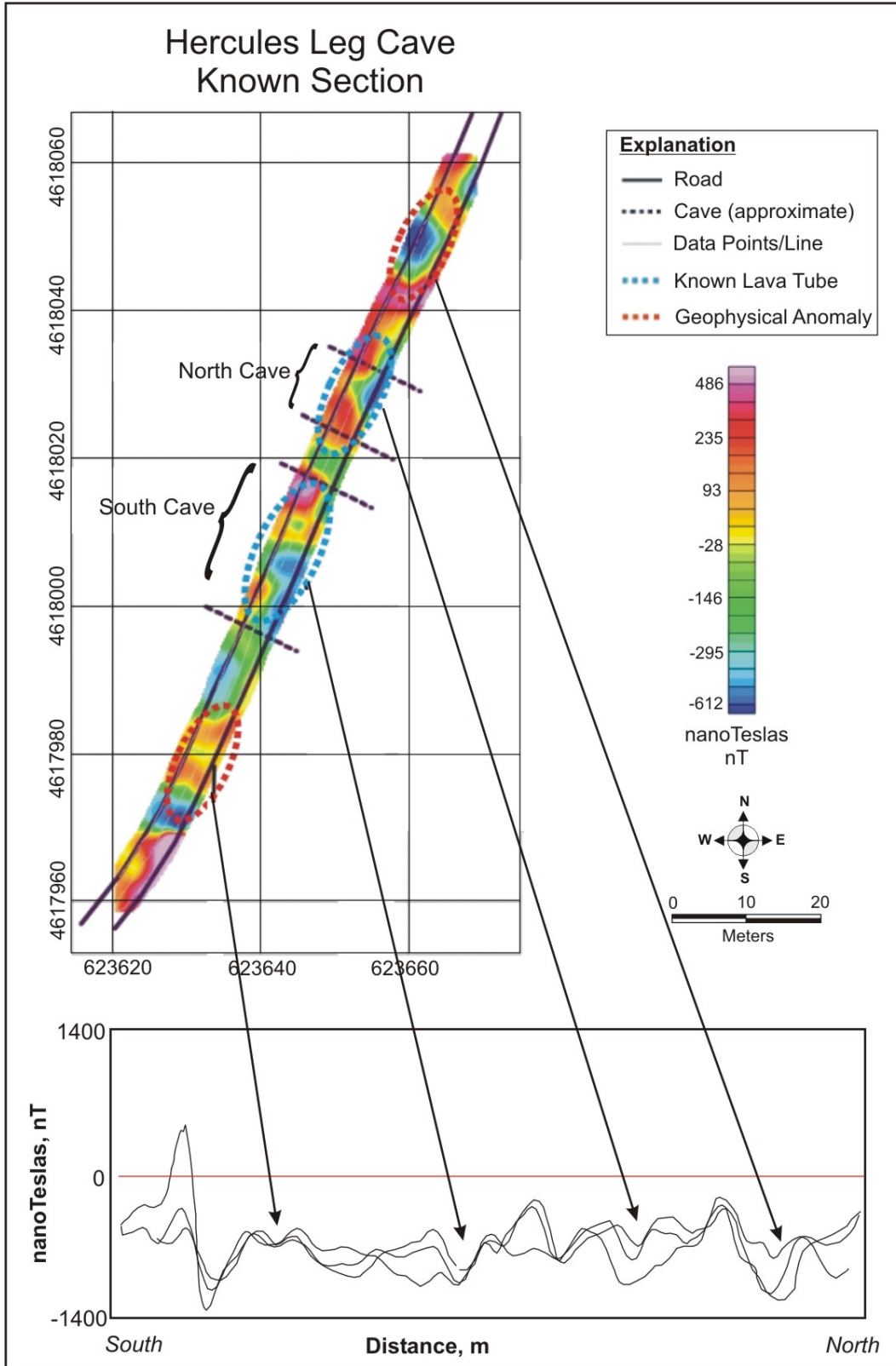


Figure 49. Map. Magnetic data collected over the known section of Hercules Leg Cave.

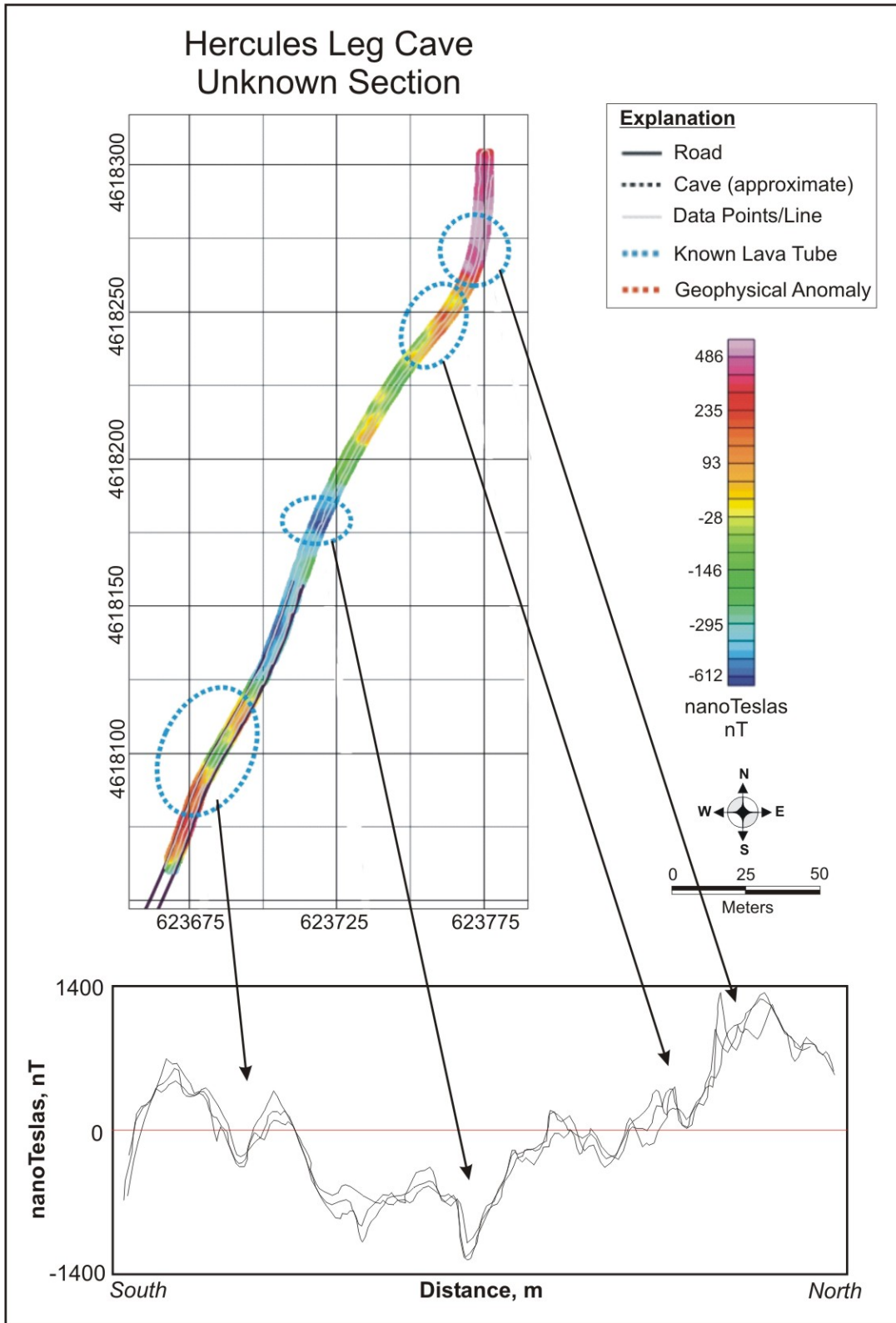


Figure 50. Map. Magnetic data collected over the unknown section of Hercules Leg Cave.

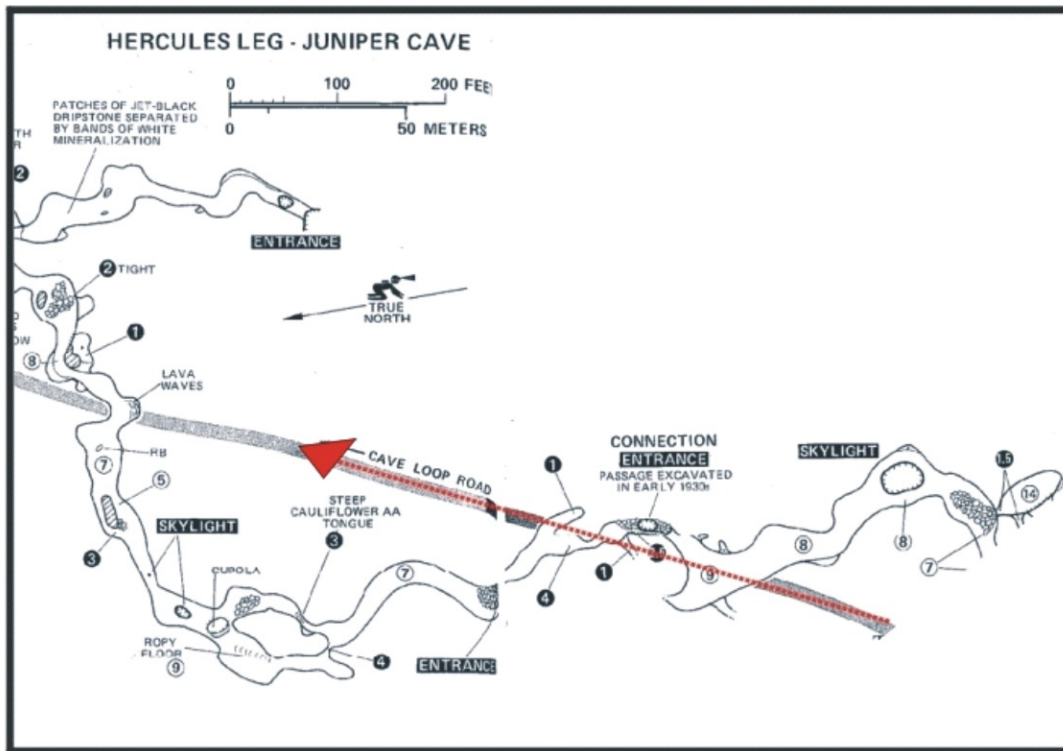


Figure 51. Drawing. Electrical resistivity survey line over Hercules Leg Cave. ⁽⁶⁾

Table 13. Electrical resistivity survey line coordinates over Hercules Leg Cave.

ID	Easting (m)	Northing (m)
Point 1 (south end point)	623628.64	4617972.26
Point 2	623639.05	4617995.62
Point 3	623660.73	4618044.87
Point 4	623680.86	4618090.54
Point 5 (north end point)	623689.58	4618114.58
All coordinates are listed in NAD 83/UTM Zone 10		

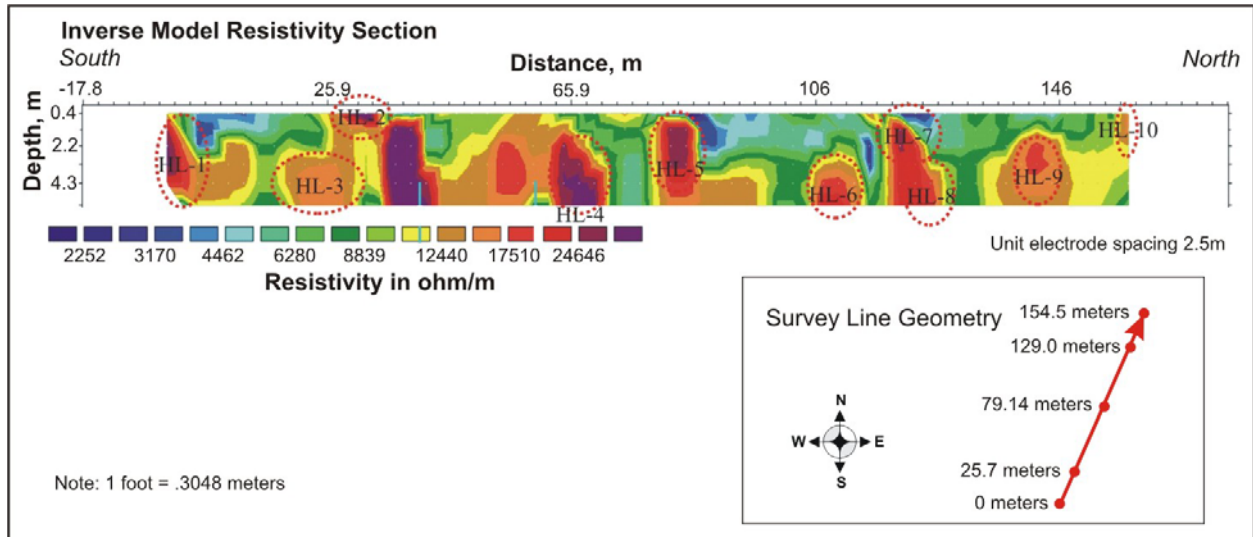


Figure 52. Cross Section. Electrical resistivity data collected over Hercules Leg Cave.

The south cave lies at approximately 42.0 m (137.8 ft) along the traverse and corresponds to a resistivity high at 40.8 m (133.9 ft). The maximum resistivity of this anomaly is 41,600 ohm-m. At this location, this cave passes under the road and immediately loops back under the road. Anomaly HL-3, while having a much smaller amplitude than the anomaly associated with the cave, could be the same cave going under the road. More information at a greater depth is needed to fully characterize this anomaly.

A more complex anomaly occurs at the second known cave, which appears to occur at a saddle between two resistivity highs, one of which is labeled HL-4. The resistivity data appears to indicate either a complex cave structure or possibly two caves.

Anomalies HL-1 and HL-10 are located on the south edge and north edge of the data, respectively. Anomaly HL-1 is quite resistive, whereas anomaly HL-10 is only mildly anomalous. Both anomalies are poorly defined since they are at the ends of the line. Therefore, it is difficult to characterize them without having more data to completely define their shapes. Anomaly HL-2 is a small, near surface anomaly with a maximum resistivity of 38,200 ohm-m. This shallow anomaly, 0.3 m (1.0 ft) below the surface, could be a blister or small surface tube. Anomaly HL-5 is located at 82.3 m (270.0 ft) and has an interpreted depth of 1.2 m (3.9 ft). This too has the potential to represent a small cave. Anomaly HL-6 is shown at 107.0 m (351.0 ft). Since this anomaly is probably located deeper than 5.5 m (18.0 ft), more information at depth is needed to characterize this anomaly. Anomalies HL-7 and HL-8 are shown as two anomalies; however, due to their close proximity, they may have resulted from the same physical feature. Their maximum resistivity values are 25,500 and 21,100 ohm-m respectively. Anomaly HL-9 is an isolated anomaly located at 142.0 m (465.9 ft) at an interpreted depth of 2.0 m (6.6 ft) to the top of the anomaly.

Electrical Conductivity

Electrical conductivity was not a proposed method for testing at LBNM due to the fact that, prior to conducting the surveys, the area was suspected as being generally resistive, with the voids being highly resistive. Although measuring the electrical conductivity is an effective method based on physics, obtaining conductivity measurements using the EM31 in this resistive environment may be difficult. However, due to the rapid data collection rate and the availability of the instrumentation, it was decided to conduct a single test of the EM31 at the Hercules Leg Cave site, taking measurements across the known cave and the region where potential, but unknown, caves may occur.

EM31 data were collected along three lines positioned along the center and along both sides of the road at Hercules Leg Cave. Data were recorded in the vertical dipole mode giving a depth of investigation of up to about 6 m. The quadrature (conductivity) and in-phase components of the electromagnetic field were recorded at 2 hertz using a Polycorder 720 to control the data recording and store the data. The data were coupled with DGPS for positioning.

During processing, the DGPS data were imported into Trimble Geomatics Office (TGO) program and it was reformatted and exported. The EM31 data were imported into the DAT31 program and analyzed for completeness. The reformatted DGPS data were then combined with the EM31 data in DAT31 and it was exported in *.xyz ASCII format. These ASCII files were then read into Oasis montaj where figures were created.

The data, shown on Figure 53, are displayed using a scale of 0 to 10 millimhos/meter (mmhos/m). There is one small conductive anomaly visible in the data and outlined in red. The anomaly is located farther north than the surveyed location of Hercules Leg Cave. This anomaly is not supported by the magnetic method, which was the only other method used at that location. The shape of the anomaly suggests a vertical electrically conductive feature. It is possible that either a spatially rapid increase in the depth of fill, or a change in its composition, could produce the anomaly.

Seismic Reflection

Figure 54 displays the approximate location of the HRSW survey line, which traverses over Hercules Leg Cave ⁽⁶⁾, continuing across an area where caves may occur. Table 14 gives the location of every tenth geophone along the geophysical survey line. The Hercules Leg Cave seismic sections are illustrated in Figure 55 and also included in Appendix D.

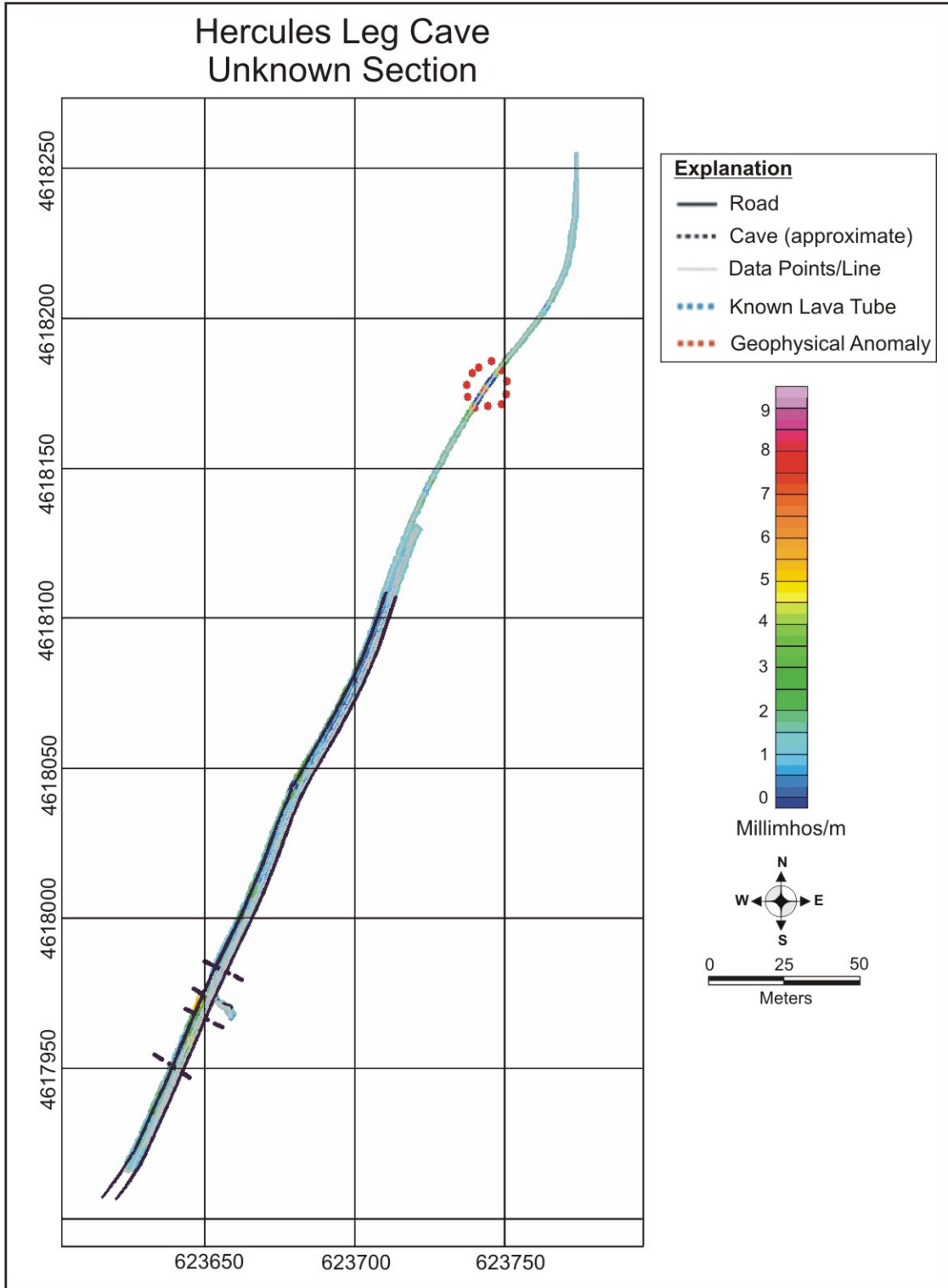


Figure 53. Map. Electrical conductivity data collected over Hercules Leg Cave.

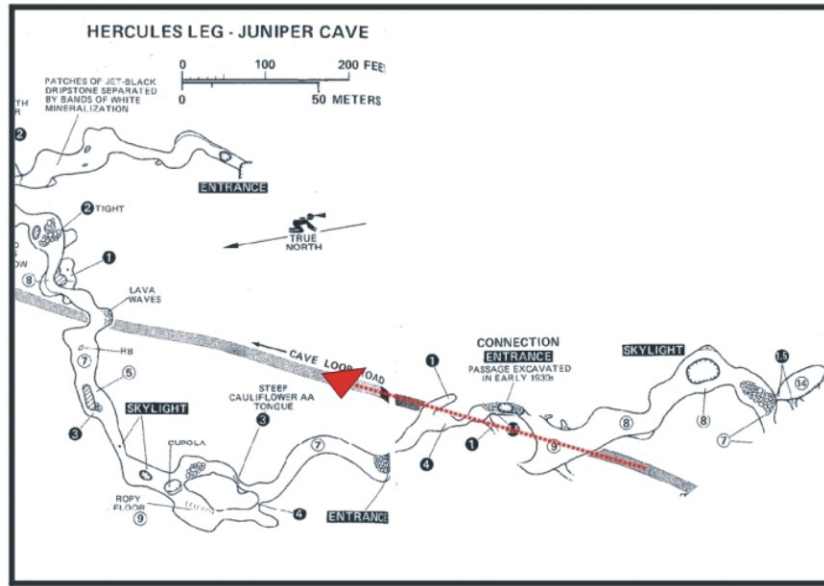


Figure 54. Map. HRSW survey line over Hercules Leg Cave. ⁽⁶⁾

Table 14. Geophone coordinate locations over Hercules Leg Cave.

ID	Easting (m)	Northing (m)	Elevation (m)
Geophone 101	623633.94	4617988.64	1502.51
Geophone 111	623636.44	4617994.16	1502.23
Geophone 121	623638.94	4617999.71	1501.92
Geophone 131	623641.44	4618005.24	1501.56
Geophone 141	623643.94	4618010.73	1501.14
Geophone 151	623646.41	4618016.23	1500.70
Geophone 161	623648.9	4618021.71	1500.27
Geophone 171	623651.41	4618027.22	1499.85
Geophone 181	623653.93	4618032.73	1499.42
Geophone 191	623656.43	4618038.25	1499.01
Geophone 201	623658.93	4618043.66	1498.61
Geophone 211	623661.38	4618049.09	1498.17
Geophone 221	623663.88	4618054.55	1497.73
Geophone 231	623666.36	4618060.02	1497.34
Geophone 241	623668.88	4618065.48	1497.00
Geophone 251	623671.39	4618070.97	1496.69
Geophone 252	623671.65	4618071.5	1496.66

All coordinates are listed in NAD 83/ UTM Zone 10

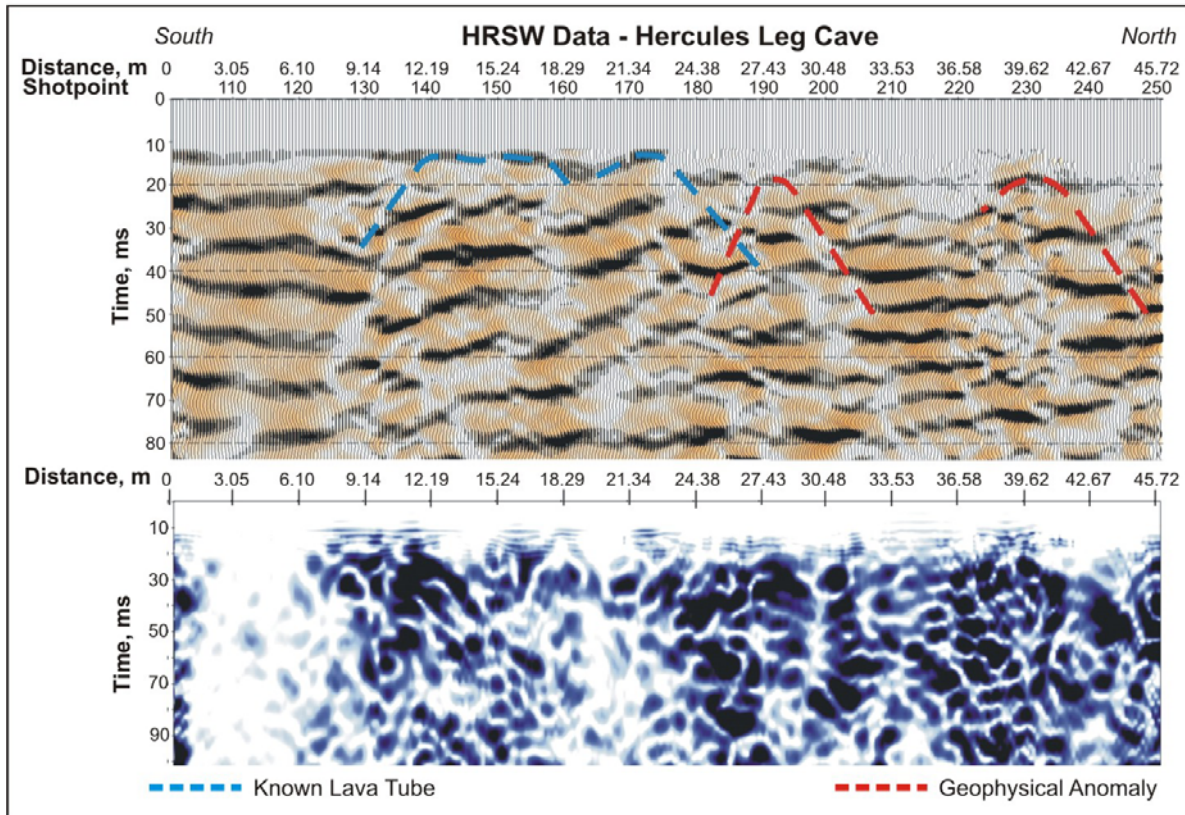


Figure 55. Cross Section. HRSW data collected over Hercules Leg Cave.

The Hercules lava tube passes twice under this profile. The southern cave, located at shot point 145, has a width of approximately 22.3 m (73.2 ft) under the seismic line. The northern cave located at shot point 174 has a width of approximately 9.8 m (32.2 ft) under the line. Both tubes are approximately 3.0 m (9.8 ft) below the ground surface. The seismic velocity in the vicinity of the known cave is 1524 m/sec (5000 ft/sec), so the reflection from the cave should occur about 4 ms below the top of the data. Zero time on this section is at an elevation of 1508.0 m (4947.5 ft).

The reflections from the top of the known caves merge to form the shallowest event between shot points 139 and 176. The top of this wide cave causes a prominent reverberation, as the s-wave energy bounces back and forth between the top of the cave and the ground surface. The reverberating energy continues to the bottom of the section. Faint diffractions are interpreted at the edge of the caves. The small separation between the two caves is not readily evident.

Although sometimes detected, caves within the top 3 to 5 m (9.8 to 16.4 ft) of the subsurface pose a significant problem in HRSW data interpretation. With targets this shallow, the acoustic waves sent into the ground may be distorted and very difficult to separate from other acoustic waves (i.e. ground roll).

Two suspected lava tubes are also interpreted on this profile. The first, centered on shot point 191.5 (628.3 ft), is interpreted based on the presence of both an arcuate reflection and faint diffractions on both sides of this reflection. This source of the anomaly is interpreted to be approximately 7.6 m (24.9 ft) deep with a horizontal dimension of about 2.4 m (7.9 ft).

The second interpreted lava tube is centered on shot point 231, and is evidenced by an arcuate reflection overlying a zone of incoherent reflectors. A faint diffraction occurs on the south side of this anomaly. The interpreted depth to the top of this possible lava tube is approximately 7.6 m (24.9 ft) and its interpreted width is about 4.6 m (15.1 ft).

4.6.3 Comparisons

Figure 56 compares the anomalous zones in the data sets collected over both the known caves at this site along with the area where there are potential, but unknown, caves. These comparisons do not include the electrical conductivity measurements, which were taken using the EM31. The known caves at Hercules Leg Cave (North and South) were detected with the HRSW, electrical resistivity, and GPR methods. The known caves are identifiable in the magnetic data; however, the locations of the known caves were needed to make an accurate interpretation. The North Cave was detected at about the same location with each of the methods. The South Cave was detected in the same general area with the HRSW reflection, magnetic, and GPR methods but is offset approximately 15.2 m (49.9 ft) to the south in the electrical resistivity data. An anomalous zone is located to the southwest of the most southern known cave in both the electrical resistivity and the magnetic data. An anomalous zone is interpreted in all the data for each of the methods just to the north of Hercules Leg North Cave. There is a slight offset, approximately 4.6 m (15.1 ft), in the HRSW data compared to the electrical resistivity, magnetic, and GPR data sets. One additional anomaly was detected to the north with the HRSW data. This anomaly was not observed in the data from any of the other methods. One additional anomalous zone was detected further north in the magnetic data, which corresponds to two anomalous zones in the electrical resistivity data. Overall, the magnetic and electrical resistivity data show anomalies that are spatially coincident while the size of the caves and small overburden thickness benefited the GPR method.

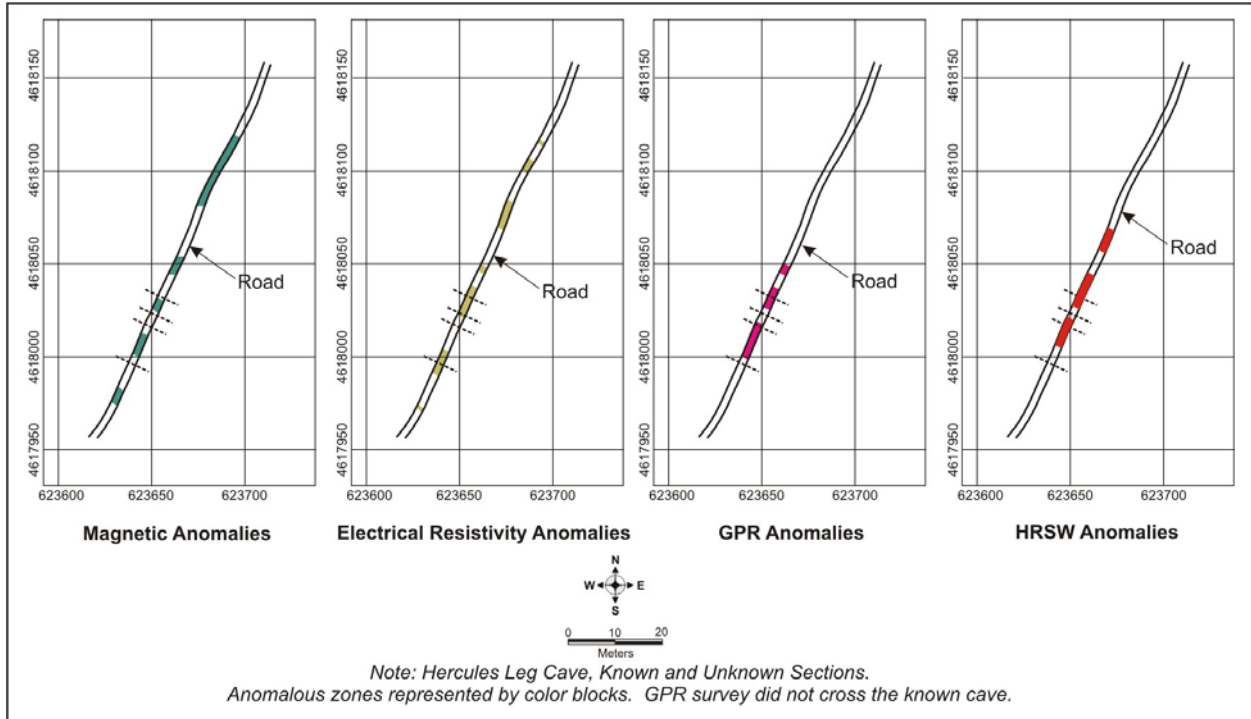


Figure 56. Map. Comparison of anomalous zones over Hercules Leg Cave.

CHAPTER 5.0. DISCUSSION OF RESULTS

The lava tubes profiled at Lava Beds National Monument manifest themselves in each of the geophysical methods. However, each of the lava tube sites has unique aspects with regard to the data collected and interpretation. All of the data interpretations were performed by field personnel, and then reviewed by more experienced geophysicists. The data from each method was interpreted independent of the other data sets, but with an understanding of the local geology at each site. The results of the geophysical surveys, by cave location, are summarized below.

Golden Dome Cave

- Although the GPR cross sections did not cross the known cave location, as mapped by the compass and chain method, there were numerous diffractions present in the data. It is unclear if the GPR method would have detected the Golden Dome Cave.
- The Golden Dome Cave location was very distinct in the magnetic data profile. Two spatially close magnetic highs were present with the cave location being positioned at the depression between the two highs. Two other anomalies, possibly indicating cave locations, were located northeast of the known lava tube.
- The seismic section over Golden Dome Cave is dominated by reverberating reflection events, indicating the presence of shallow scoria beds in this area. An obscure reflection event occurs at the top of the cave, as well as diffractions on each side.

Indian Well Cave

- The thick overburden present severely limited the usefulness of the GPR method. Numerous diffractions are present in the data but are not considered to be associated with the cave.
- Indian Well Cave was successfully located with the magnetic data profile. Two other possible cave locations were selected northwest from the known lava tube. Both anomalies indicate a positive anomaly in one line of the profile data while the other two profile lines show a negative response.
- Several anomalies, including one selected over the cave, are visible in the resistivity (TR2) data. The anomaly over the cave is just visible at the deepest portion (bottom) of the section. An increase in the array length (increasing the dipole separation) might be useful for future surveys to delineate deep, large voids.
- The seismic section over the Indian Well Cave is relatively free of reverberating seismic energy, indicating an absence of shallow scoria beds. The tube can be identified by a reflection from the cave top, a diffraction from the west edge, and a zone of relatively noisy data later in time.

Monument Road Cave

- Multiple diffractions are present in the GPR data, but vary in amplitude from line to line. This lava tube was not imaged using GPR.
- Monument Road Cave was successfully located with the magnetic method. In the magnetic profile, a positive magnetic anomaly is observed. Another anomaly is found to the north of the known cave location and was proposed as a possible lava tube site.
- Two well-defined anomalies are clearly evident in the electrical resistivity data. The known cave was easily interpreted from the data as well as a second anomaly to the south.
- The Monument Road Cave is evident from the arcuate reflection in the HRSW data from the top of the cave. However, the section is composed of predominantly reverberating seismic energy, bouncing back and forth between a shallow scoria bed and the surface.

Bearpaw Bridge

- The electrical resistivity data were successful at locating the lava tube at Bearpaw Bridge. High resistivity values indicate the location of the lava tube.

Hercules Leg Cave

- The known caves were clearly identified by the GPR data. The depth to the roof and the width of the caves were easily distinguished from the raw and processed data.
- Magnetic anomalies were observed over the two known caves. Information concerning the locations of these caves aided in the selection of these anomalies. Two other anomalies, with profiles similar to the profile over the known caves, were selected in this section. Within the unknown section of the Hercules Leg Cave survey site, a very distinctive trough in the data appears in the middle of the line, suggesting a cave. Also, one possible cave location was proposed to the southwest and two others were proposed northeast of the middle of the survey line.
- Several anomalies are present in the electrical resistivity data, but do not have the continuity associated with them compared to the anomalies at Indian Well or Monument Road Cave. This may indicate that the source of these anomalies is comparatively small, suggesting small voids.
- The EM31 data collected showed no anomalies in the vicinity of the known cave.
- Hercules Leg Cave is wide enough under the seismic line that it traps seismic energy between the top of the cave and the ground surface, causing strong reverberations. Again the thin overburden present may be disguising the exact shape and size of the known voids.

Overall, each known lava tube was detected with at least two geophysical methods. Table 15 is a reference guide of the final results from all geophysical surveys. It is important to note that

although the lava tube was interpreted at each location, the data processing and interpretation for certain geophysical methods were aided by knowledge of the general lava tube location.

The large voids at the Indian Well and Monument Road Cave sites were easily detected with the magnetic and electrical resistivity data. The ease of data acquisition using the magnetic or electrical resistivity methods makes them more favorable for lava tube detection at LBNM, especially for data collection over long distances. These data sets may also be relatively quickly processed and interpreted. Anomalies interpreted from the magnetic or electrical resistivity methods may then be further investigated using the HRSW or GPR method.

The HRSW method is effective at determining depths as well as providing width estimates over voids thought to have more than 3.0 m (9.8 ft) of overburden. Although the lava tubes are visible in the HRSW data sets, they would be difficult to locate without some prior knowledge of their locations. A known site is important to be able to calibrate the processing and interpretation steps. Once the characteristics of a known cave are observed in the data, then other anomalies can be interpreted using similar criteria. It is therefore recommended that, for future work, shear wave reflection surveys be “calibrated” against a known cave in the local area.

The GPR method was effective at detecting voids down to depths of 4.0 m (13.1 ft) without “calibration,” and may be a more practical method for determining shallow void characteristics where individual anomalies are not distinguishable in either the magnetic or electrical resistivity methods. GPR could be used to assist in determining the depths of anomalies in the magnetic or resistivity data, providing the sources of these anomalies were less than about 4.0 m (13.1 ft) deep.

5.1 SURVEY METHOD EVALUATION

The evaluation of the geophysical methods, based on the results described above, demonstrated their ability to detect the presence of subsurface voids and to characterize the vertical and horizontal extent of the voids. However, their ability to accurately and economically detect the presents of voids under specific geologic settings varies from method to method. Table 16 summarizes the methods’ detection capabilities, their production rates, and their cost effectiveness for lava tube detection. In examining the table, it shows that none of the methods are capable of determining the height of the lava tube.

Table 15. Reference guide of the final results from the geophysical surveys at LBNM.

Location	Method	Detected Known Lava Tube	Surveyed Dimensions			Interpreted Dimensions from Data		
			Depth	Width	Height	Depth	Width	Height
			(m)	(m)	(m)	(m)	(m)	(m)
Golden Dome Cave	GPR	NA	4	4	2.7	NA	NA	NA
	Magnetics	Y	4	4	2.7	NA	4 to 10	NA
	Electrical Resistivity	NA	4	4	2.7	NA	NA	NA
	HRSW	Y*	4	4	2.7	4	3	NA
Indian Well Cave	GPR	NA	8.8	7.9	8.5	NA	NA	NA
	Magnetics	Y	8.8	7.9	8.5	NA	8 to 18	NA
	Electrical Resistivity	Y	8.8	7.9	8.5	6	7	NA
	HRSW	Y*	8.8	7.9	8.5	9	8	NA
Monument Road Cave	GPR	N	5.5	12.2	5.5	3 to 5	3 to 5	NA
	Magnetics	Y	5.5	12.2	5.5	NA	3 to 10	NA
	Electrical Resistivity	Y	5.5	12.2	5.5	2 to 3	12	NA
	HRSW	Y*	5.5	12.2	5.5	12	6	NA
Bearpaw Bridge	GPR	NA	6.4	15.2	3	NA	NA	NA
	Magnetics	NA	6.4	15.2	3	NA	NA	NA
	Electrical Resistivity	Y	6.4	15.2	3	2 to 3	10	NA
	HRSW	NA	6.4	15.2	3	NA	NA	NA
Hercules Leg North	GPR	Y	3.4	9.8	0.9	2	12	NA
	Magnetics	N	3.4	9.8	0.9	NA	NA	NA
	Electrical Resistivity	Y	3.4	9.8	0.9	1	6	NA
	HRSW	Y*	3.4	9.8	0.9	3	9	NA
Hercules Leg South	GPR	Y	2.7	22.3	2.4	2	21	NA
	Magnetics	N	2.7	22.3	2.4	NA	NA	NA
	Electrical Resistivity	Y	2.7	22.3	2.4	1	4	NA
	HRSW	Y*	2.7	22.3	2.4	3	3	NA

* - Processing and interpretation were aided by the knowledge of the general lava tube location

Table 16. Geophysical survey methods’ capabilities, production rates, and cost effectiveness for lava tube detection.

Geophysical Method	Data Acquisition Speed	Data Processing and Interpretation	Cost-effectiveness ¹	Survey Location Estimates ²		
				Depth (m)	Width (m) ⁷	Height (m)
GPR	Walking ³	16 hrs/day of collection ⁵	2	< 4m	< ±20%	NA
Magnetics	Walking ³	16 hrs/day of collection ⁵	2	3 - 9	< ±40%	NA
Electrical Resistivity	Walking ³	16 hrs/day of collection ⁵	2	3 - 9	< ±20%	NA
HRSW	200-300 shots/day ⁴	6-10 days/day of collection ⁶	4	3 - 9	< ±20%	NA

¹ – cost-effectiveness is based on scale of 1-5 with 1 being the best. Factors include collection rates, known lava tube detection rate, interpreted size and depth.

² – estimates are based on results from this report only.

³ – in certain cases these instruments may be mounted to a vehicle or cart for higher data collection rates.

⁴ – estimates using the Land Streamer instead of normal geophones.

⁵ – higher collection rates may require more processing and interpretation time.

⁶ – an increase in the days of data collection will not necessarily increase the processing and interpretation time.

⁷ – the estimate of the width of the lava tube from the data was within listed percentage of the actual width of the known lava tube.

CHAPTER 6.0. QUALITY ASSURANCE AND QUALITY CONTROL

In order to ensure the highest quality geophysical data, a multi-layer approach to Quality Assurance and Quality Control (QA/QC) was implemented. Before shipping equipment to job sites, rigorous tests were conducted to ensure all equipment is functioning properly.

Quality control is obtained in the field by highly trained geophysicists. Survey parameters and acquisition procedures are agreed to by at least two geophysicists, who are then responsible for conducting the surveys. When time allows, survey data is recorded a second time, either in the same or opposite directions, to ensure repeatability. Data were then compared during the data processing and interpretation steps. Data are also returned to the home office for analysis by senior geophysicists within the QA/QC department.

During data processing and interpretation, the geophysicists discuss results and interpretations with the internal QA/QC department on a daily basis. Ideas and alternate techniques are discussed and implemented to provide clients with the most accurate data possible.

Report writing is generally handled by the processing geophysicists. Draft reports are generated and circulated within the QA/QC department as well as given to at least one additional senior geophysicist.

The different layers of this QA/QC approach ensure a high quality product is produced for each and every client.

During the completion of this report the Project Manager for this project used the following Blackhawk personnel for QA/QC:

- Kanaan Hanna – Senior Engineer, senior review;
- Jim Hild – Senior Geophysicist, data processing and interpretation;
- Steve Hodges – Consulting Geophysicist (Satori Enterprises), data acquisition;
- Natasa Mekic – Senior Geophysicist, data processing and general QA/QC activities.
- Dr. Ed Wightman – Senior Geophysicist. Provides general QA/QC activities.

CHAPTER 7.0. CONCLUSIONS AND RECOMMENDATIONS

The results of this study and the method evaluations revealed the following conclusions and recommendations.

7.1 CONCLUSION

The methods described below are listed in order of their capability and cost-effectiveness in detecting near surface voids.

Ground Penetrating Radar

- Effective in detecting voids to 4.0 m without calibration.
- Practical for determining shallow void characteristics.

Magnetics

- Rapid data collection, processing, and interpretation.
- Field survey can be conducted over large area.

Electrical Resistivity

- Effective in detecting voids at each site.
- Difficult to collect data in confined areas, over single lane roads, or over roads with tight curves.

High Resolution Shear Wave

- Effective in identifying each of the known caves.
- Effective in locating voids with greater overburden.
- Data processing and interpretation is time consuming and requires experienced geophysicist.

7.2 RECOMMENDATIONS

The combined GPR and magnetic methods would be the most economical and least time consuming for detecting voids over large areas. These geophysical methods can locate and characterize voids whose depths range between 0 to 9 m (0 to 30 ft). Magnetic surveys should be performed first as a reconnaissance tool in order to locate the position of magnetic anomalies that may indicate the presence of potential voids. A focused GPR survey would then be conducted to evaluate each magnetic anomaly and to determine the depth and lateral extent of the features.

CERTIFICATION AND DISCLAIMER

All geophysical data analysis, interpretations, conclusions, and recommendations in this document have been prepared under the supervision of and reviewed by Blackhawk senior geophysicists.

This geophysical investigation was conducted using sound scientific principles and state-of-the-art technology. A high degree of professionalism was maintained during all aspects of the project from the field investigation and data acquisition, through data processing, interpretation, and reporting. The results and interpretations were limited by the data obtained in the field and from the client. All original field data files, field notes, observations, and other pertinent information are maintained in the project files at the Blackhawk's Golden office, and are available to the client for a minimum of five years.

A geophysicist's certification of interpreted geophysical conditions comprises a declaration of his/her professional judgment. It does not constitute a warranty or guarantee, expressed or implied, nor does it relieve any other party of its responsibility to abide by contract documents, applicable codes, standards, regulations, or ordinances.

ACKNOWLEDGEMENT

The authors would like to express their sincere appreciation to Mr. Khamis Y. Haramy and Mr. Matthew DeMarco, geotechnical engineers of FHWA-CFLHD, for their guidance, valuable technical assistance, and review during the course of this investigation. The authors would also like to thank Mr. Linden Snyder and Mr. Roger Surdahl of the FHWA-CFLHD for their technical advice and review of this report.

The staff at Lava Beds National Monument is gratefully acknowledged for their insight, information, and assistance during data collection.

REFERENCES

1. Lava Beds National Monument Website. Retrieved August 2, 2005 from http://www.nps.gov/labe/content/HISTORY_Main.htm
2. Resource Management Plan, Lava Beds National Monument. December 1999. Retrieved August 2, 2005 from <http://data2.itc.nps.gov/parks/labe/ppdocuments/1999RMP.pdf>.
3. Dorman, C. Personal communication regarding lava tube occurrences at Lava Beds National Monument. October 2003.
4. Lava Beds National Monument Website. Retrieved October 1, 2003 from <http://www.nps.gov/carto/LABE.html>
5. Alt, D. and D.W. Hyndman. Roadside Geology of Northern and Central California. Vancouver: Mountain Press Publishing Company, 2000. p 370.
6. Larson, C. and J. Larson. Lava Beds Book. Vancouver: ABC Publishing, 1989. pp 24-25, 29-32, 41-43.
7. Wightman et al. Application of Geophysical Methods to Highway Related Problems. Federal Highway Administration, Central Federal Lands Highway Division. Project No. DTFH68-02-P-00083. September 2003
8. Ray, M.W. "Electronic Technology Being Used to Map Salt Water Contamination in Developing Areas of Central Oklahoma." Oklahoma House of Representatives Media Division Website. Retrieved on February 27, 2002 from <http://www.lsb.state.ok.us/house/NEWS6262.htm>
9. Wolfe, P.J., E.C. Hauser, and B.H. Richard. Identifying Potential Collapse Features Under Highways. Ohio Department of Transportation. State Job Number 14700(0). Department of Geological Sciences, Wright State University. Dayton, Ohio, March 2003.
10. "Pellissippi Case Study." Advanced Geosciences, Inc Company Website. January 19, 2002. Retrieved on February 20, 2004 from <http://www.agiusa.com/pellissippi.shtml>.
11. Miyamoto et al. "Ground Penetrating Radar to detect lava tubes: preliminary results of a GPR application to Fuji volcano, Japan." Retrieved on February 20, 2004 from <http://www.lpi.usra.edu/meetings/lpsc2002/pdf/1482.pdf>.
12. Olhoeft et al. "Hot and Cold Lava Tubes Characterization with Ground Penetrating Radar." In GPR 2000, Proc. of the 8th International Conference on Ground Penetrating Radar, Gold Coast, Australia, 22-25 May 2000, D. A. Noon, G. F. Stickley, and D. Longstaff, eds., SPIE vol. 4084, p. 482-487.

13. Taylor, R. S. "Applications of Terrain Conductivity M." Retrieved on February 20, 2004 from <http://www.dualem.com/abib.html>
14. Clark, J.C. "Double Feature at the Bijou: Shear Wave Vibroseis Reflection Seismic Acquired Within a Working Movie Theater."
15. National Parks Service. Lava Beds National Monument – Geology. February 26, 2001. Retrieved on February 12, 2004 from <http://www.nps.gov/labe/Geology.html>
16. Donnelly-Nolan, J. M. and D.E. Champion. *Geologic Map of Lava Beds National Monument, Northern California*. Map I-1804. Scale 1: 24,000. Reston, Virginia. Department of the Interior – Geological Survey, 1998.
17. Sims, M., Weinberg, and D., Vollmer. *Monument Road Cave Lava Beds National Monument, California*. Scale 1:360. 1992. Received from LBNM officials on October 10, 2003.

APPENDIX A - PHOTOGRAPHS FROM LBNM



Devil's Homestead Lava Flow



Seismic Doghouse at Golden Dome

Figure 57. Photos. Site conditions.



Hercules Leg Cave

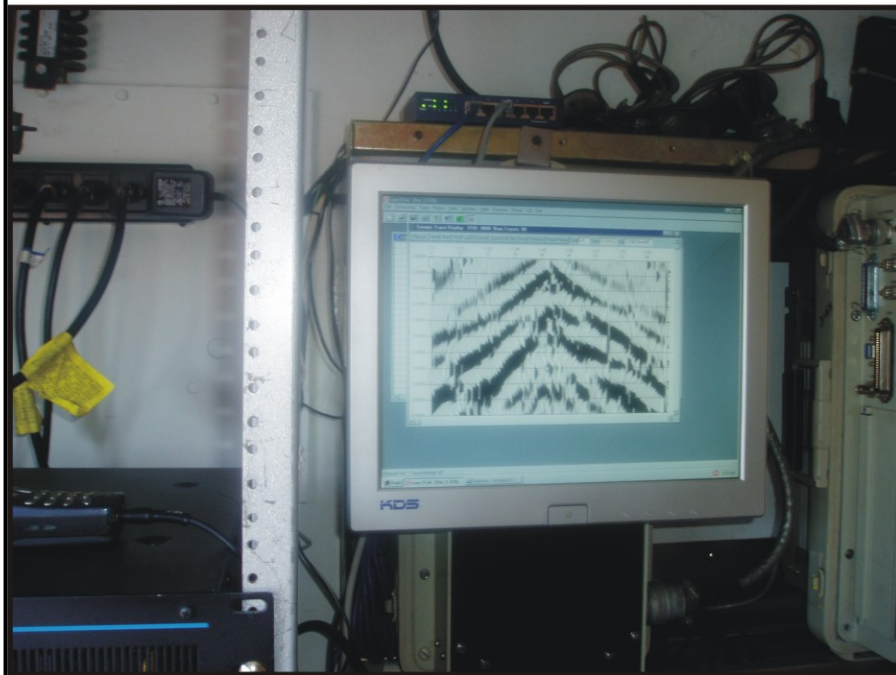


LandStreamer and MicroVibe at Hercules Leg

Figure 58. Photos. Site conditions.



GSSI Sir-2000 Control Unit In Back Of Automobile



Seismic Data Displayed Inside of Doghouse

Figure 59. Photos. Site conditions.



Wildlife at LBNM



The Natural Terrain at LBNM

Figure 60. Photos. Site conditions.

APPENDIX B - SURVEY PARAMETERS

Table 17. GPR survey parameters.

GPR - General Data Acquisition Parameters			
Samples/Scan	1024		
Bits/Sample	16		
Scans/Meter	40*wheel mode only		
Scans/Second	32*automatic mode only		
M/Mark	5		
Dielectric Constant	6		
Golden Dome Cave			
Wheel Mode	Antenna Frequency		
	100 MHz	200 MHz	400 MHz
Range	500 nanoseconds (ns)	300ns	150ns
Vertical LowPass Filter	675 MHz	690 MHz	1460 MHz
Vertical HighPass Filter	40 MHz	40 MHz	90 MHz
Horizontal Stacking	3	3	5
Range Gain	-1,5,10,22,49,58,63,67	1,40,49,58,61,64,70,72	-4,31,46,55,59,59,59,61
Hercules Leg Cave			
Wheel/Automatic Mode	Antenna Frequency		
	100 MHz	200 MHz	400 MHz
Range	500ns	300ns	150ns
Vertical LowPass Filter	590 MHz	980 MHz	1460 MHz
Vertical HighPass Filter	35 MHz	60 MHz	90 MHz
Horizontal Stacking	3	3	5
Range Gain	-5,4,20,32,40,50,55,60	1,40,49,58,61,64,70,72	-4,31,46,55,59,59,59,61
Indian Well Cave			
Wheel Mode	Antenna Frequency		
	100 MHz	200 MHz	400 MHz
Range	500ns	300ns	150ns
Vertical LowPass Filter	590 MHz	980 MHz	1460 MHz
Vertical HighPass Filter	35 MHz	60 MHz	90 MHz
Horizontal Stacking	3	3	5
Range Gain	-1,8,32,43,52,58,63,67	1,40,49,58,61,64,70,72	-4,31,46,55,59,59,59,61
Monument Road Cave			
Automatic Mode	Antenna Frequency		
	200 MHz	400 MHz	
Range	300ns	150ns	
Vertical LowPass Filter	975 MHz	1240 MHz	
Vertical HighPass Filter	60 MHz	75 MHz	
Horizontal Stacking	3	5	
Range Gain	1,36,53,65,70,70,71,72	-4,35,52,65,70,70,71,72	

Table 18. Geometrics OhmMapper TR2 array parameters.

	Line #	Receiver #	F	P	S	C	N	spacing	Rope Length
Hercules Leg Cave South to North	0	2	3.2	10	10	10		1	5
	0	1	8.2	10	5	10		0.5	5
	2	2	3.2	10	15	10		1.5	10
	2	1	8.2	10	10	10		1	10
Hercules Leg Cave North to South	1	2	3.2	10	10	10		1	5
	1	1	8.2	10	5	10		0.5	5
	3	2	3.2	10	15	10		1.5	10
	3	1	8.2	10	10	10		1	10
Indian Well Cave South to North	1	2	3.2	10	10	10		1	5
	1	1	8.2	10	5	10		0.5	5
	3	2	3.2	10	15	10		1.5	10
	3	1	8.2	10	10	10		1	10
Indian Well Cave North to South	0	2	3.2	10	10	10		1	5
	0	1	8.2	10	5	10		0.5	5
	4	2	3.2	10	15	10		1.5	10
	4	1	8.2	10	10	10		1	10
Monument Road Cave South to North	2	2	3.2	10	15	10		1.5	10
	2	1	8.2	10	10	10		1	10
	4	2	3.2	10	10	10		1	5
	4	1	8.2	10	5	10		0.5	5
Monument Road Cave North to South	1	2	3.2	10	15	10		1.5	10
	1	1	8.2	10	10	10		1	10
	3	2	3.2	10	10	10		1	5
	3	1	8.2	10	5	10		0.5	5
Bearpaw Bridge East to West	1	2	3.2	10	15	10		1.5	10
	1	1	8.2	10	10	10		1	10
	3	2	3.2	10	10	10		1	5
	3	1	8.2	10	5	10		0.5	5
Bearpaw Bridge West to East	0	2	3.2	10	15	10		1.5	10
	0	1	8.2	10	10	10		1	10
	2	2	3.2	10	10	10		1	5
	2	1	8.2	10	5	10		0.5	5

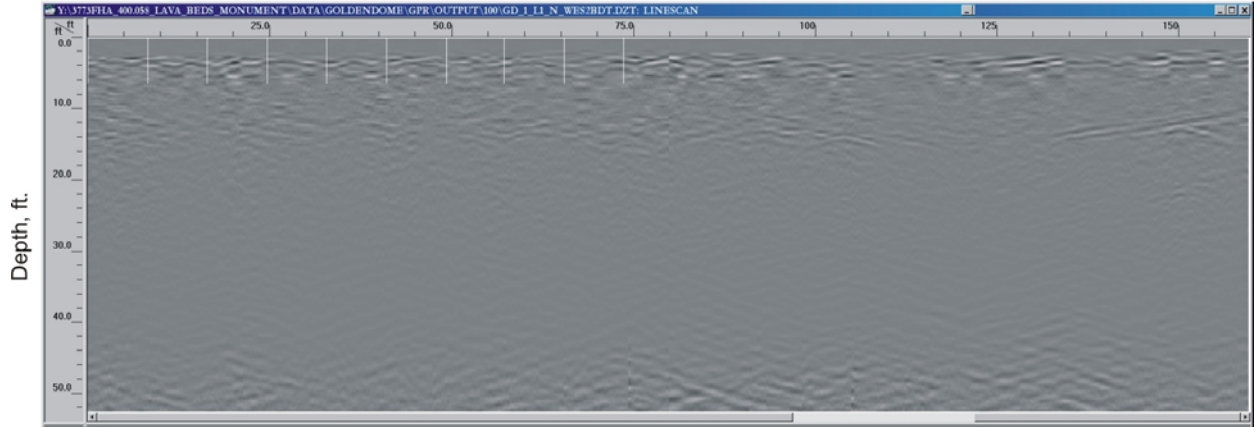
F = Operator offset, P = Receiver Dipole
S = Rope Length For Calculations, C = Transmitter Dipole

Table 19. High Resolution Shear Wave reflection survey parameters.

Shot Spacing	.61 m (2 ft)
Geophone Group Interval	.61 m (2 ft)
Nominal CDP Fold	48
Maximum Offset	29.0 m (95 ft)
Minimum Offset	.305 m (1 ft)
Spread Geometry	Symmetric Split Spread 48/48 – (57.9 meter total active array)
Seismograph	2 OYO DAS-1 Recorders (Master/Slave)
Number of Channels	96
Sample Rate	0.25 ms
Record Length	0.25 second
Field Filters	3/18 – Out Hz/dB
Seismic Source	Bay MicroVib, - 136 kilogram of peak ground force 20 to 450 Hz, Linear, 4 second sweep, 4 to 6 sweep/station
Geophones	1 X 40 OYO SMC70 40 Hz Shear Wave phone
Cables	96-channel Land Streamer
Rollbox	I/O Inc. RLS-240M

APPENDIX C - GPR CROSS SECTIONS

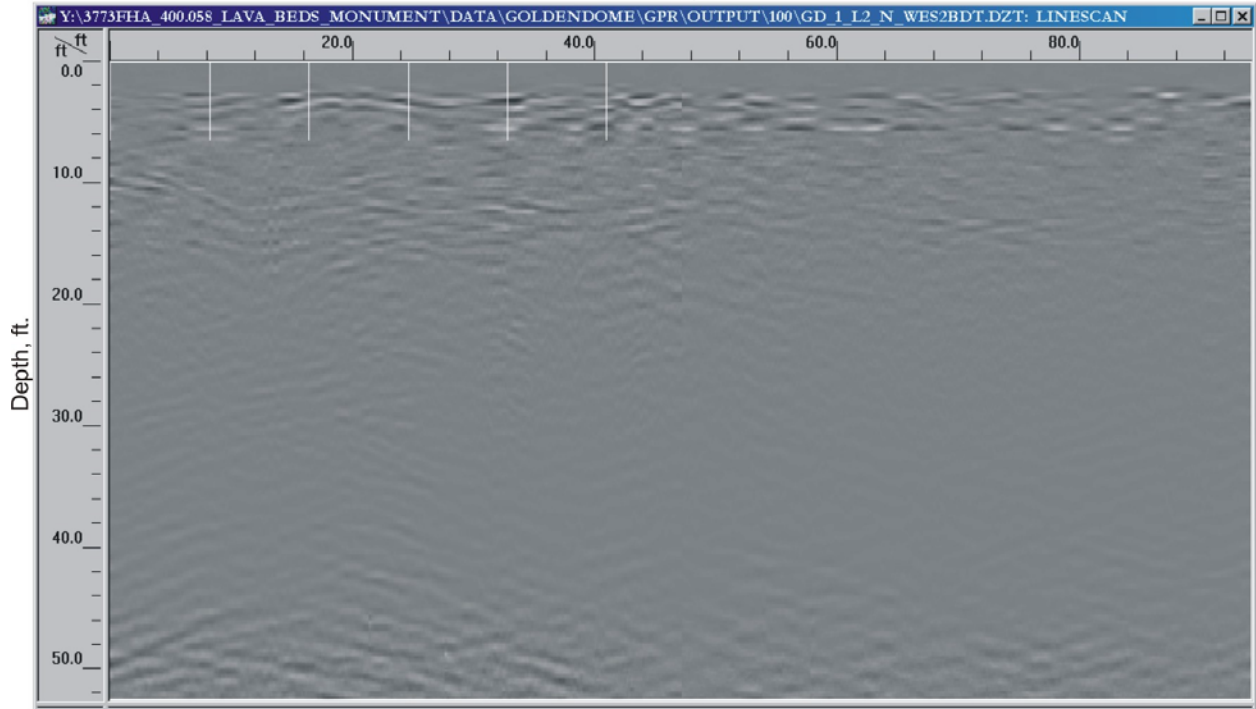
Processed GPR Data 100 MHz Antenna - Line 1
Golden Dome Cave
Distance, ft.



Note: 1 foot = .3048 meters

Figure 61. Cross Section. GPR data.

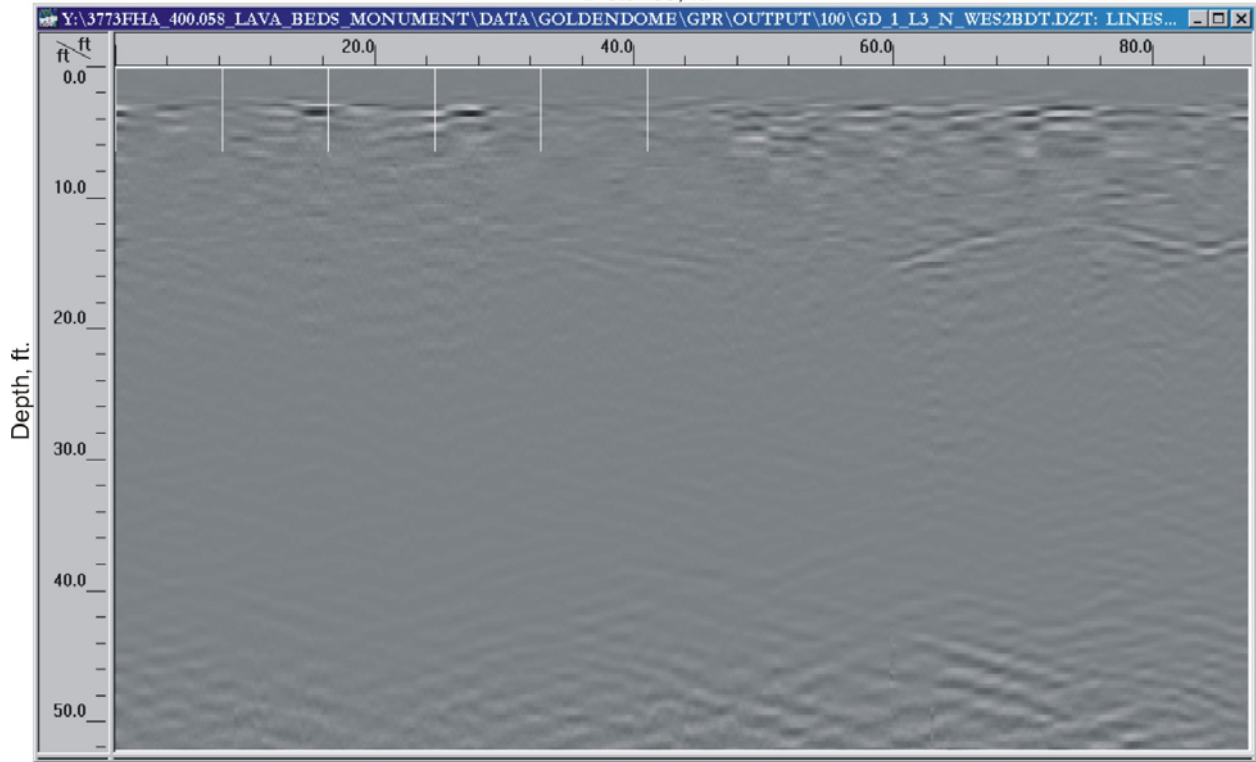
Processed GPR Data 100 MHz Antenna - Line 2
Golden Dome Cave
Distance, ft.



Note: 1 foot = .3048 meters

Figure 62. Cross Section. GPR data.

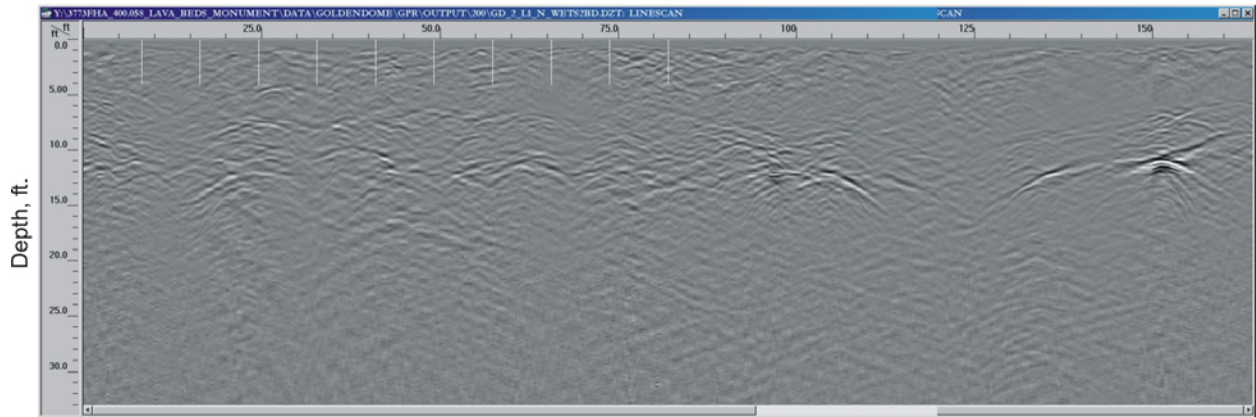
Processed GPR Data 100 MHz Antenna - Line 3
Golden Dome Cave
Distance, ft.



Note: 1 foot = .3048 meters

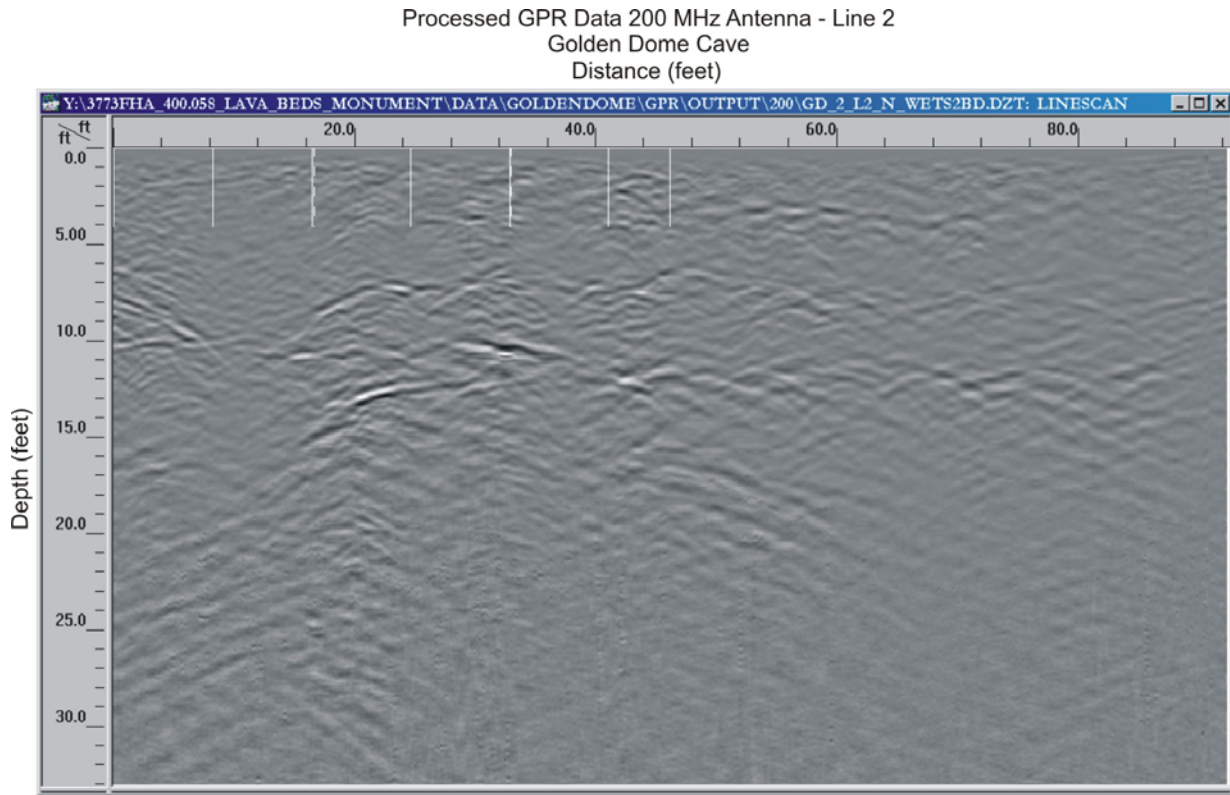
Figure 63. Cross Section. GPR data.

Processed GPR Data 200 MHz Antenna - Line 1
Golden Dome Cave
Distance, ft.



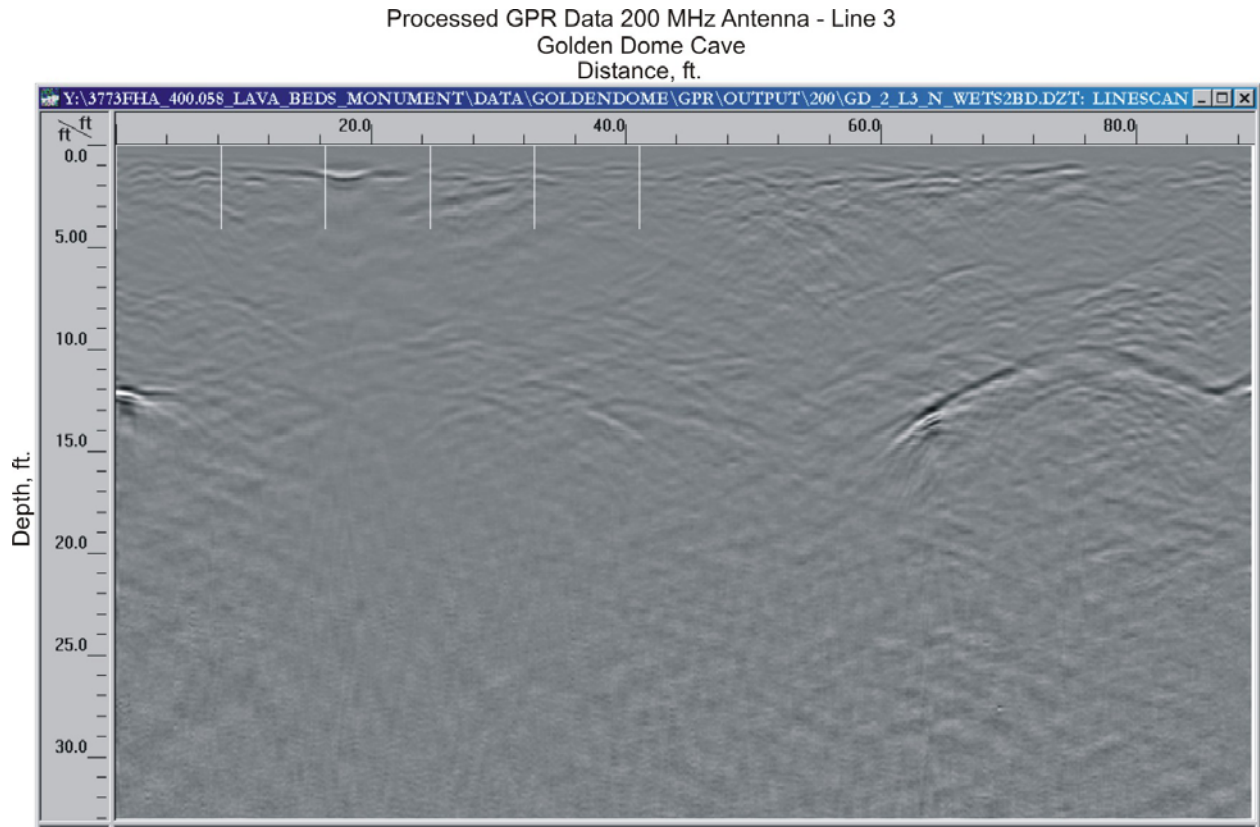
Note: 1 foot = .3048 meters

Figure 64. Cross Section. GPR data.



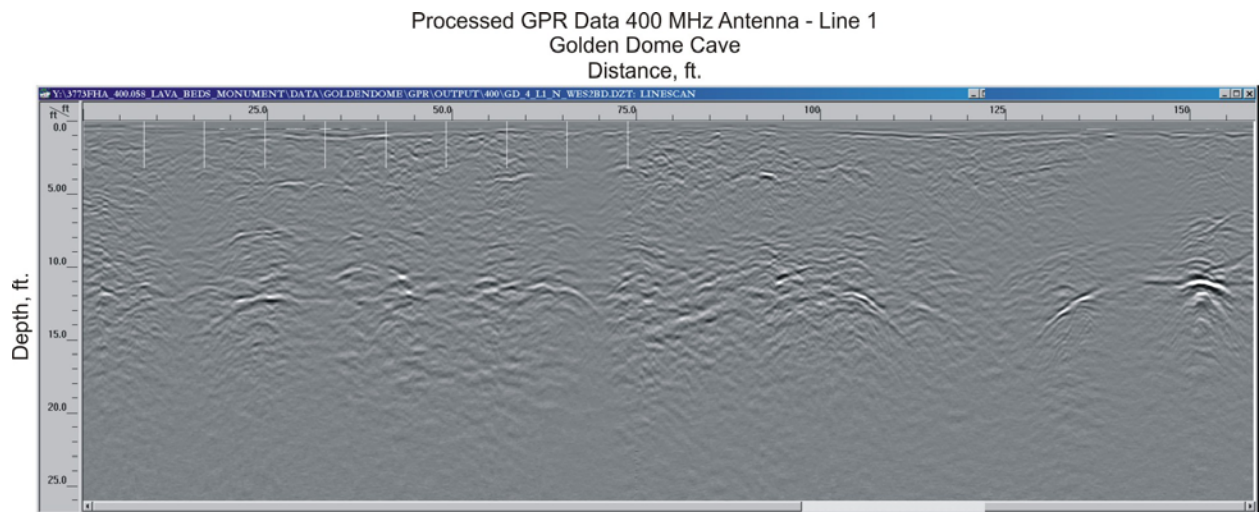
Note: 1 foot = .3048 meters

Figure 65. Cross Section. GPR data.



Note: 1 foot = .3048 meters

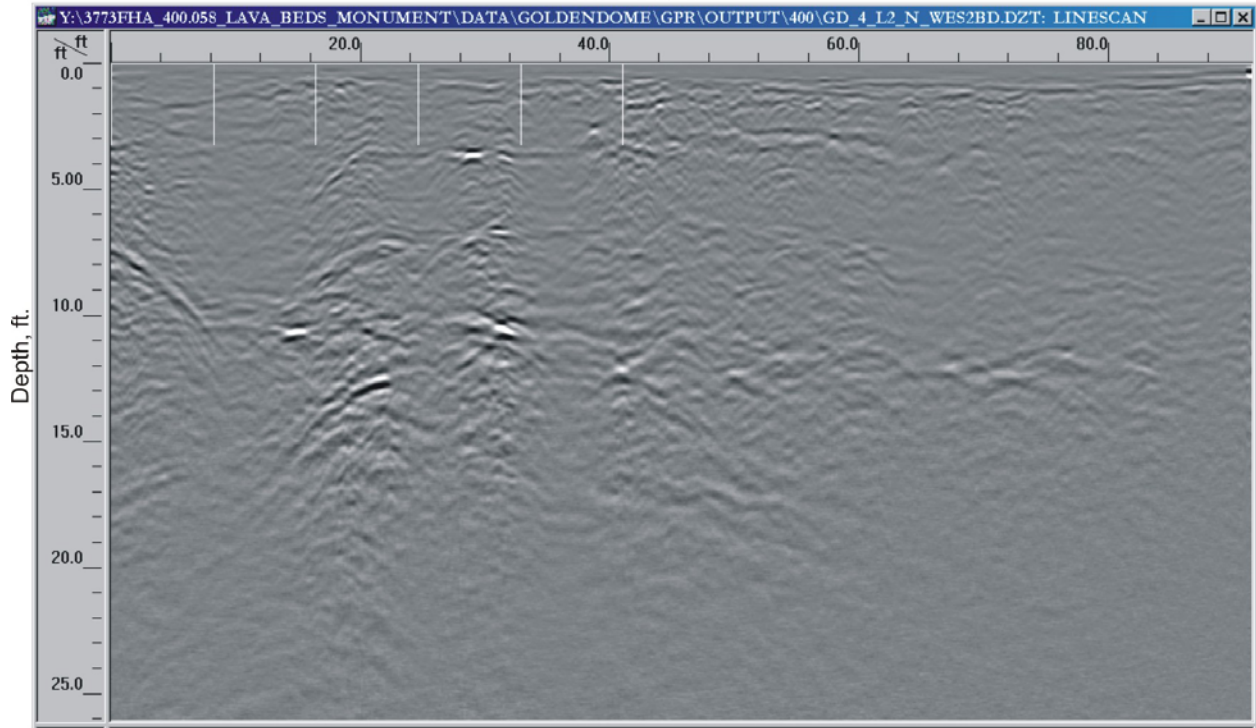
Figure 66. Cross Section. GPR data.



Note: 1 foot = .3048 meters

Figure 67. Cross Section. GPR data.

Processed GPR Data 400 MHz Antenna - Line 2
Golden Dome Cave
Distance, ft.



Note: 1 foot = .3048 meters

Figure 68. Cross Section. GPR data.

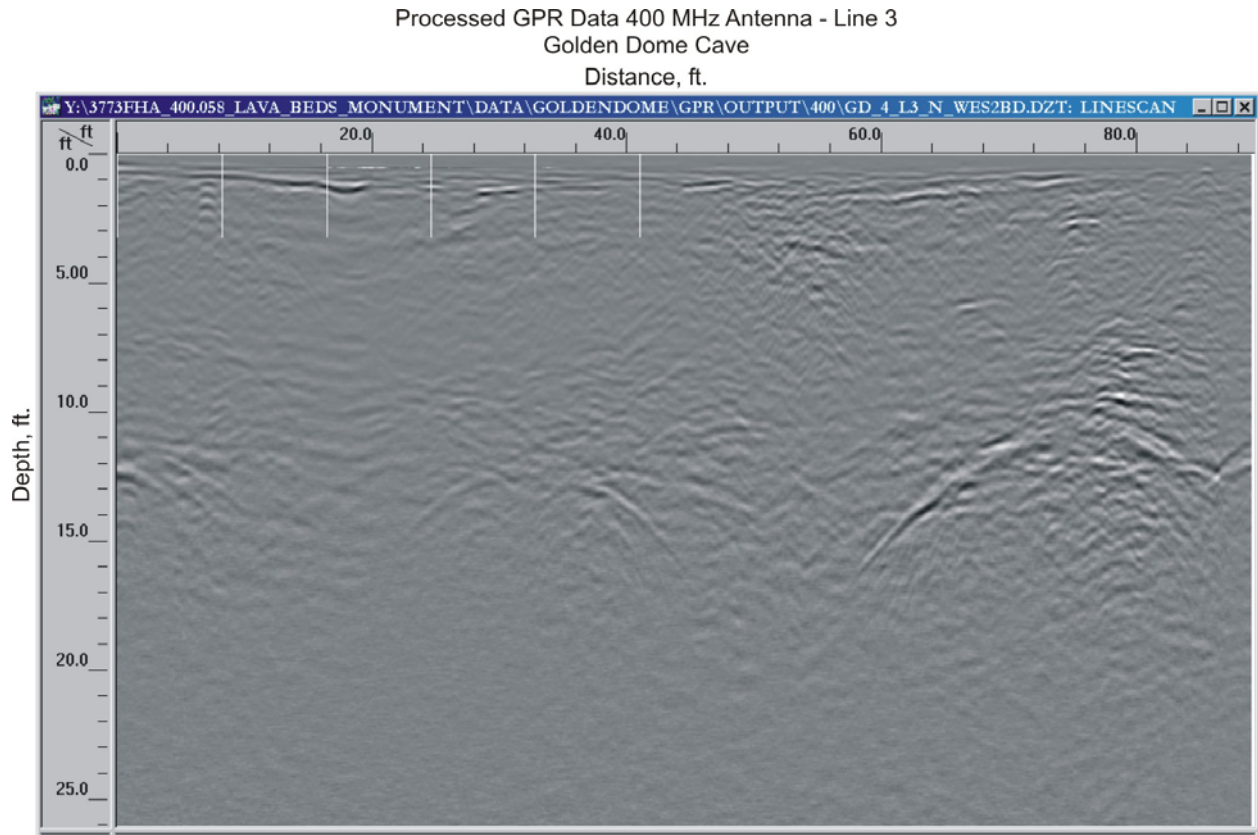


Figure 69. Cross Section. GPR data.

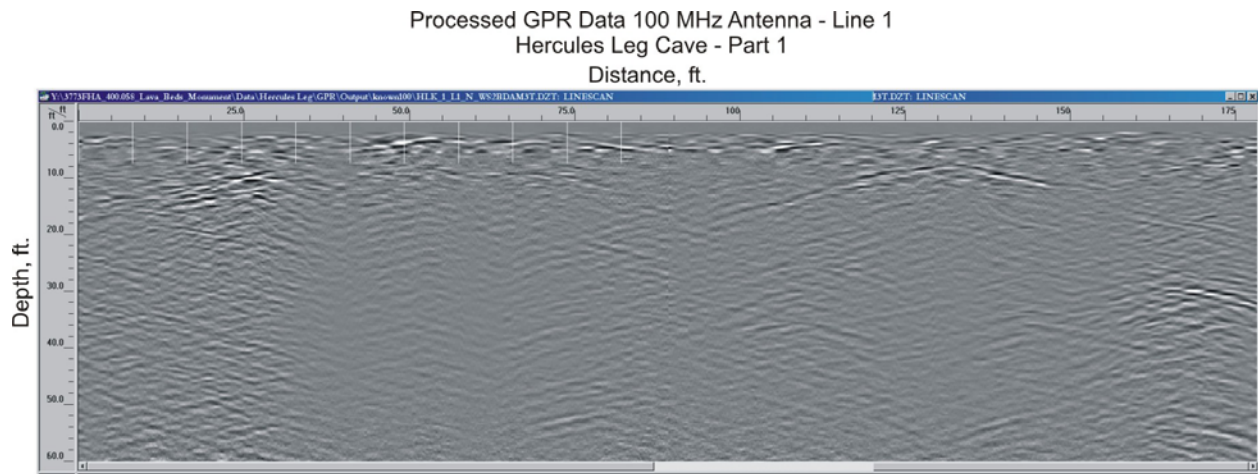
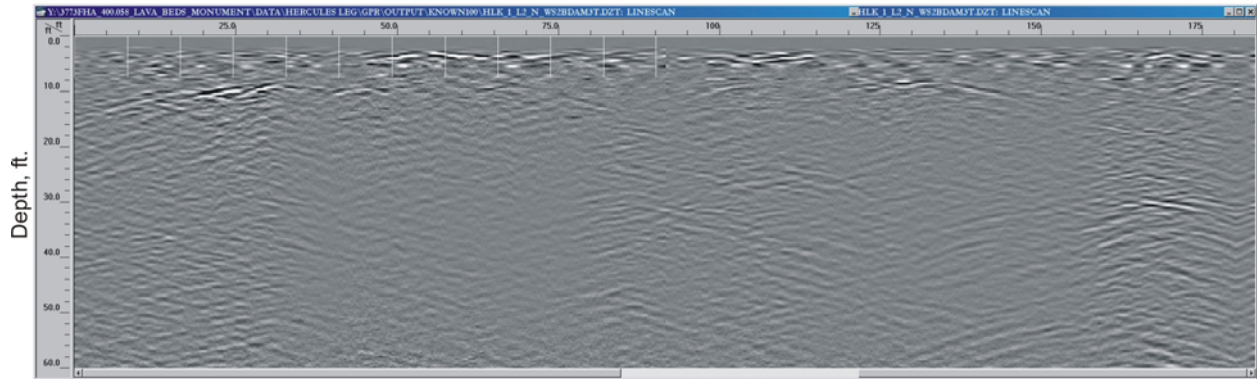


Figure 70. Cross Section. GPR data.

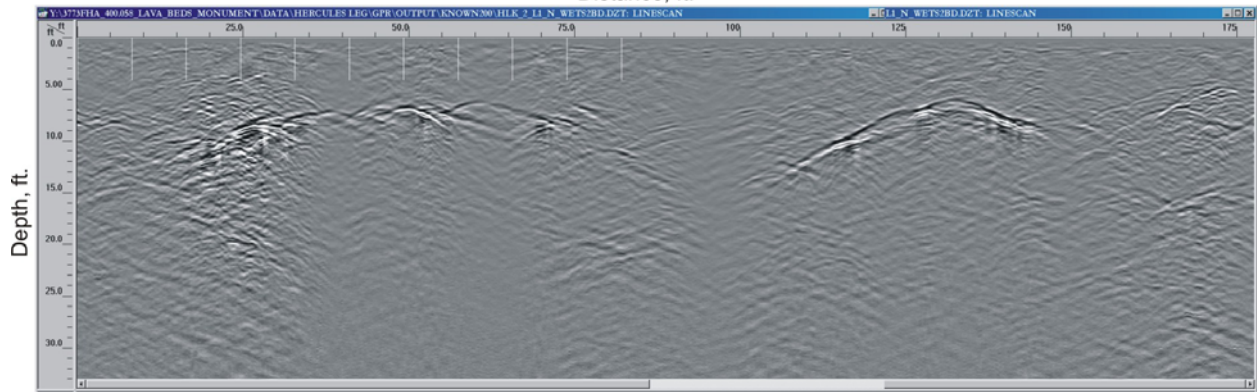
Processed GPR Data 100 MHz Antenna - Line 2
Hercules Leg Cave - Part 1
Distance, ft.



Note: 1 foot = .3048 meters

Figure 71. Cross Section. GPR data.

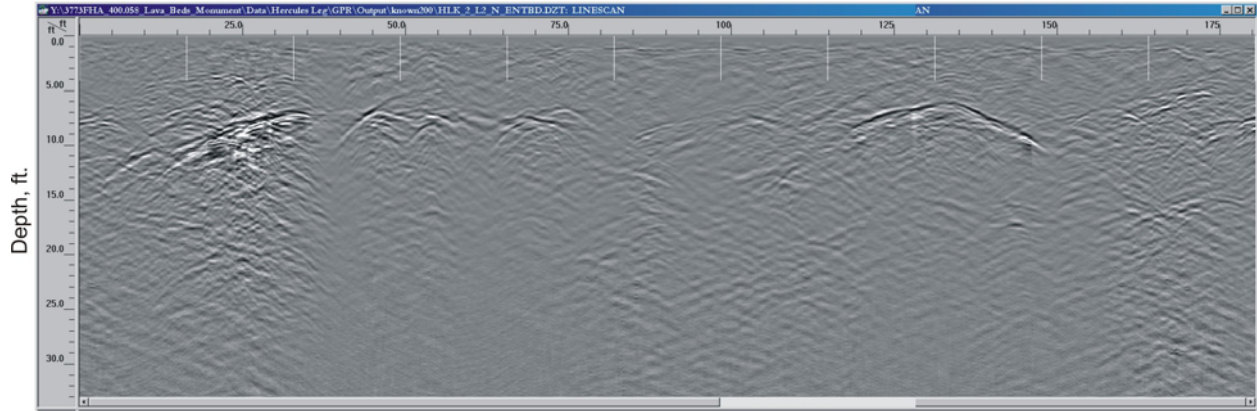
Processed GPR Data 200 MHz Antenna - Line 1
Hercules Leg Cave - Part 1
Distance, ft.



Note: 1 foot = .3048 meters

Figure 72. Cross Section. GPR data.

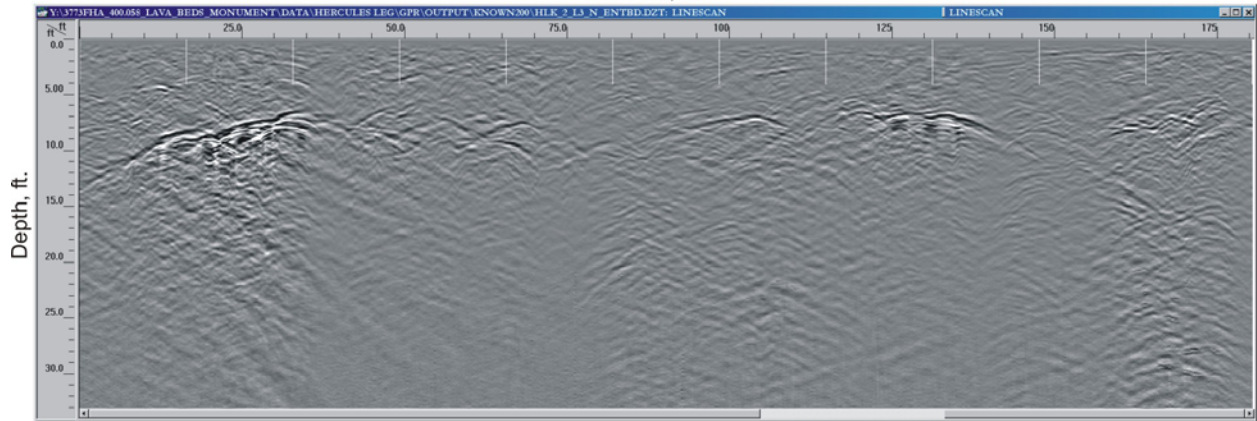
Processed GPR Data 200 MHz Antenna - Line 2
Hercules Leg Cave - Part 1
Distance, ft.



Note: 1 foot = .3048 meters

Figure 73. Cross Section. GPR data.

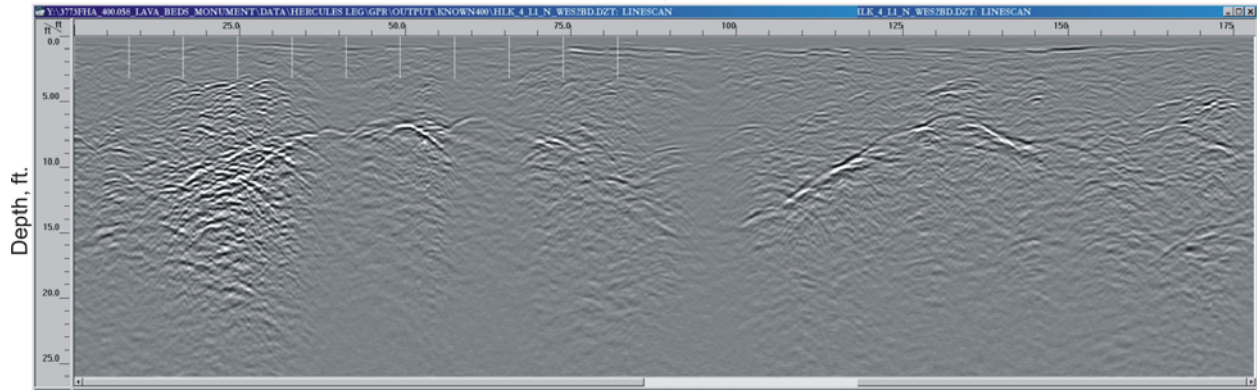
Processed GPR Data 200 MHz Antenna - Line 3
Hercules Leg Cave - Part 1
Distance, ft.



Note: 1 foot = .3048 meters

Figure 74. Cross Section. GPR data.

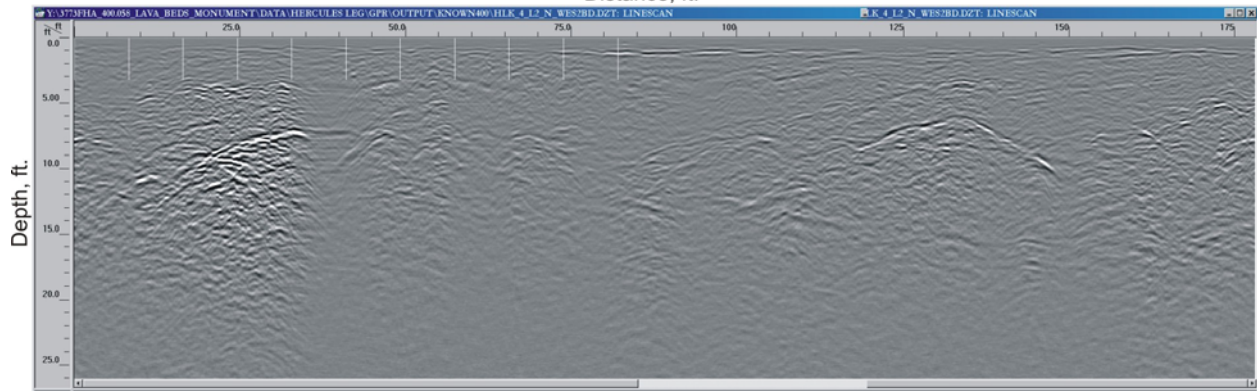
Processed GPR Data 400 MHz Antenna - Line 1
Hercules Leg Cave - Part 1
Distance, ft.



Note: 1 foot = .3048 meters

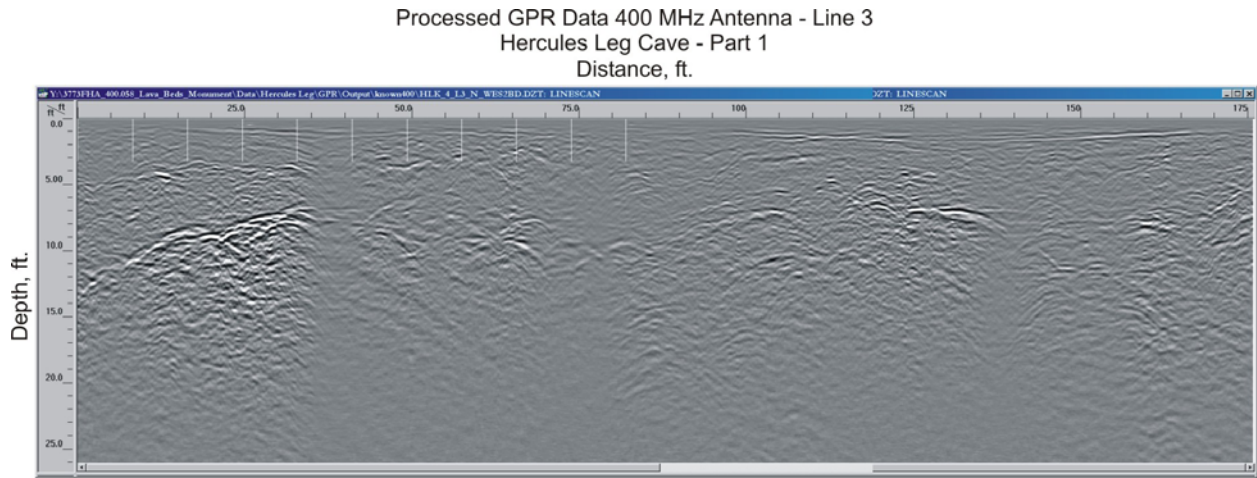
Figure 75. Cross Section. GPR data.

Processed GPR Data 400 MHz Antenna - Line 2
Hercules Leg Cave - Part 1
Distance, ft.



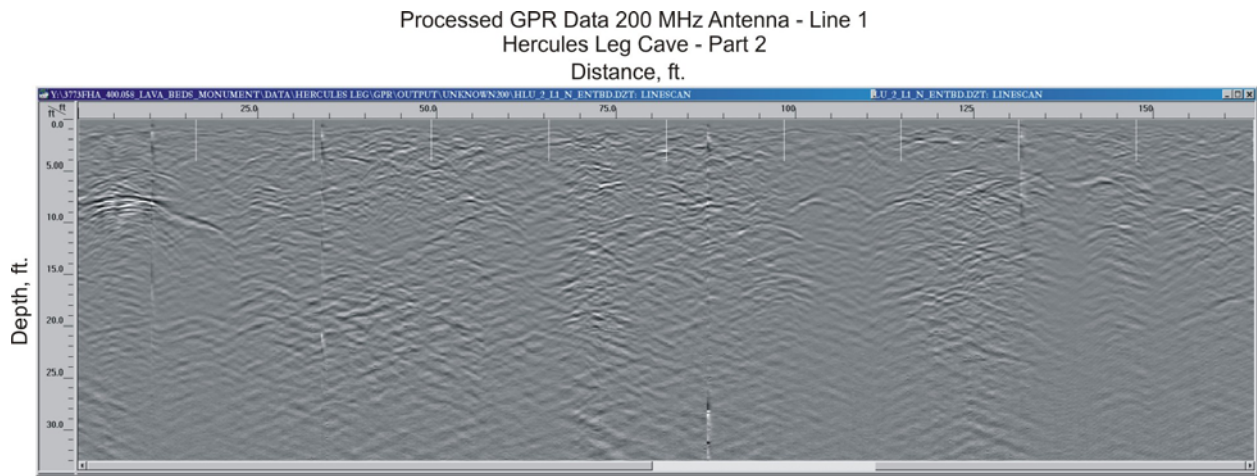
Note: 1 foot = .3048 meters

Figure 76. Cross Section. GPR data.



Note: 1 foot = .3048 meters

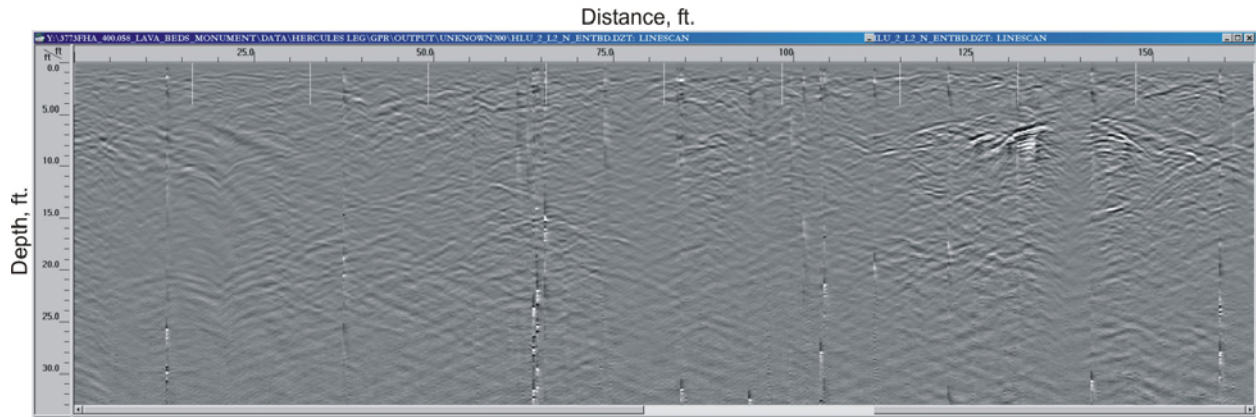
Figure 77. Cross Section. GPR data.



Note: 1 foot = .3048 meters

Figure 78. Cross Section. GPR data.

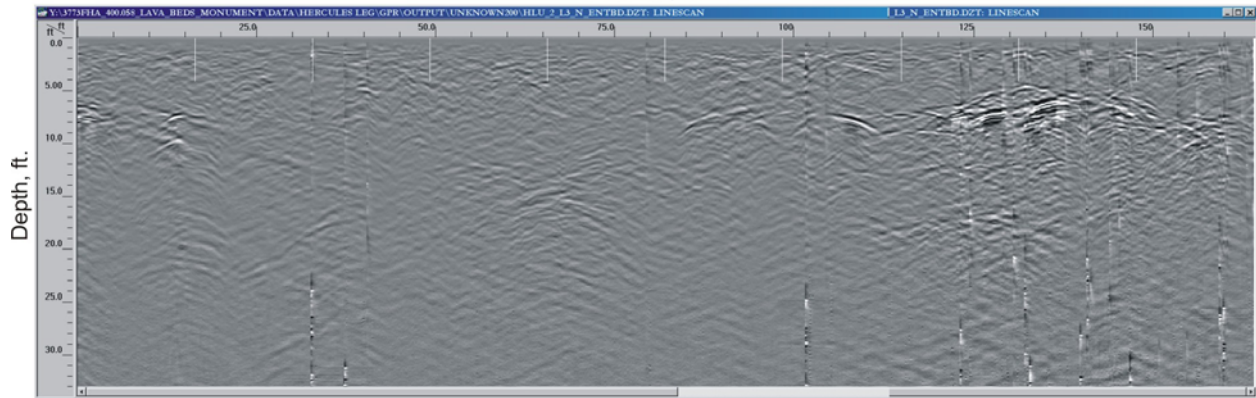
Processed GPR Data 200 MHz Antenna - Line 2
Hercules Leg Cave - Part 2



Note: 1 foot = .3048 meters

Figure 79. Cross Section. GPR data.

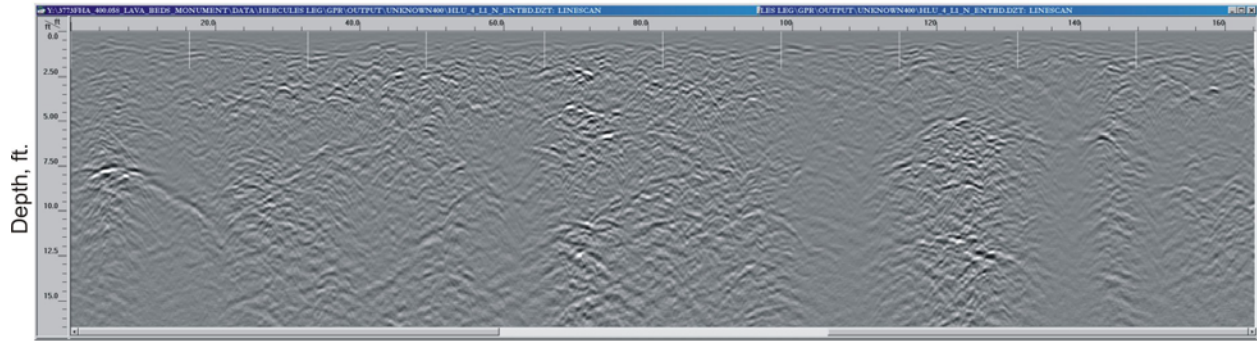
Processed GPR Data 200 MHz Antenna - Line 3
Hercules Leg Cave - Part 2
Distance, ft.



Note: 1 foot = .3048 meters

Figure 80. Cross Section. GPR data.

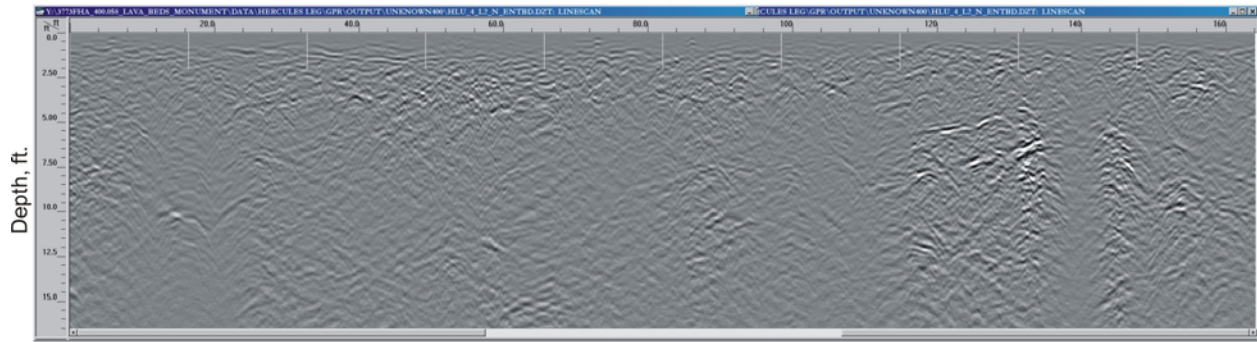
Processed GPR Data 400 MHz Antenna - Line 1
Hercules Leg Cave - Part 2
Distance, ft.



Note: 1 foot = .3048 meters

Figure 81. Cross Section. GPR data.

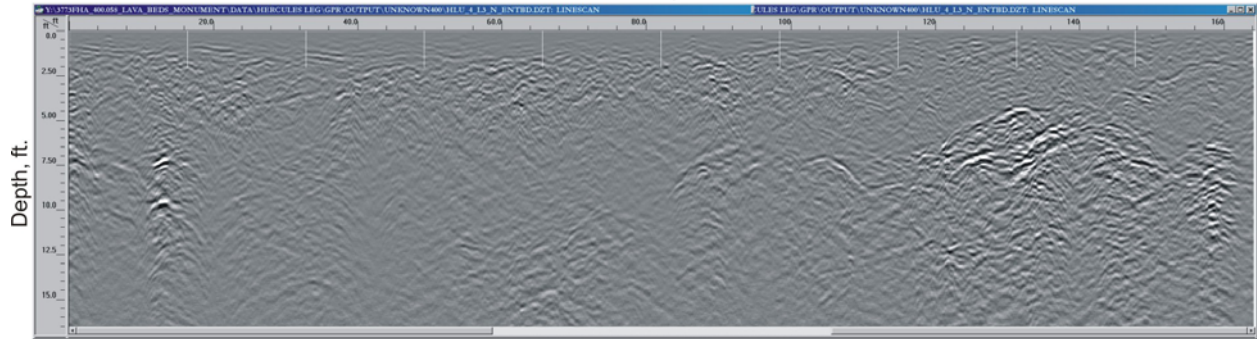
Processed GPR Data 400 MHz Antenna - Line 2
Hercules Leg Cave - Part 2
Distance, ft.



Note: 1 foot = .3048 meters

Figure 82. Cross Section. GPR data.

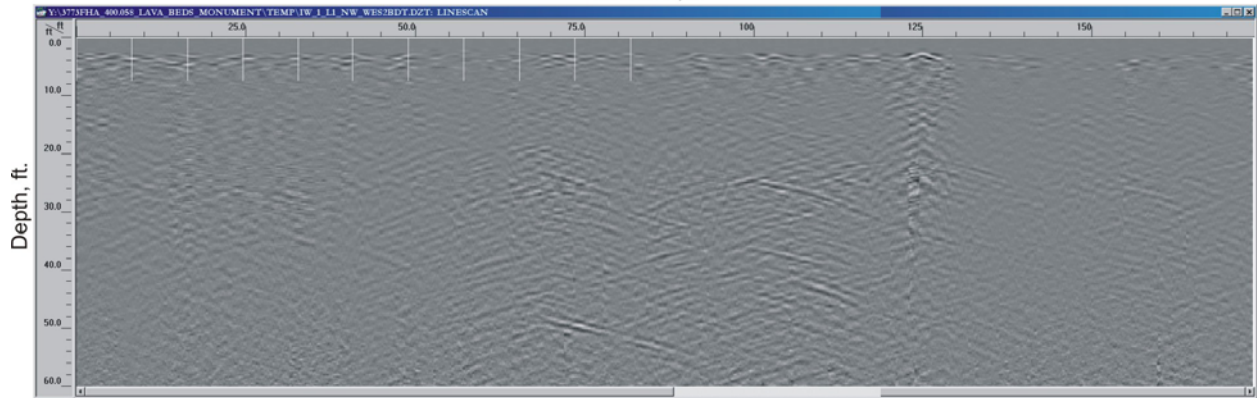
Processed GPR Data 400 MHz Antenna - Line 3
Hercules Leg Cave - Part 2
Distance, ft.



Note: 1 foot = .3048 meters

Figure 83. Cross Section. GPR data.

Processed GPR Data 100 MHz Antenna - Line 1
Indian Well Cave
Distance, ft.



Note: 1 foot = .3048 meters

Figure 84. Cross Section. GPR data.

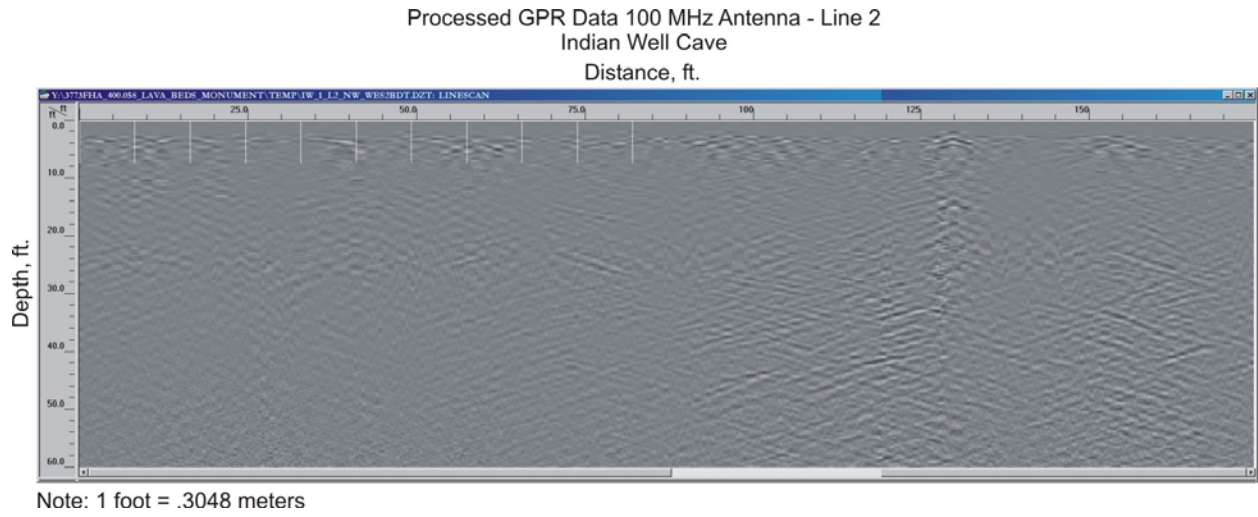


Figure 85. Cross Section. GPR data.

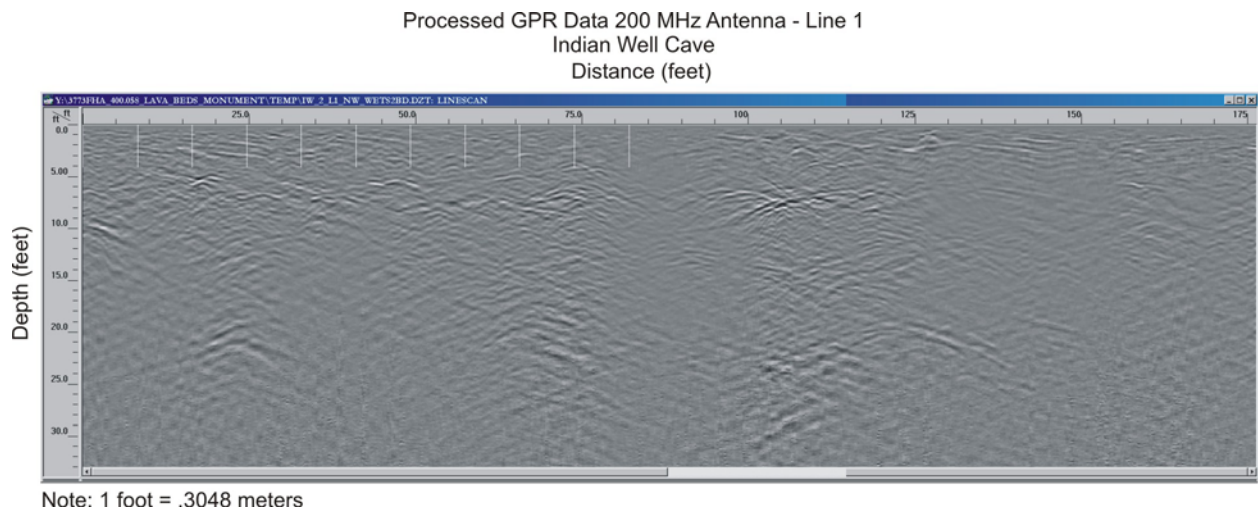
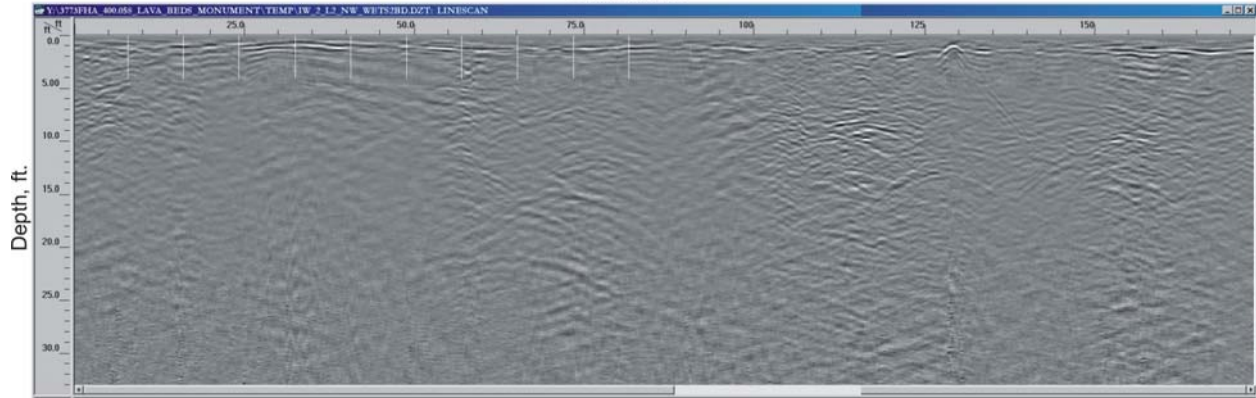


Figure 86. Cross Section. GPR data.

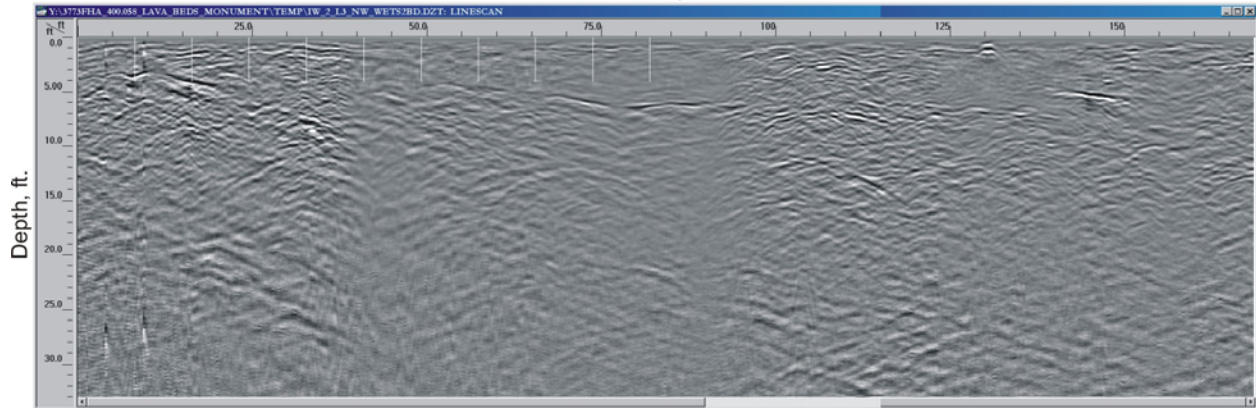
Processed GPR Data 200 MHz Antenna - Line 2
Indian Well Cave
Distance, ft.



Note: 1 foot = .3048 meters

Figure 87. Cross Section. GPR data.

Processed GPR Data 200 MHz Antenna - Line 3
Indian Well Cave
Distance, ft.



Note: 1 foot = .3048 meters

Figure 88. Cross Section. GPR data.

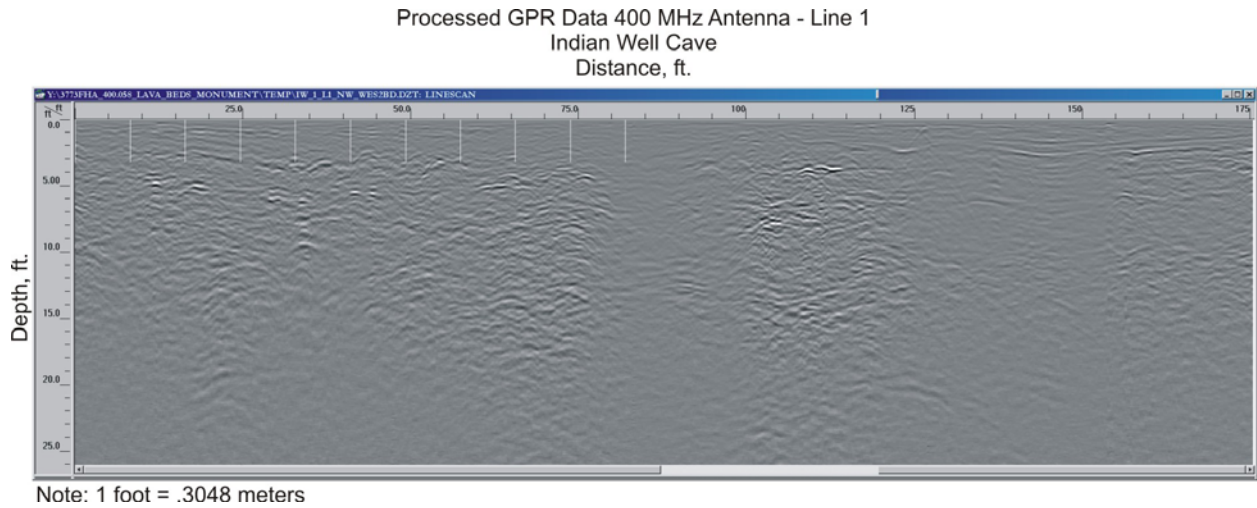


Figure 89. Cross Section. GPR data.

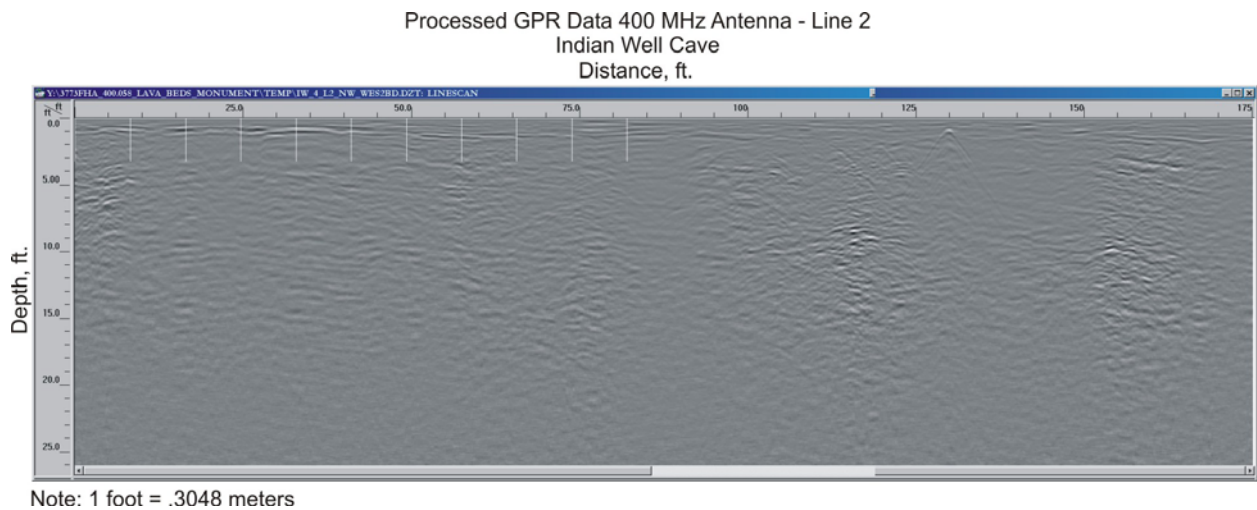
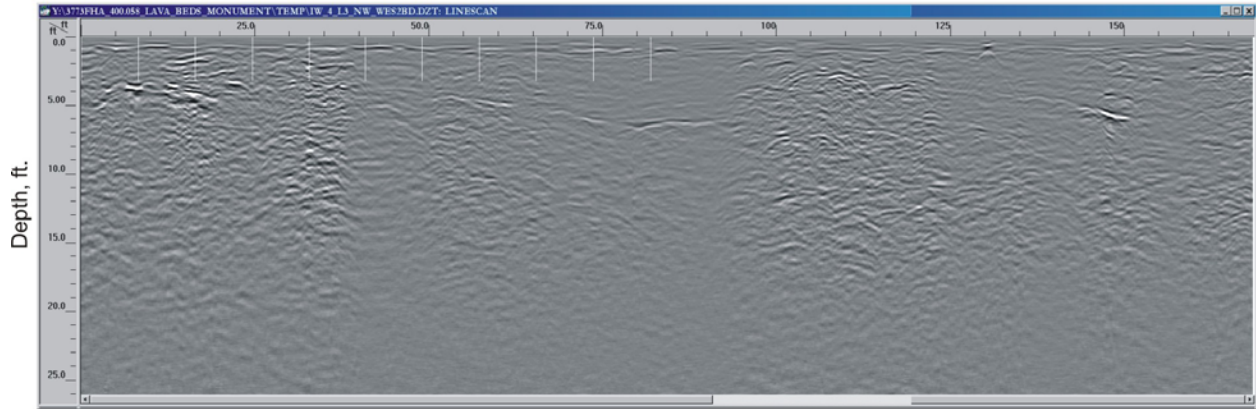


Figure 90. Cross Section. GPR data.

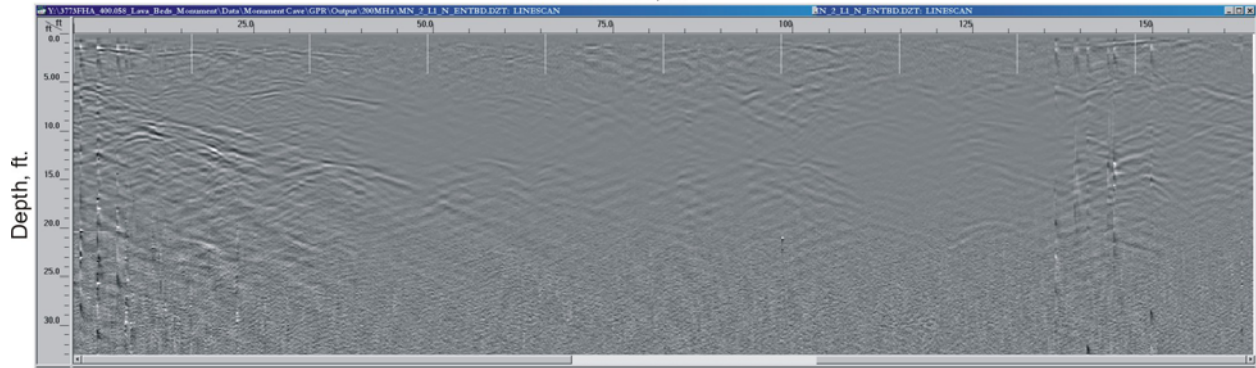
Processed GPR Data 400 MHz Antenna - Line 3
Indian Well Cave
Distance, ft.



Note: 1 foot = .3048 meters

Figure 91. Cross Section. GPR data.

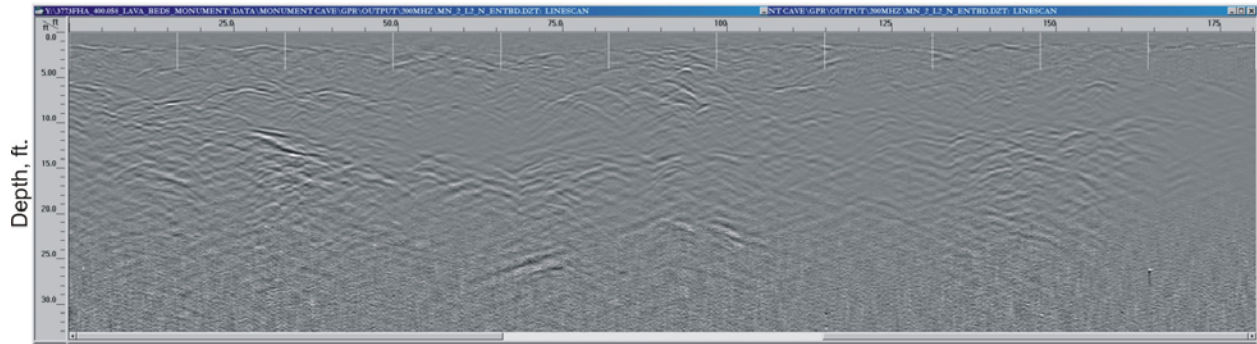
Processed GPR Data 200 MHz Antenna - Line 1
Monument Road Cave
Distance, ft.



Note: 1 foot = .3048 meters

Figure 92. Cross Section. GPR data.

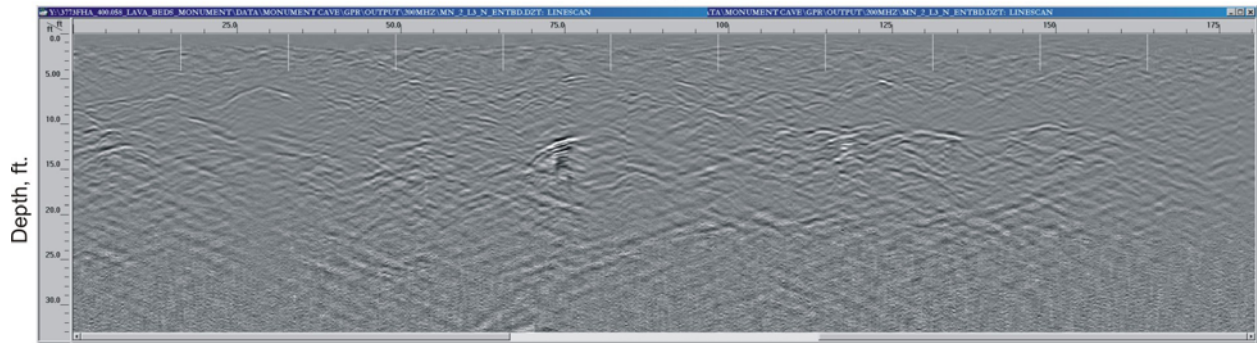
Processed GPR Data 200 MHz Antenna - Line 2
Monument Road Cave
Distance, ft.



Note: 1 foot = .3048 meters

Figure 93. Cross Section. GPR data.

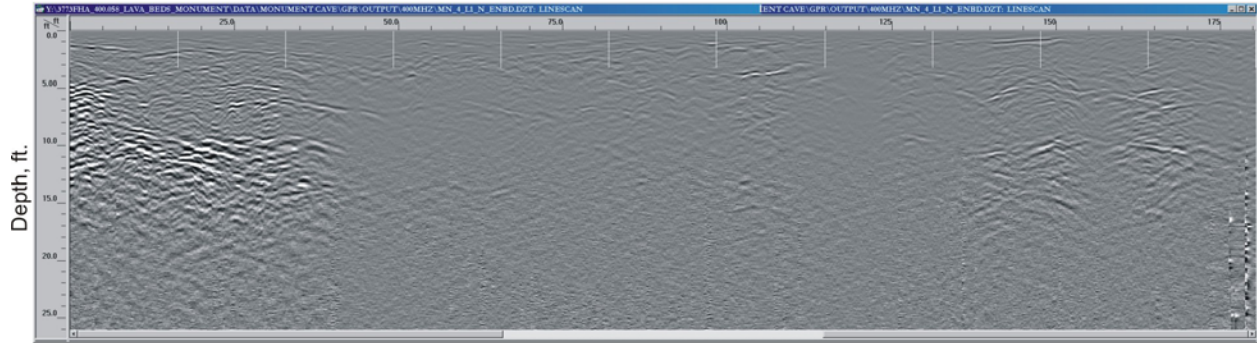
Processed GPR Data 200 MHz Antenna - Line 3
Monument Road Cave
Distance, ft.



Note: 1 foot = .3048 meters

Figure 94. Cross Section. GPR data.

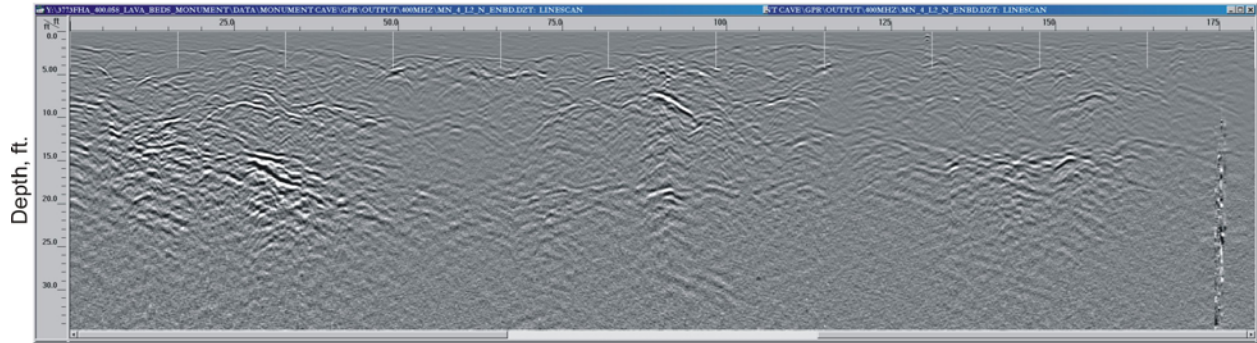
Processed GPR Data 400 MHz Antenna - Line 1
Monument Road Cave
Distance, ft.



Note: 1 foot = .3048 meters

Figure 95. Cross Section. GPR data.

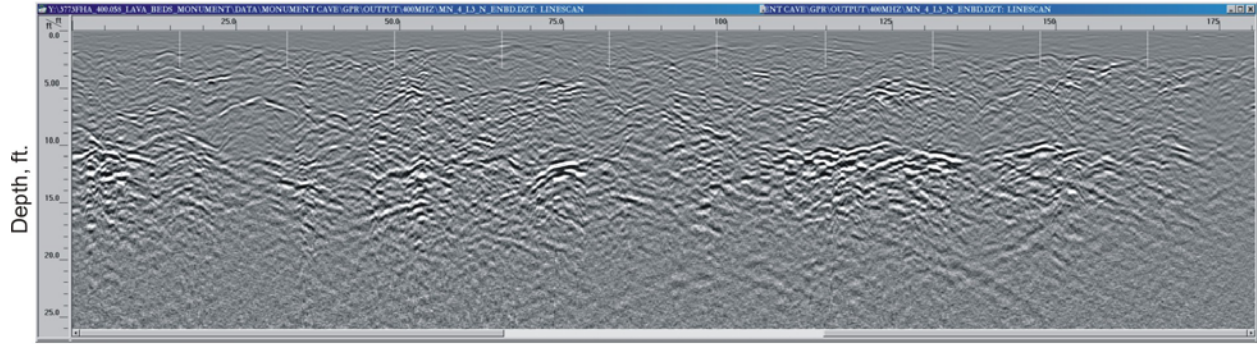
Processed GPR Data 400 MHz Antenna - Line 2
Monument Road Cave
Distance, ft.



Note: 1 foot = .3048 meters

Figure 96. Cross Section. GPR data.

Processed GPR Data 400 MHz Antenna - Line 3
Monument Road Cave
Distance, ft.



Note: 1 foot = .3048 meters

Figure 97. Cross Section. GPR data.

APPENDIX D - HIGH RESOLUTION SHEAR WAVE CROSS SECTIONS

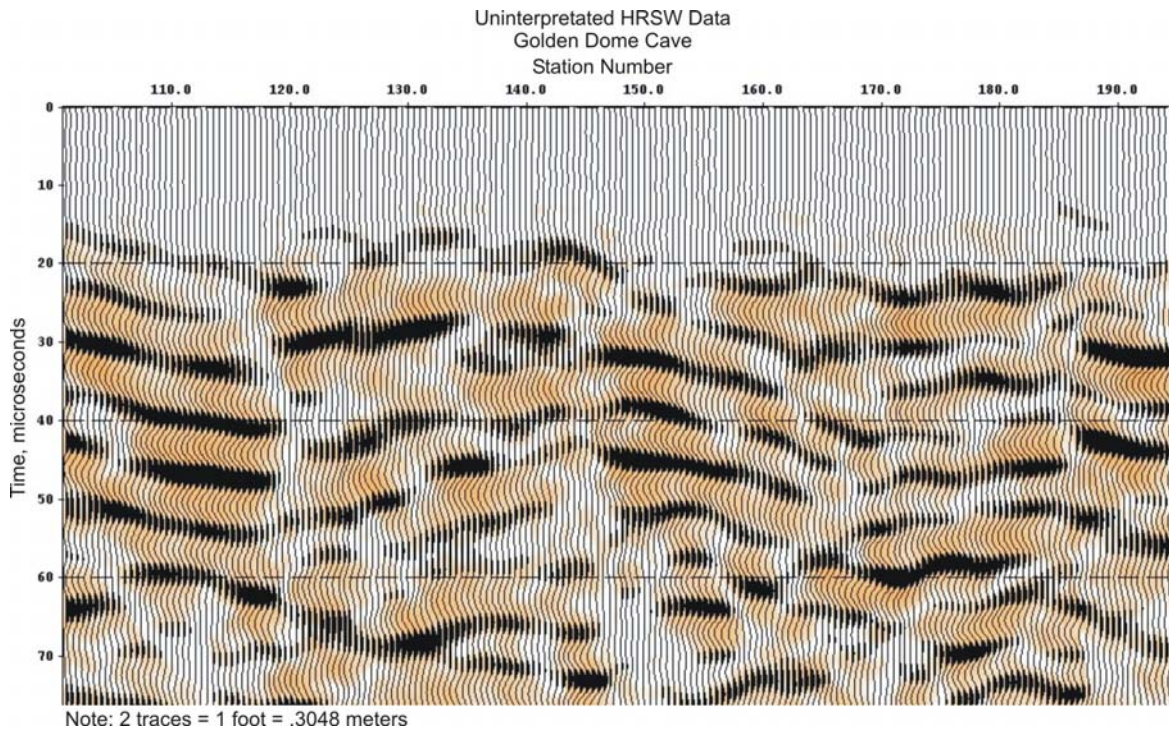


Figure 98. Cross Section. Uninterpreted HRSW data.

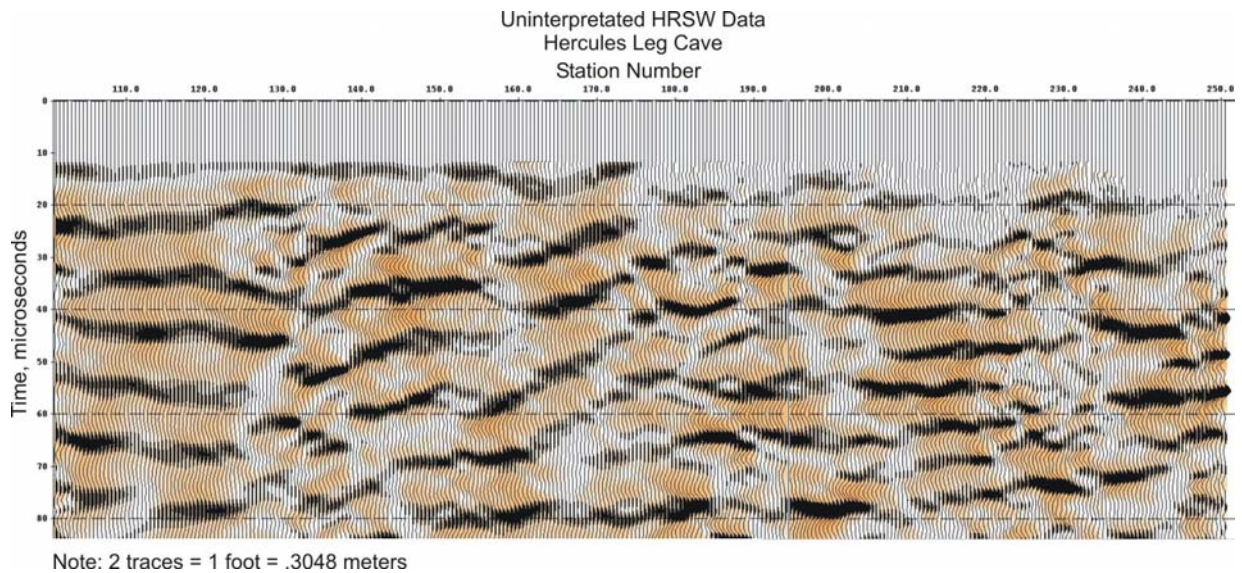


Figure 99. Cross Section. Uninterpreted HRSW data.

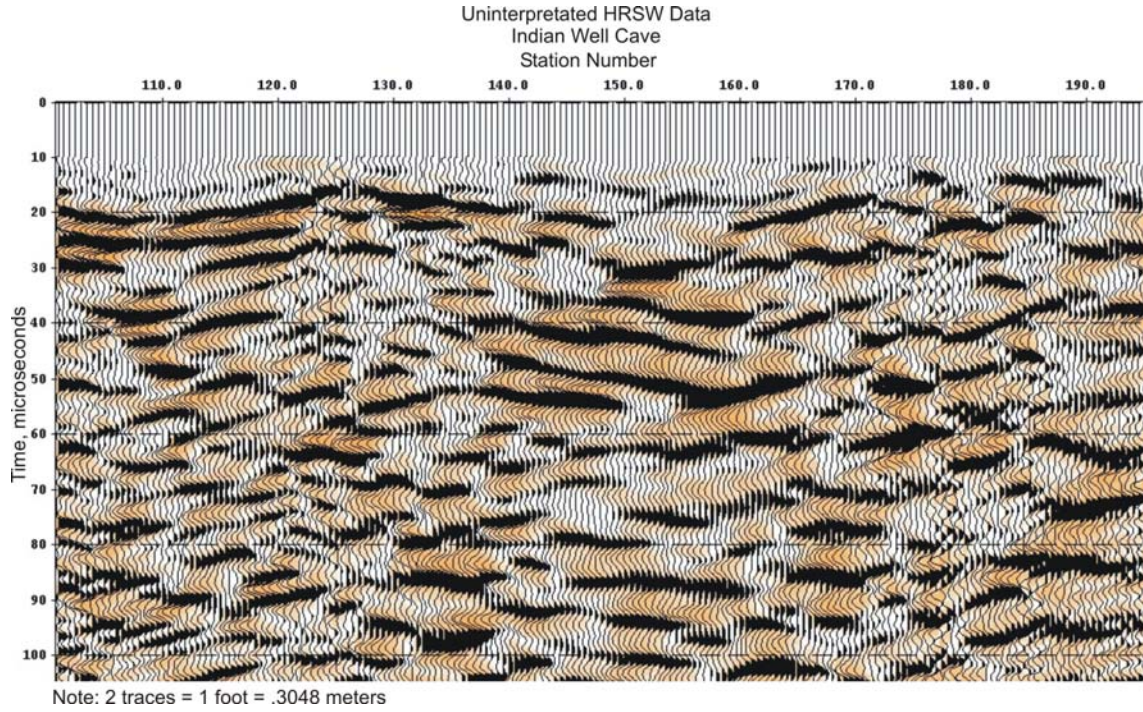


Figure 100. Cross Section. Uninterpreted HRSW data.

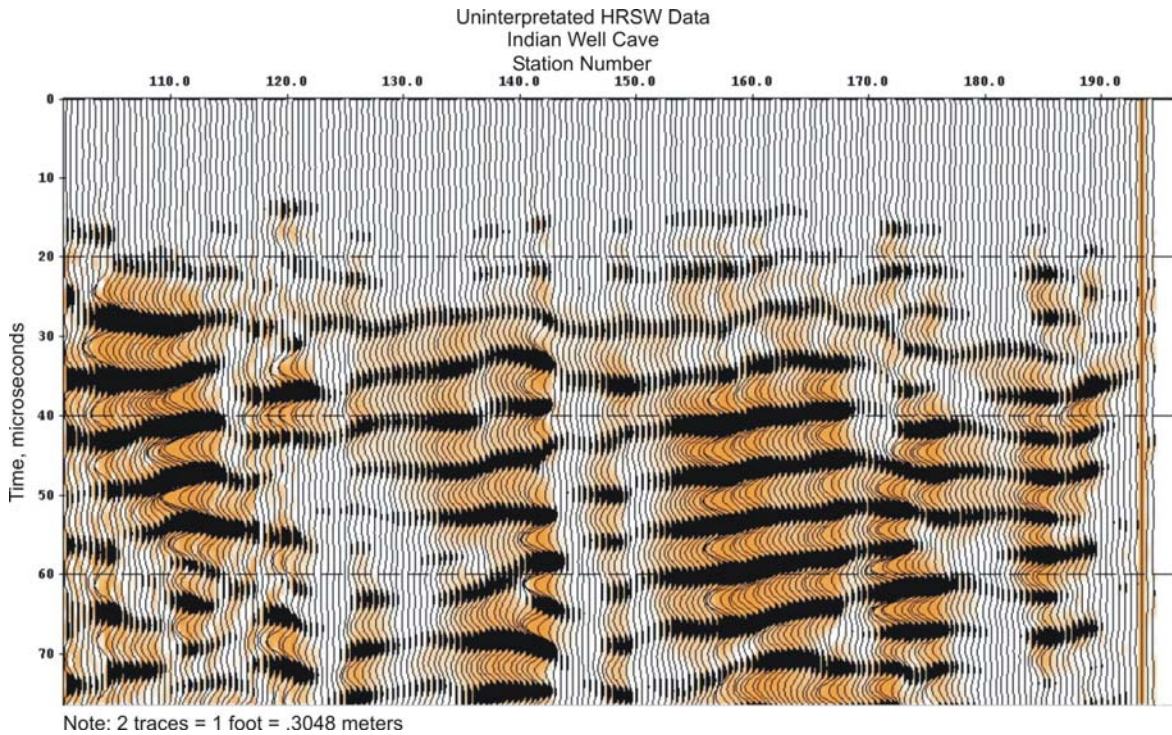
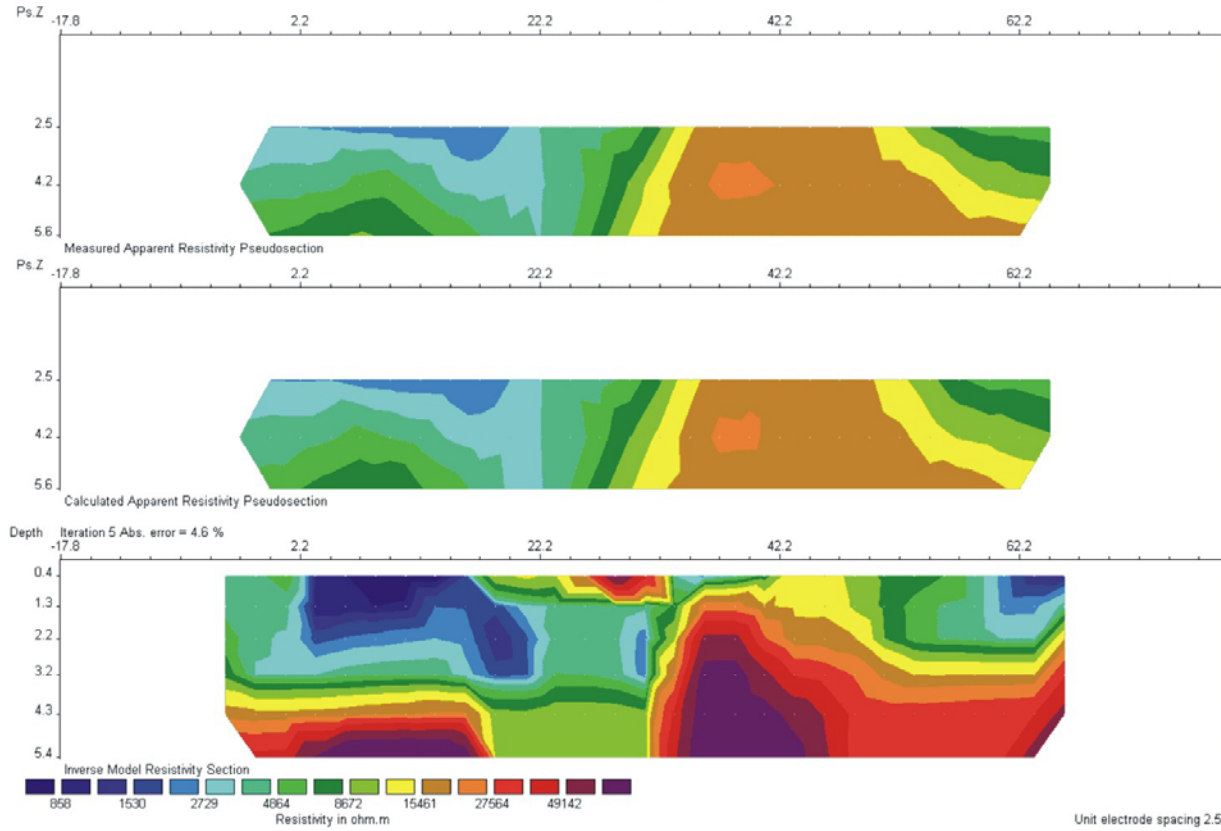


Figure 101. Cross Section. Uninterpreted HRSW data.

APPENDIX E - ELECTRICAL RESISTIVITY CROSS SECTIONS

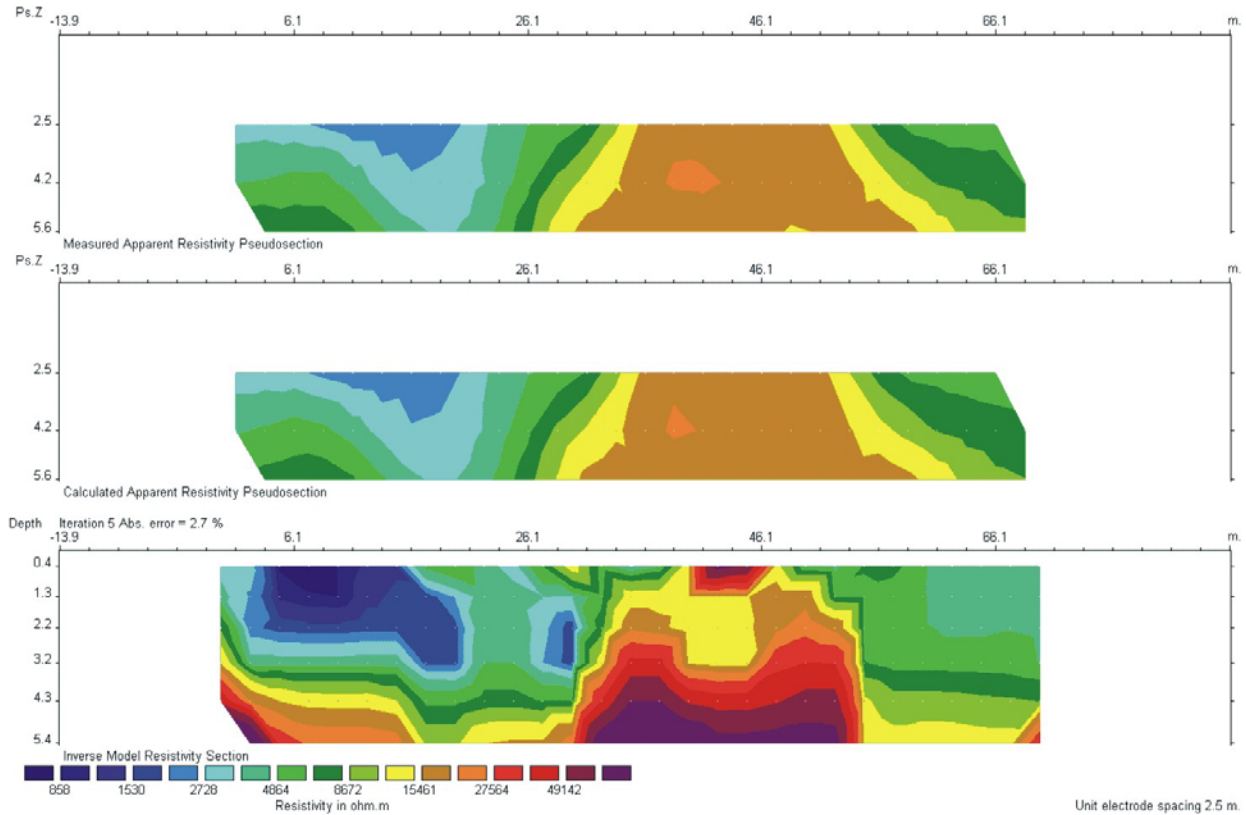
Electrical Resistivity 2-D Vertical Cross Section
Bearpaw Bridge - East to West



Note: 1 foot = .3048 meters

Figure 102. Cross Section. Electrical Resistivity Vertical 2-D.

Electrical Resistivity 2-D Vertical Cross Section
 Bearpaw Bridge - West to East



Note: 1 foot = .3048 meters

Figure 103. Cross Section. Electrical Resistivity Vertical 2-D.

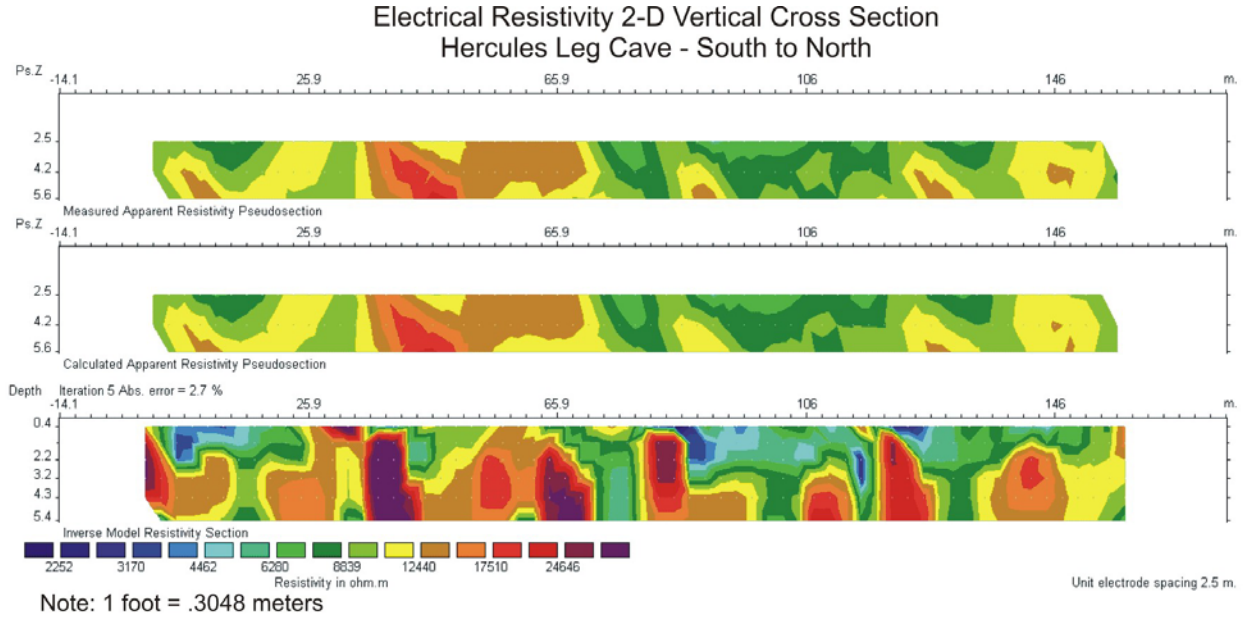


Figure 104. Cross Section. Electrical Resistivity Vertical 2-D.

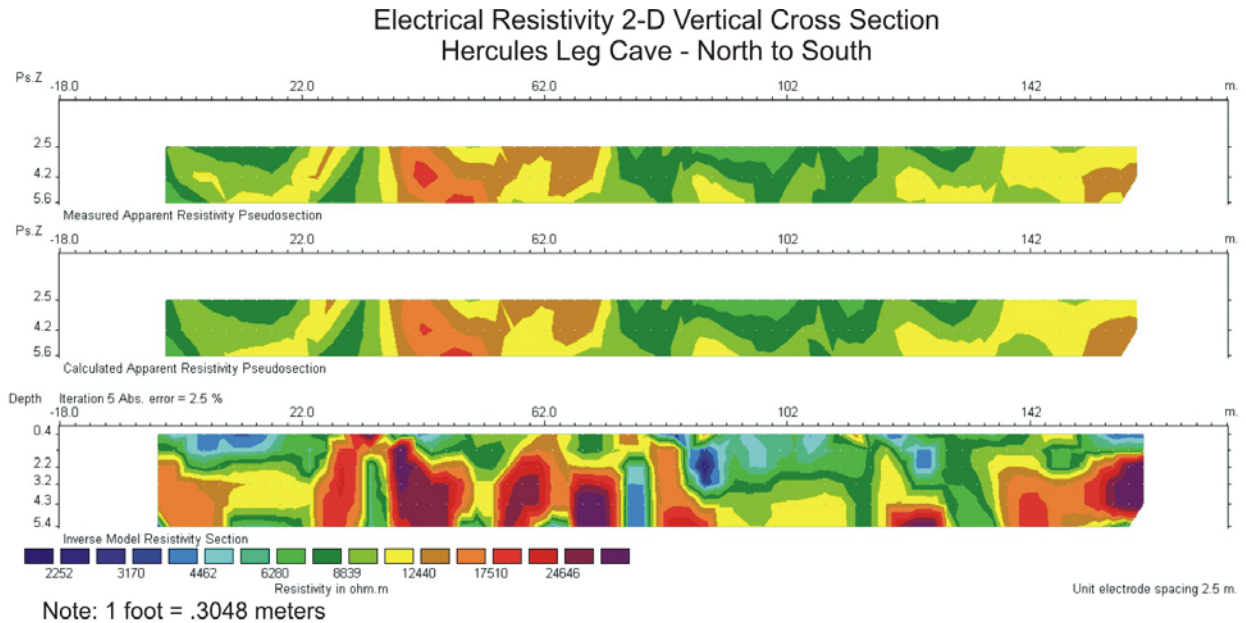


Figure 105. Cross Section. Electrical Resistivity Vertical 2-D.

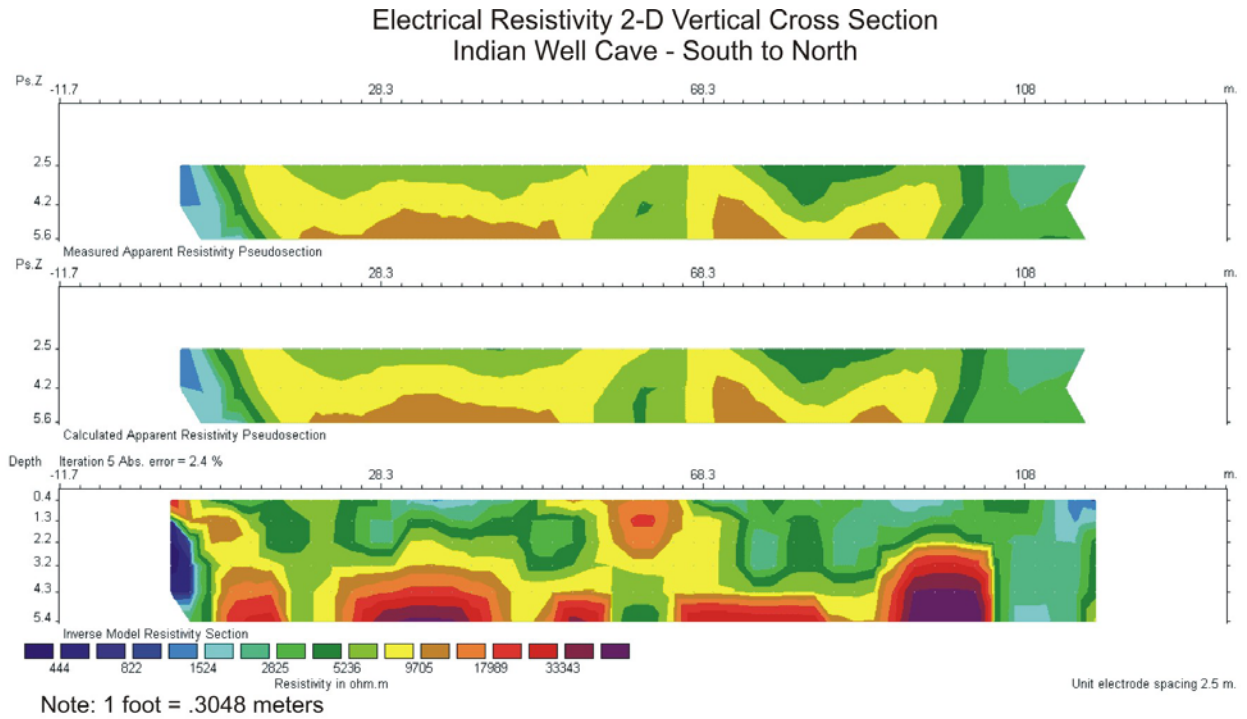


Figure 106. Cross Section. Electrical Resistivity Vertical 2-D.

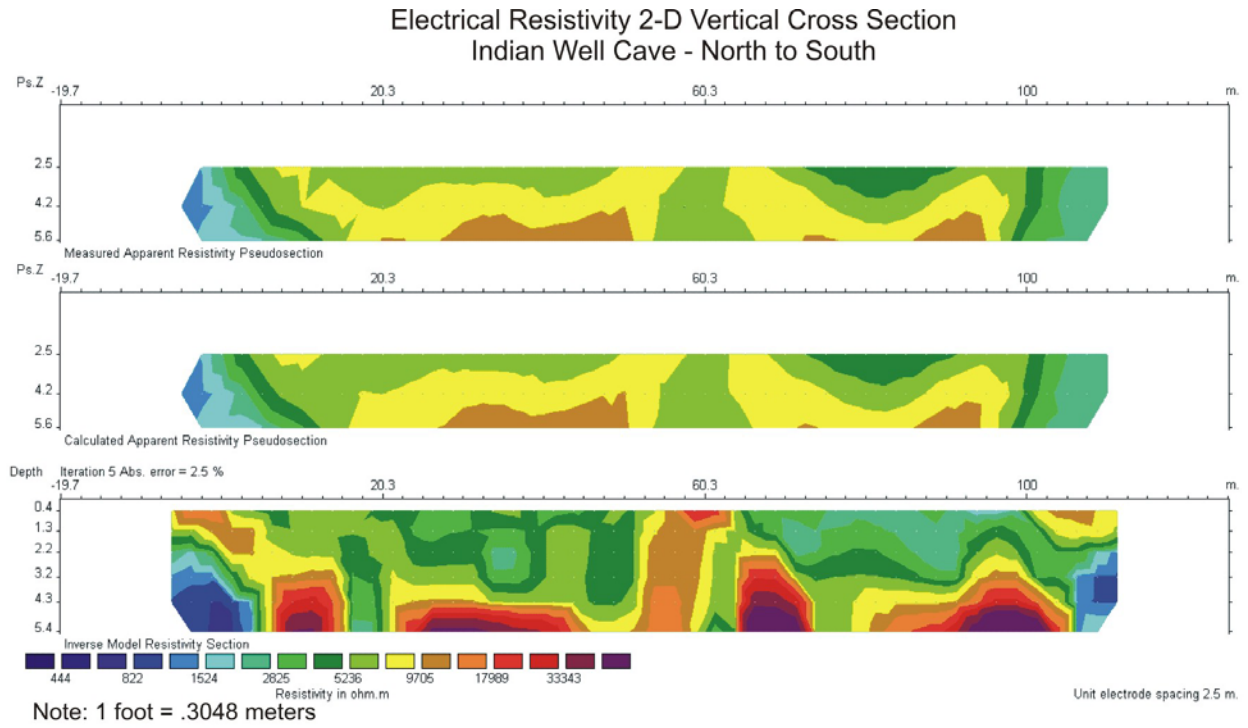


Figure 107. Cross Section. Electrical Resistivity Vertical 2-D.

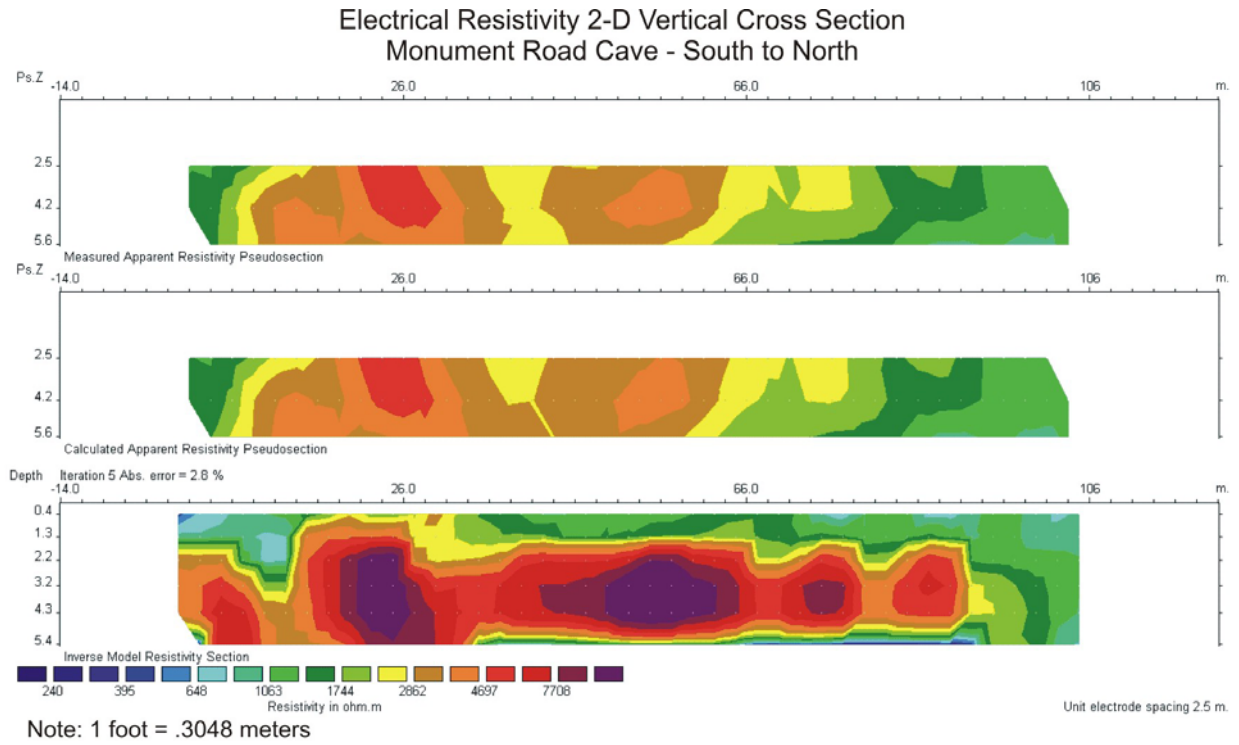


Figure 108. Cross Section. Electrical Resistivity Vertical 2-D.

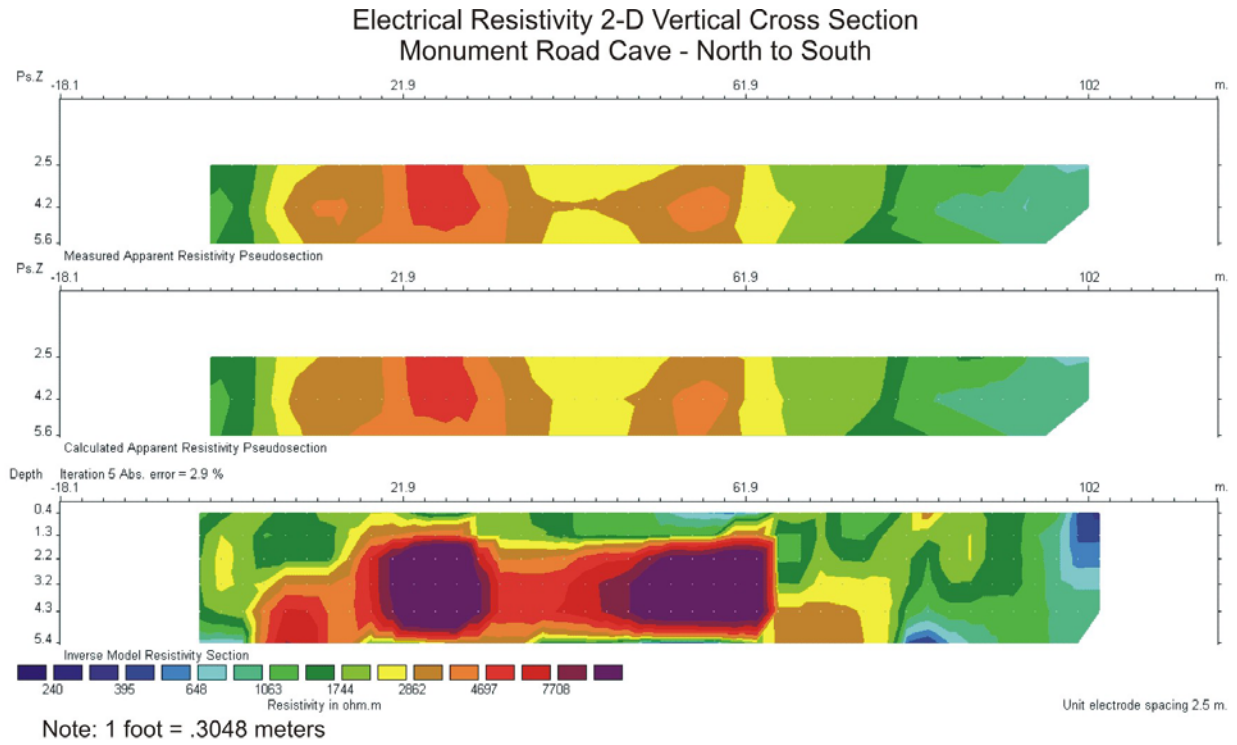


Figure 109. Cross Section. Electrical Resistivity Vertical 2-D.

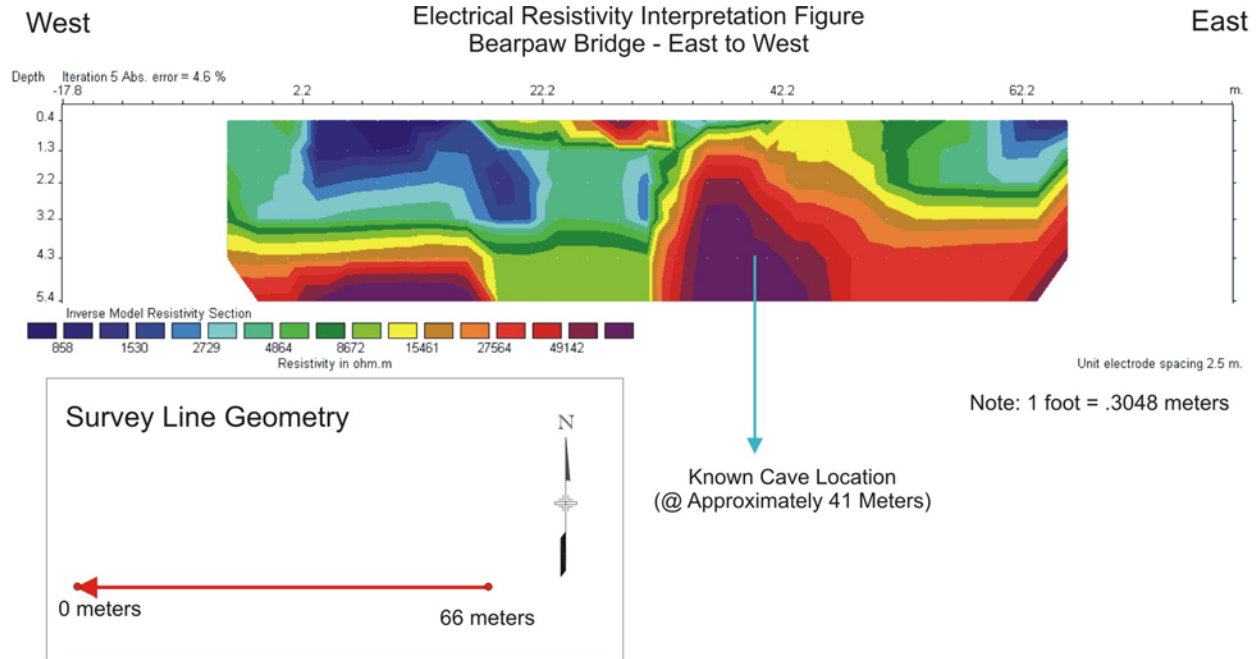


Figure 110. Cross Section. Electrical Resistivity Interpretation.

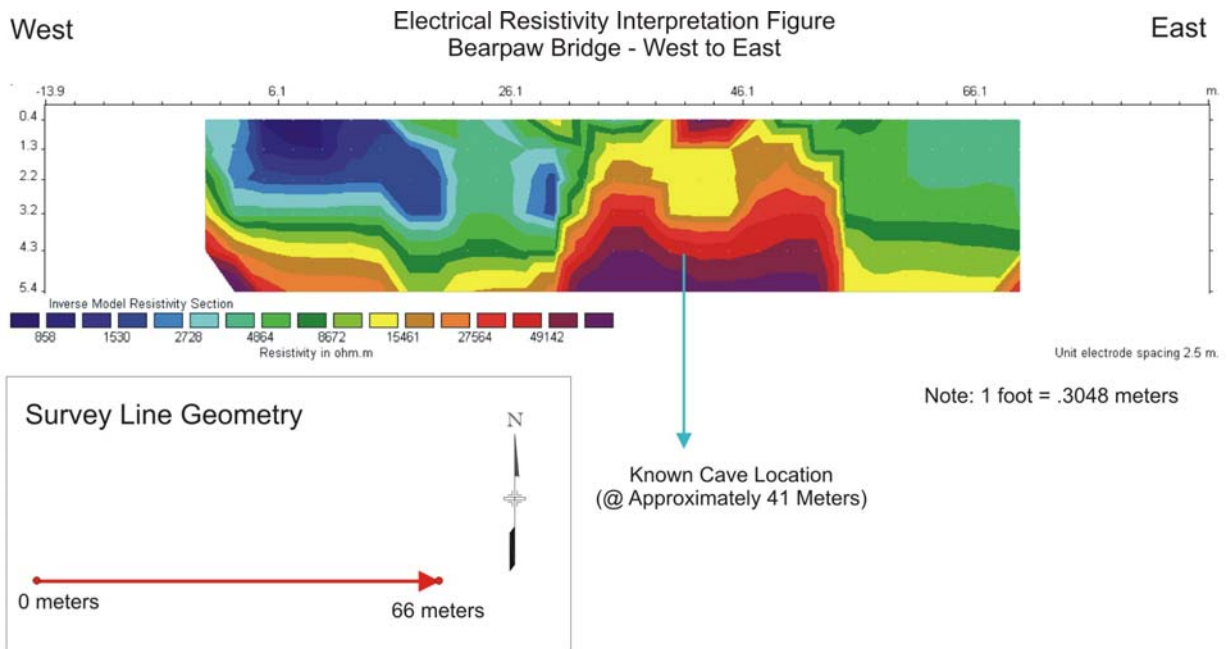


Figure 111. Cross Section. Electrical Resistivity Interpretation.

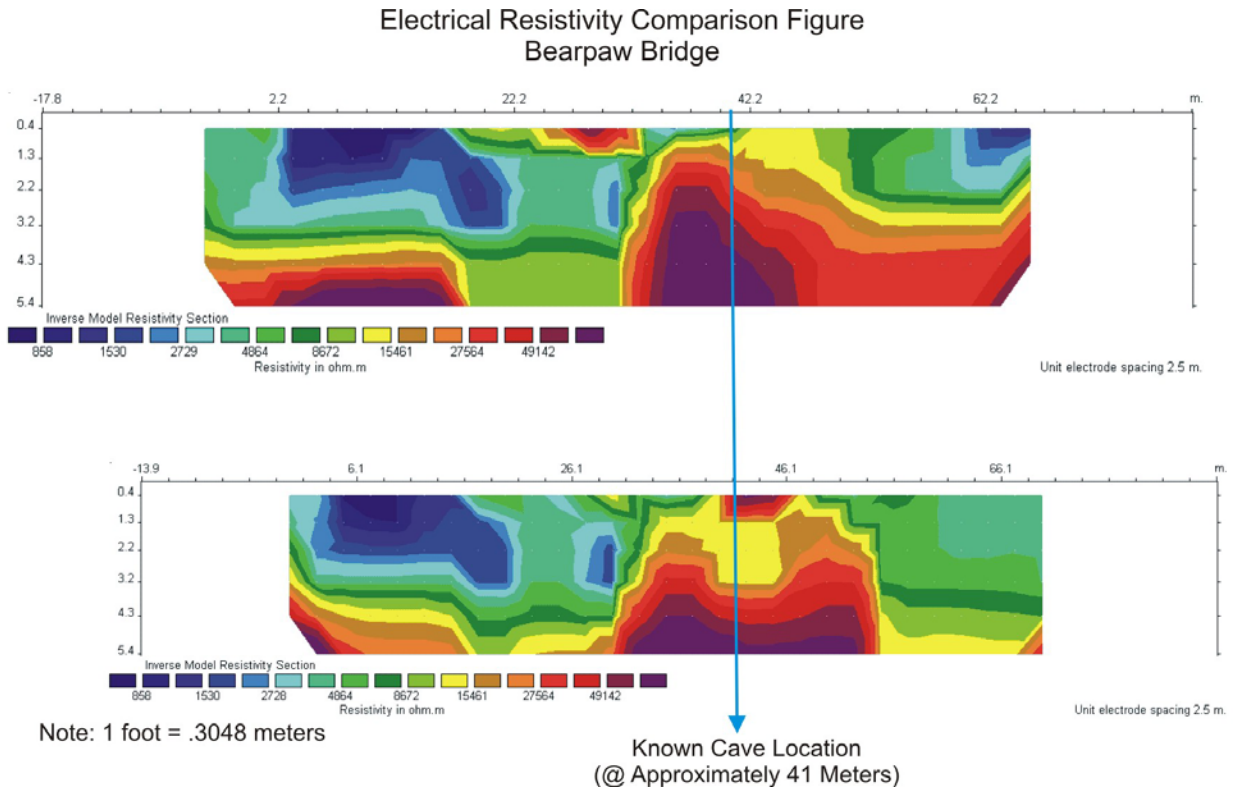


Figure 112. Cross Section. Electrical Resistivity Comparison.

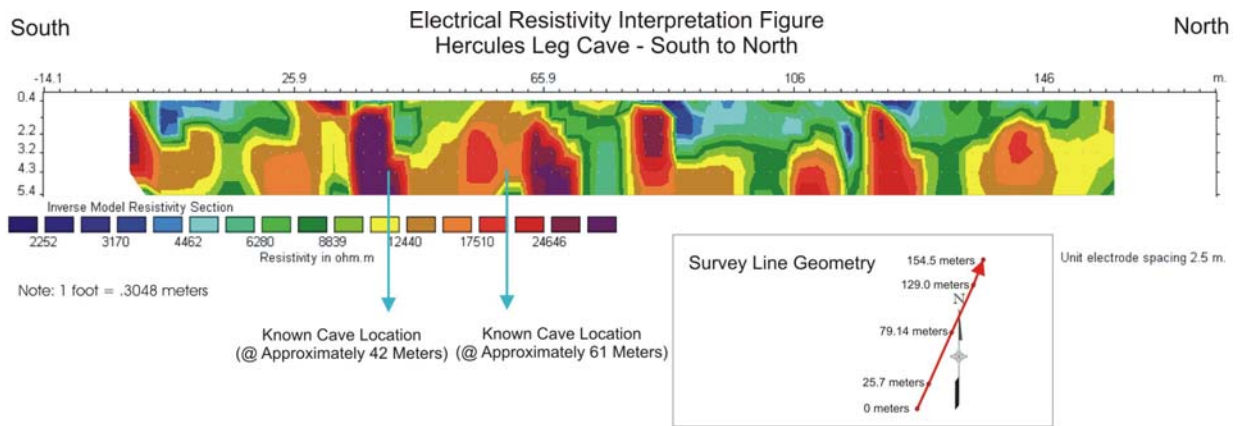


Figure 113. Cross Section. Electrical Resistivity Interpretation.

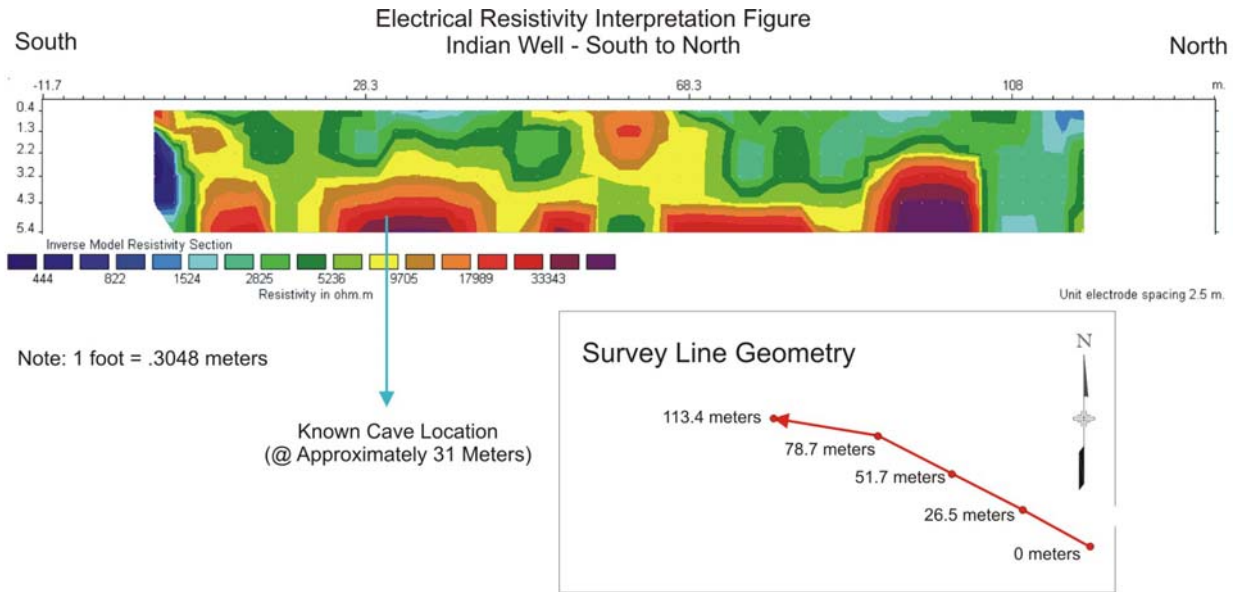


Figure 116. Cross Section. Electrical Resistivity Interpretation.

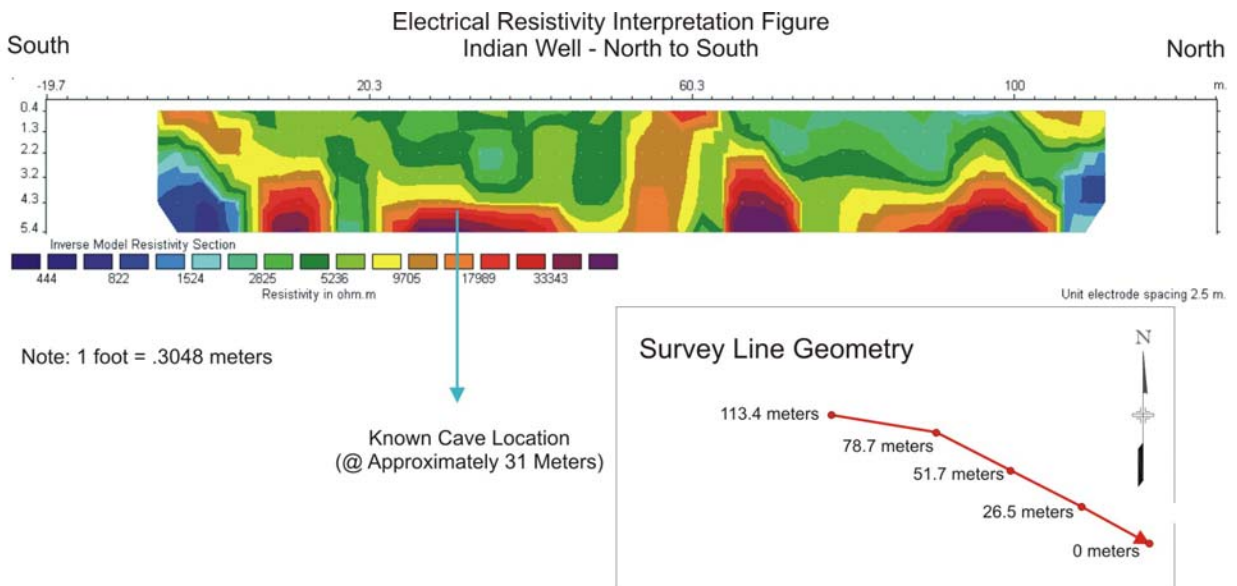


Figure 117. Cross Section. Electrical Resistivity Interpretation.

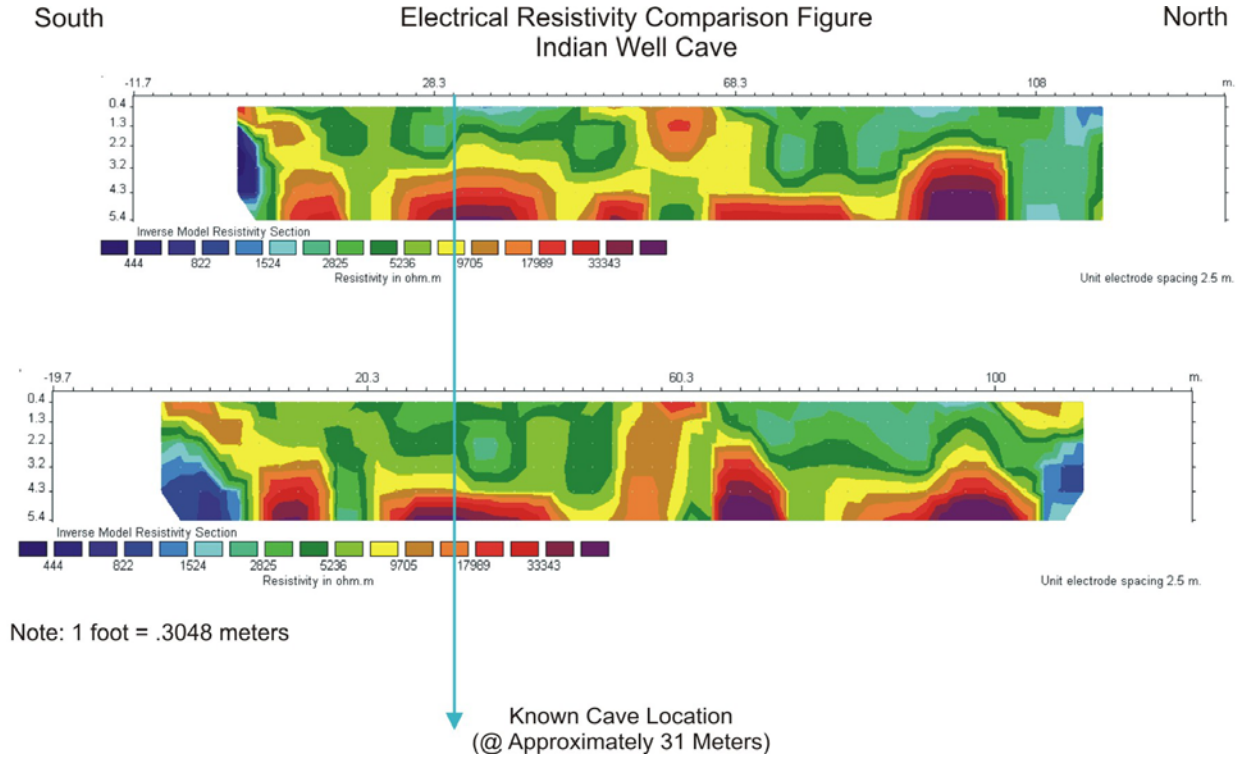


Figure 118. Cross Section. Electrical Resistivity Comparison.

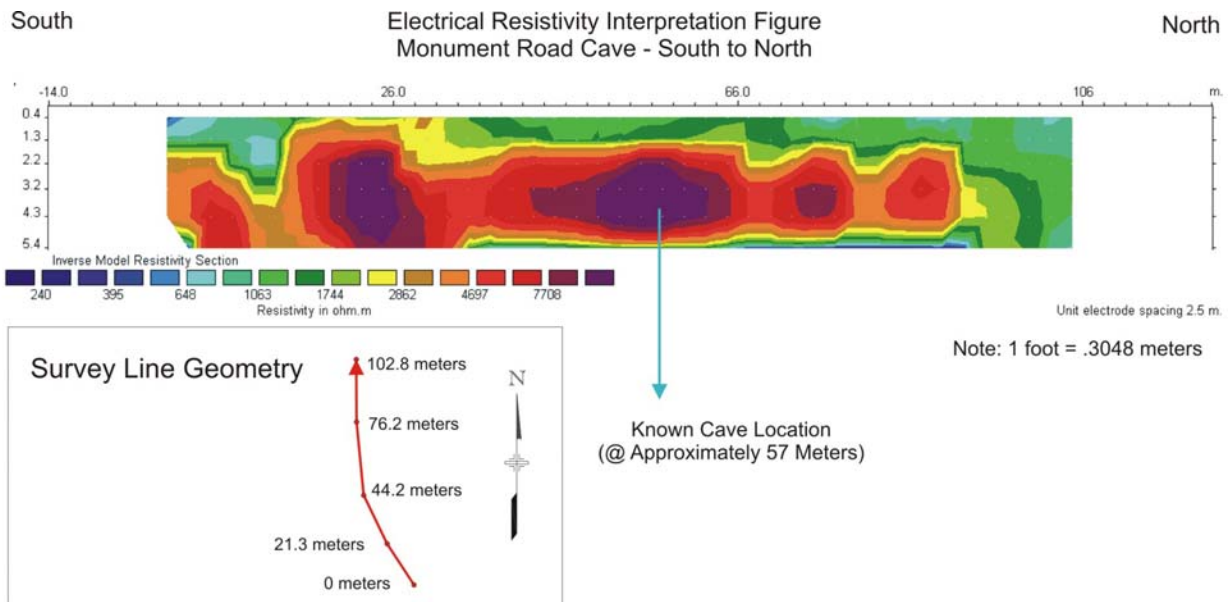


Figure 119. Cross Section. Electrical Resistivity Interpretation.

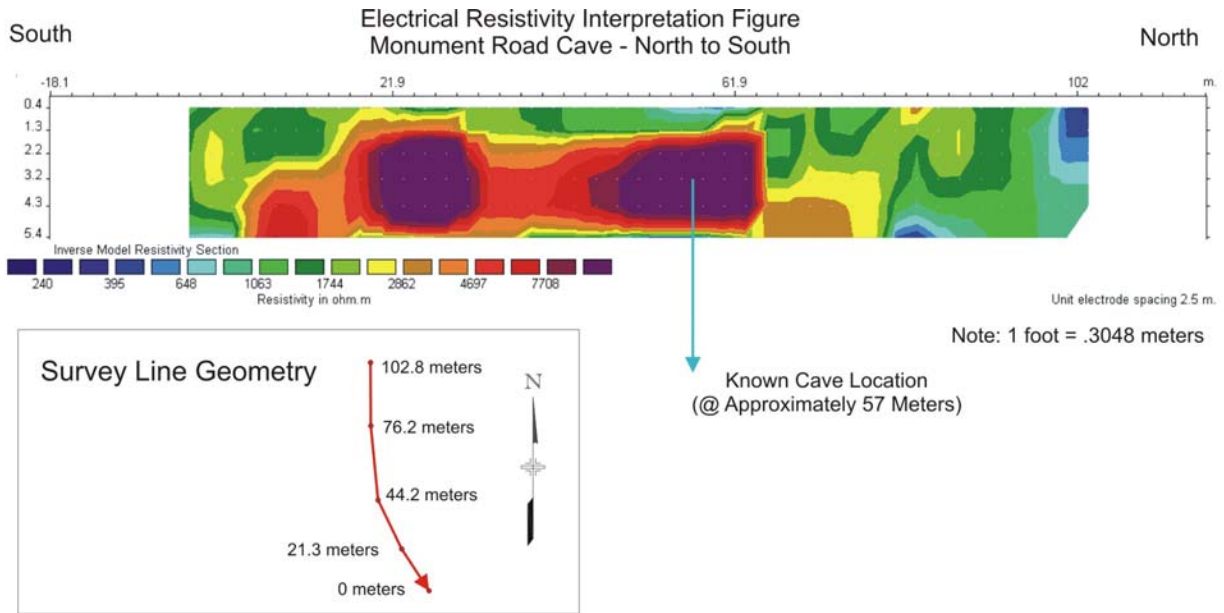


Figure 120. Cross Section. Electrical Resistivity Interpretation.

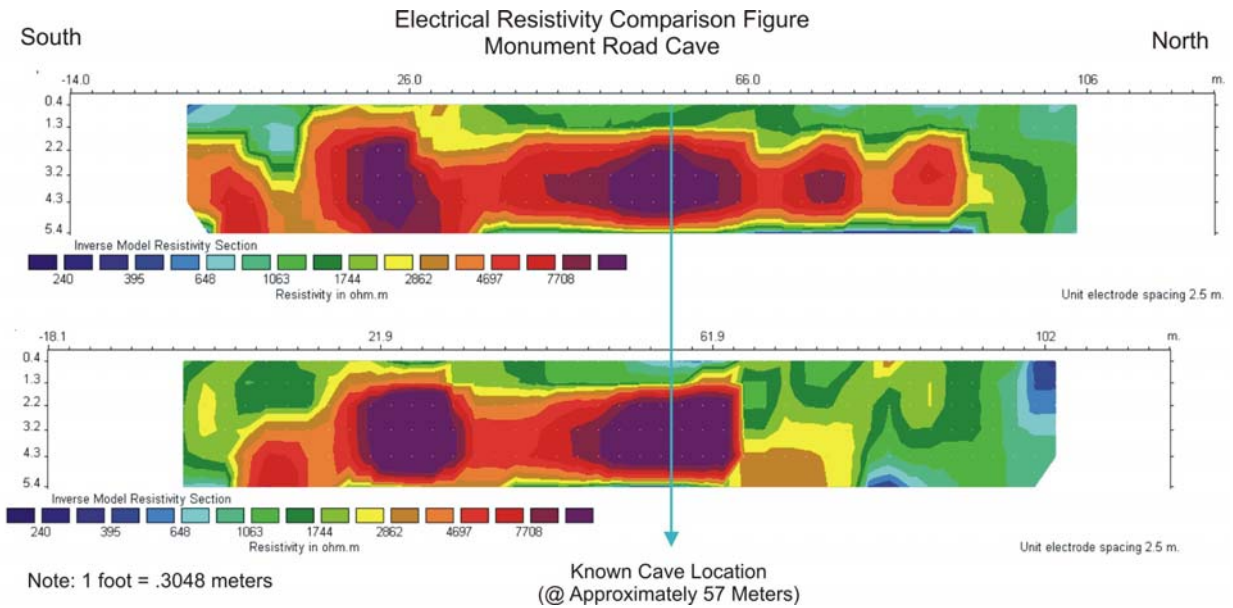


Figure 121. Cross Section. Electrical Resistivity Comparison.